

---

Doctoral Dissertations

Student Theses and Dissertations

---

Summer 2011

## Preliminary model development of metal complexation of polyester derivatives of 2,2'-biimidazole

Shelonda Rena Taylor Finch

Follow this and additional works at: [https://scholarsmine.mst.edu/doctoral\\_dissertations](https://scholarsmine.mst.edu/doctoral_dissertations)

 Part of the [Chemistry Commons](#)

Department: Chemistry

---

### Recommended Citation

Finch, Shelonda Rena Taylor, "Preliminary model development of metal complexation of polyester derivatives of 2,2'-biimidazole" (2011). *Doctoral Dissertations*. 63.

[https://scholarsmine.mst.edu/doctoral\\_dissertations/63](https://scholarsmine.mst.edu/doctoral_dissertations/63)

This thesis is brought to you by Scholars' Mine, a service of the Missouri S&T Library and Learning Resources. This work is protected by U. S. Copyright Law. Unauthorized use including reproduction for redistribution requires the permission of the copyright holder. For more information, please contact [scholarsmine@mst.edu](mailto:scholarsmine@mst.edu).

PRELIMINARY MODEL DEVELOPMENT  
OF METAL COMPLEXATION OF POLYESTER  
DERIVATIVES OF 2,2'-BIIMIDAZOLE

by

SHELONDA RENA TAYLOR FINCH

A DISSERTATION

Presented to the Faculty of the Graduate School of the  
MISSOURI UNIVERSITY OF SCIENCE AND TECHNOLOGY

In Partial Fulfillment of the Requirements for the Degree

DOCTOR OF PHILOSOPHY

in

CHEMISTRY

2011

Approved by

Harvest L. Collier, Advisor  
Russell G. Baughman  
Frank D. Blum  
Ekkehard Sinn  
David J. Westenberg



## ABSTRACT

The objective of this study was to develop a chemical model for metal ion complex formation by a macroligand system with multi-metal binding sites using 2,2'-biimidazole as the starting molecule of the ligand system. Prior studies in this laboratory guided the selection of diesters and hydroxyethyl derivatives of 2,2'-biimidazole as model monomers. In addition, metal ion complexation studies with 2,2'-biimidazole derivatives were conducted. As a result, crystal structures of 1,1'-di(methylpropionato)-2,2'-biimidazole, 2,2'-bis(1H-imidazolium) dinitrate and silver 2,2'-bis(1H-imidazolium) trinitrate, were reported. The crystal structures indicated a dependence upon the binding ability of the protonated 2,2'-biimidazole and counter ions. Transesterification of the diesters and diols revealed oligomeric formation in dimers to pentamers. Upon mixing the esters and oligomers with metal salts, associated metal salts formed.

## ACKNOWLEDGEMENTS

I would like to thank Dr. Harvest L. Collier for his guidance, support, wisdom, patience, and encouragement during my graduate studies at UMR, now Missouri University of Science and Technology. I would also like to thank my advisory committee: Dr. Russell G. Baughman (Truman State University), Dr. Frank D. Blum (Oklahoma State University), Dr. Ekkehard Sinn (Western Michigan University), and Dr. David J. Westenberg. I would like to recognize Dr. V. Prakash Reddy for his assistance and time in explaining concepts and processes to me. I would also like to thank Dr. Amitava Choudhury for single crystal x-ray determinations. In addition, I would like to thank the Collier Research Group of past and present for assistance in experiments along with helpful and insightful discussions.

For financial support, I would like to thank the Chemistry Department, the Minority Engineering Program, and the Missouri Alliance for Graduate Education for the Professorate sponsored by the National Science Foundation. I not only gained monetary payment, but many memories and teaching experiences by the interactions with undergraduate students.

Finally, I would like to thank my family and friends for their encouragement and emotional support. Specifically, I thank my mother, Chizuko Taylor, a strong and wise woman who is a hard example to follow. And also I thank my biggest fan and cheerleader, Hisako Sobierajski, who passed away August 1, 2002 never in doubt of my success.

## TABLE OF CONTENTS

	Page
ABSTRACT.....	iii
ACKNOWLEDGEMENTS.....	iv
LIST OF FIGURES.....	ix
LIST OF SCHEMES.....	xii
LIST OF TABLES.....	xiii
INSTRUMENTATION.....	xvi
SECTION	
1 INTRODUCTION.....	1
1.1 OVERVIEW.....	1
1.2 SIGNIFICANCE OF METAL ION BINDING POLYMER MODEL DEVELOPMENT.....	2
1.2.1 Specificity.....	5
1.2.2 Equilibrium Process.....	8
1.3 TRANSESTERIFICATION.....	8
2 2,2'-BIIMIDAZOLE.....	12
2.1 HISTORY OF 2,2'-BIIMIDAZOLE.....	12
2.2 SYNTHESIS OF 2,2'-BIIMIDAZOLE.....	17
2.3 SYNTHESIS OF 2,2-BIS(1H-IMIDAZOLIUM) DINITRATE.....	18
2.4 2,2'-BIIMIDAZOLE ESTER DERIVATIVES.....	25
2.4.1 Previously reported 1,1'-diesters of 2,2'-biimidazole.....	26
2.4.1.1 1,1'-Di(methylacetato)-2,2'-Biimidazole, DMAB.....	26
2.4.1.2 1,1'-Di(methylpropionato)-2,2'-Biimidazole, DMPB.....	27
2.4.1.3 1,1'-Di(ethylpropionato)-2,2'-Biimidazole, DEPB.....	28

2.4.1.4	1,1'-Di(ethylacrylate)-2,2'-Biimidazole, DEA*B .....	30
2.4.2	New 2,2'-biimidazole diesters synthesized.....	31
2.4.2.1	1,1'-Di(ethylacetato)-2,2'-Biimidazole, DEAB .....	31
2.4.2.2	1,1'-Di(methylacrylate)-2,2'-Biimidazole, DMA*B .....	32
2.5	ALCOHOLS.....	33
2.5.1	1-Hydroxyethyl-2,2'-Biimidazole, mono-HEB .....	33
2.5.2	1,1'-Di(hydroxyethyl)-2,2'-Biimidazole, HEB .....	35
2.5.3	N, N'- Bis(2-hydroxyethyl)ethylenediamine, mock-HEB.....	37
3	METAL COMPLEXES OF 2,2'-BIIMIDAZOLE .....	39
3.1	METAL COMPLEXES OF 2,2'-BIIMIDAZOLE .....	39
3.1.1	Silver Complexes.....	42
3.1.2	Cadmium Complexes.....	42
3.1.3	Cobalt Complexes.....	42
3.1.4	Chromium Complexes .....	43
3.1.5	Copper Complexes.....	43
3.1.6	Iron Complexes.....	43
3.1.7	Iridium Complexes.....	43
3.1.8	Manganese Complexes .....	43
3.1.9	Molybdenum Complexes .....	44
3.1.10	Nickel Complexes.....	44
3.1.11	Osmium Complexes.....	44
3.1.12	Rhenium Complexes.....	45
3.1.13	Ruthenium Complexes.....	45
3.1.14	Vanadium Complexes.....	45
3.1.15	Zinc Complexes .....	45

3.2	SILVER BIS(1H-IMIDAZOLIUM) TRINITRATE.....	46
3.3	METAL COMPLEXATION OF 2,2'-BIIMIDAZOLE DERIVATIVES .....	49
4	POLYMERIZATION OF 2,2'-BIIMIDAZOLE AND DERIVATIVES .....	51
4.1	BACKGROUND ON POLYMERS OF 2,2'-BIIMIDAZOLE.....	51
4.2	TRANSESTERIFICATION.....	51
4.2.1	Acid vs. Base Catalyzed. ....	53
4.2.2	Enzyme Catalyzed .....	54
4.2.3	Viscometry.....	54
4.2.4	Experimental .....	58
4.2.5	Results and Discussion .....	59
4.2.5.1	Reaction I – HEB:DMPB.....	59
4.2.5.2	Reaction II – HEB:DEPB .....	61
4.2.5.3	Reaction III – DEPB:mock-HEB with EtOH. ....	65
4.2.5.4	Reaction IV – DEPB:mock-HEB with H <sub>2</sub> O .....	66
4.2.5.5	Comparison of Reactions.....	69
4.2.6	Molecular Weight Determination .....	74
5	METAL COMPLEXATION OF POLYMERIC 2,2'-BIIMIDAZOLE AND DERIVATIVES .....	75
5.1	METAL COMPLEX POLYMERIZED .....	75
5.2	POLYMER CHELATED BY A METAL.....	76
5.3	2,2'-BIIMIDAZOLE OR 2,2'-BIIMIDAZOLE DERIVATIVE DIRECTLY POLYMERIZED BY A METAL SALT.....	76
5.4	EXPERIMENTAL – SYNTHESIS OF LIGAND WITH COPPER(II) ACETATE.....	76
6	SUMMARY .....	79
6.1	OUTCOMES.....	79



6.1.1 Monomer Ligand. ....	79
6.1.2 Parent Polymer.....	81
6.1.3 Monomer Complex. ....	82
6.1.4 Polymer Complex. ....	82
6.2 FURTHER STUDY .....	83
APPENDICES	
A. INFRARED SPECTRA .....	85
B. CRYSTALLOGRAPHIC TABLES .....	96
C. NUCLEAR MAGNETIC RESONANCE SPECTRA.....	111
D. THERMOGRAVIMETRIC ANALYSIS SPECTRA .....	113
REFERENCES .....	118
VITA.....	130

## LIST OF FIGURES

	Page
Figure 1.1. Strategic model for 2,2'-biimidazole-based esters.....	3
Figure 1.2. Macromolecular ligand-metal-ion binding models.....	6
Figure 2.1. Diprotonated 2,2'-biimidazole with bromide and chloride counter ions from the x-y plane.....	23
Figure 2.2. Protonated 2,2'-biimidazole with nitrate counter ions.....	23
Figure 2.3. Asymmetric unit of [bimH <sub>2</sub> ][NO <sub>3</sub> ] <sub>2</sub> .....	24
Figure 2.4. Unit cell of 2,2'-bis(1H-imidazolium) dinitrate.....	24
Figure 2.5. Unit cell of 2,2'-bis(1H-imidazolium) dinitrate.....	25
Figure 3.1. Ellipsoid / OR TEP diagram of silver 2,2-bis(1H-imidazolium) trinitrate.....	48
Figure 3.2. Unit cell silver bis(1H-imidazolium) trinitrate along x-y face.....	48
Figure 3.3. Preliminary crystallographic determination of silver nitrate with 1,1'-di(ethylpropionato)-2,2'-biimidazole.....	50
Figure 4.1. The ideal Huggins, Kraemer, and Mark-Houwink-Sakurada relationships.....	57
Figure 4.2. Plot of $\eta_{red}$ and $\eta_{inh}$ versus concentration of HEB:DMPB in DMF at 25°C.....	60
Figure 4.3. DSC overlay of HEB, DMPB, and HEB:DMPB product.....	62
Figure 4.4. Plot of $\eta_{red}$ and $\eta_{inh}$ versus concentration of HEB:DEPB in DMF at 25°C.....	63
Figure 4.5. DSC Overlay of HEB, DEPB, and HEB:DEPB product.....	64
Figure 4.6. Plot of $\eta_{red}$ and $\eta_{inh}$ versus concentration of DEPB:mock-HEB with ethanol in DMF at 25°C.....	65
Figure 4.7. DSC overlay of DEPB, mock-HEB, DEPB:mock-HEB w EtOH, and DEPB:mock-HEB w H <sub>2</sub> O.....	67
Figure 4.8. Plot of $\eta_{red}$ and $\eta_{inh}$ versus concentration of DEPB:mock-HEB with water using DMF at 25°C.....	68

Figure 4.9. IR overlay of HEB:DMPB, HEB:DEPB, DEPB:mock-HEB w EtOH, and DEPB:mock-HEB w H <sub>2</sub> O.....	70
Figure 4.10. TGA overlay of HEB:DMPB, HEB:DEPB, DEPB:mock-HEB w EtOH, DEPB:mock-HEB w H <sub>2</sub> O.....	72
Figure 4.11. DSC overlay of HEB:DMPB, HEB:DEPB, DEPB:mock-HEB w EtOH, DEPB:mock-HEB w H <sub>2</sub> O.....	73
Figure 5.1. Strategic model for 2,2'-biimidazole-based esters.....	75
Figure 6.1. Strategic model for 2,2'-biimidazole-based esters.....	79
Figure 6.2. Strategic model for 2,2'-biimidazole-based esters with focus on monomer.....	80
Figure 6.3. Strategic model for 2,2'-biimidazole-based esters with focus on parent polymer.....	81
Figure 6.4. Strategic model for 2,2'-biimidazole-based esters with focus on monomer complex.....	82
Figure 6.5. Strategic model for 2,2'-biimidazole-based esters with focus on polymer complex.....	83
Figure A.1. Infrared spectrum of 2,2'-biimidazole.....	86
Figure A.2. Infrared spectrum of 1,1'-di(methylacetato)-2,2'-biimidazole.....	87
Figure A.3. Infrared spectrum of 1,1'-di(ethylpropionato)-2,2'-biimidazole.....	88
Figure A.4. Infrared spectrum of 1,1'-di(ethylacrylate)-2,2'-biimidazole.....	89
Figure A.5. Infrared spectrum of 1-hydroxyethyl-2,2'-biimidazole.....	90
Figure A.6. Infrared spectrum of 1,1'-di(hydroxyethyl)-2,2'-biimidazole.....	91
Figure A.7. Infrared spectrum of HEB:DMPB product.....	92
Figure A.8. Infrared spectrum of HEB:DEPB product.....	93
Figure A.9. Infrared spectrum of DEPB:mock-HEB product with ethanol.....	94
Figure A.10. Infrared spectrum of DEPB:mock-HEB product with water.....	95
Figure C.1. Proton NMR spectra at 20°, 50°, and 75° C (from bottom to top) of 2,2'-bis(1H-imidazolium) dinitrate.....	112

Figure C.2. Carbon NMR spectra at 20°, 50°, and 75°C (from bottom to top) of 2,2'-bis(1H-imidazolium) dinitrate. ....	112
Figure D.1. Thermal gravimetric spectrum of 2,2'-biimidazole.....	114
Figure D.2. Thermal gravimetric spectrum of mock-HEB.....	115
Figure D.3. Thermal gravimetric spectrum of DEPB.....	116
Figure D.4. Thermal gravimetric spectrum of DEPB:mock-HEB.....	117

## LIST OF SCHEMES

	Page
Scheme 1.1. Structure of 2,2'-biimidazole (I) and histidine (II). .....	2
Scheme 1.2. Protonation and deprotonation of 2,2'-biimidazole with redox pairs and corresponding pK <sub>a</sub> s .....	4
Scheme 1.3. Metal complexes. ....	7
Scheme 1.4. General overview of synthetic pathways of a macromolecular coordination compound with 2,2'-biimidazole moiety. ....	9
Scheme 1.5. General transesterification reaction scheme.....	10
Scheme 1.6. Transesterification reaction using diester and diol.....	11
Scheme 2.1. Reaction scheme for the synthesis of 2,2'-biimidazole.....	18
Scheme 2.2. Diagram of 2,2'-biimidazole for bond lengths.....	22
Scheme 2.3. Structure of 1,1'-di(methylacetato)-2,2'-biimidazole. ....	27
Scheme 2.4. Structure of 1,1'-di(methylpropionato)-2,2'-biimidazole. ....	28
Scheme 2.5. Structure of 1,1'-di(ethylpropionato)-2,2'-biimidazole. ....	29
Scheme 2.6. Structure of 1,1'-di(ethylacrylate)-2,2'-biimidazole. ....	30
Scheme 2.7. Structure of 1,1'-di(ethylacetato)-2,2'-biimidazole. ....	31
Scheme 2.8. Structure of 1,1'-di(methylacrylate)-2,2'-biimidazole. ....	33
Scheme 2.9. Structure of 1-hydroxyethyl-2,2'-biimidazole. ....	34
Scheme 2.10. Structure of 1,1'-di(hydroxyethyl)-2,2'-biimidazole. ....	36
Scheme 2.11. Structure of N,N'-bis(2-hydroxyethyl)ethylenediamine.....	38
Scheme 3.1. Metal complexes. ....	40
Scheme 4.1. General transesterification reaction scheme.....	52
Scheme 4.2. Transesterification reaction using diester and diol.....	52
Scheme 4.3. Acid-catalyzed transesterification mechanism.....	53
Scheme 4.4. Base-catalyzed transesterification mechanism.....	54

## LIST OF TABLES

	Page
Table 2.1. Crystal Structures of 2,2'-Biimidazole and Protonated 2,2'-Biimidazole .....	15
Table 2.2. Selected Bond Lengths for Protonated 2,2'-Biimidazole.....	22
Table 3.1. Crystal Information for Various Metal - 2,2'-Biimidazole Compounds.....	41
Table 3.2. Crystal Structures of Metals with 2,2'-Biimidazole Derivatives .....	49
Table 4.1. TGA Values of 2,2'-Biimidazole, mock-HEB, DEPB and Reaction Product .....	69
Table 4.2. TGA Values of Reaction Products.....	71
Table 4.3. Molecular Weight and Mer Determination.....	74
Table 5.1. Amounts of Copper(II) Acetate and Ligands Used and Mixture Recovered .....	77
Table 5.2. Elemental Analysis of Copper(II) Acetate and Ligand Recovered with Metal Ligand Ratios .....	78
Table B.1. Crystal Data and Structure Refinement for [biimH <sub>2</sub> ][NO <sub>3</sub> ] <sub>3</sub> .....	97
Table B.2. Atomic Coordinates ( x 10 <sup>4</sup> ) and Equivalent Isotropic Displacement Parameters (Å <sup>2</sup> x 10 <sup>3</sup> ) for [biimH <sub>2</sub> ][NO <sub>3</sub> ] <sub>3</sub> .....	98
Table B.3. Bond Lengths [Å] and Angles [°] for [biimH <sub>2</sub> ][NO <sub>3</sub> ] <sub>3</sub> .....	99
Table B.4. Anisotropic Displacement Parameters (Å <sup>2</sup> x 10 <sup>3</sup> ) for [biimH <sub>2</sub> ][NO <sub>3</sub> ] <sub>3</sub> .....	101
Table B.5. Hydrogen Coordinates ( x 10 <sup>4</sup> ) and Isotropic Displacement Parameters (Å <sup>2</sup> x 10 <sup>3</sup> ) for [biimH <sub>2</sub> ][NO <sub>3</sub> ] <sub>3</sub> .....	102
Table B.6. Crystal Data and Structure Refinement for Ag(biimH) <sub>2</sub> (NO <sub>3</sub> ) <sub>3</sub> .....	103
Table B.7. Atomic Coordinates ( x 10 <sup>4</sup> ) and Equivalent Isotropic Displacement Parameters (Å <sup>2</sup> x 10 <sup>3</sup> ) for Ag(biimH) <sub>2</sub> (NO <sub>3</sub> ) <sub>3</sub> .....	104
Table B.8. Bond Lengths [Å] and Angles [°] for Ag(biimH) <sub>2</sub> (NO <sub>3</sub> ) <sub>3</sub> .....	105

Table B.9. Anisotropic Displacement Parameters ( $\text{\AA}^2 \times 10^3$ ) for Ag(biimH) <sub>2</sub> (NO <sub>3</sub> ) <sub>3</sub> .....	107
Table B.10. Hydrogen Coordinates ( $\times 10^4$ ) and Isotropic Displacement Parameters ( $\text{\AA}^2 \times 10^3$ ) for Ag(biimH) <sub>2</sub> (NO <sub>3</sub> ) <sub>3</sub> .....	108
Table B.11. Torsion Angles [ $^\circ$ ] for Ag(biimH) <sub>2</sub> (NO <sub>3</sub> ) <sub>3</sub> .....	109

## NOMENCLATURE

## Abbreviations

biim .....	biimidazole
H <sub>2</sub> biim .....	2,2'-bis(1H-imidazolium)
CV.....	Cyclic Voltammetry
DEAB.....	1,1'-Di(ethylacetato)-2,2'-biimidazole
DEA*B.....	1,1'-Di(ethylacrylate)-2,2'-biimidazole
DEPB.....	1,1'-Di(ethylpropionato)-2,2'-biimidazole
DMF.....	Dimethylformamide
DMAB.....	1,1'-Di(methylacetato)-2,2'-biimidazole
DMA*B.....	1,1'-Di(methylacrylate)-2,2'-biimidazole
DMPB.....	1,1'-Di(methylpropionato)-2,2'-biimidazole
EtOH.....	ethanol
HEB.....	1,1'-Di(hydroxyethyl)-2,2'-biimidazole
mock-HEB.....	N,N'-Bis(2-hydroxyethyl)ethylenediamine
mono-HEB.....	1-Hydroxyethyl-2,2'-biimidazole
OR TEP.....	Oak Ridge Thermal Ellipsoid Plot
TGA.....	thermogravimetric analysis
TMAH.....	tetramethylammonium hydroxide



## INSTRUMENTATION

NMR: Varian Unity / Inova with an Oxford 400 MHz magnet.

Elemental Analysis: Perkin-Elmer 2400C C, H, & N Elemental Analyzer.

TGA: Perkin-Elmer TG/S/2 Thermogravimetric Analyzer; Netzsch at Materials Research Center at the Missouri University of Science and Technology.

DSC: TA-DSC at Materials Research Center at the Missouri University of Science and Technology.

FTIR: Perkin-Elmer model 1750 Fourier Transform Infrared Spectrometer; KBr pellets.

UV-Vis: Hewlett Packard 8452A Diode Array Spectrometer.

CV: EG&G Princeton Applied Research Potentiostat/Galvanostat Model 273.

X-ray Crystallography: Bruker Smart Apex I Single Crystal XRD.

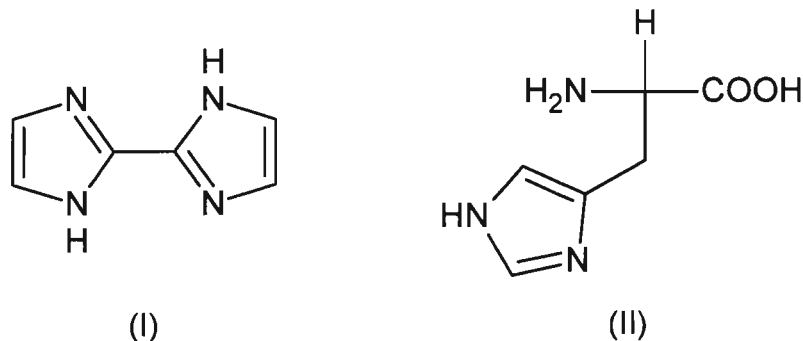
# 1 INTRODUCTION

## 1.1 OVERVIEW

The objective of this investigation was to initiate a study to establish the mechanism by which metal ion complexation occurs in a biimidazole containing macromolecular ligand system, thus developing a chemical model for metal ion complex formation by a macroligand system with multi-metal binding sites using 2,2'-biimidazole as the starting molecule for the ligand system. Three possible pathways were explored. One possible route was to form a monomer complex with subsequent polymerization. Secondly, the monomer could be polymerized first and then the metal complexed to it. Thirdly, and ultimately, the monomer could be polymerized and complexed in a concerted reaction. Prior success in the synthesis of 2,2'-biimidazole polymers, the inherent metal-binding characteristics of 2,2'-biimidazole polymers, and the lack of metal-binding studies with 2,2'-biimidazole polymers led to this study. The motivation for this study came about due to the inherent metal-binding characteristics of 2,2'-biimidazole, prior success for the preparation of 2,2'-biimidazole polymers, and the lack of metal-binding studies with 2,2'-biimidazole. The first report of 2,2'-biimidazole (structure given in Scheme 1.1. (I)) was in 1858. [1] Since that time, research interest has arisen based on its biheterocyclic composition, solid state stability and chemical reactivity. The similarity of the amine group of the amino acid histidine (Scheme 1.1. (II)) with the imidazole ring of 2,2'-biimidazole has led to studies of the biological activity of 2,2'-biimidazole. [2-6] Cromer *et al.* reported the crystal structure of 2,2'-biimidazole with the five atoms of the heterocycle were coplanar within 0.002 Å but the two rings had a dihedral angle of about 4.6° with a residual R-factor of 5.4%. [7]

The rigidity of these rings leads to limited solubility in common organic solvents.

Incorporating functional groups on the ring, specifically at the pyrrole nitrogen atom, less stringent solubility tactics are required for the synthesis, selection and isolation of product derivatives.



Scheme 1.1. Structure of 2,2'-biimidazole (I) and histidine (II).

## 1.2 SIGNIFICANCE OF METAL ION BINDING POLYMER MODEL DEVELOPMENT

The metal binding polymer model design, illustrated in Figure 1.1, incorporates four key elements and how they relate to one another. These four components are: 1) monomer, 2) parent polymer, 3) monomer complex, and 4) polymer complex. The generalized monomer structure can be represented quite easily. The other three key points can have a variety of different architectures due to the nature of the metal and the functionality of the heterocycle. Because of the characteristics of 2,2'-biimidazole and its ability to protonate and deprotonate (diagram of redox pairs of 2,2'-biimidazole given in Scheme 1.2 of different oxidation states), different morphologies of compounds exist.

[8, 9]

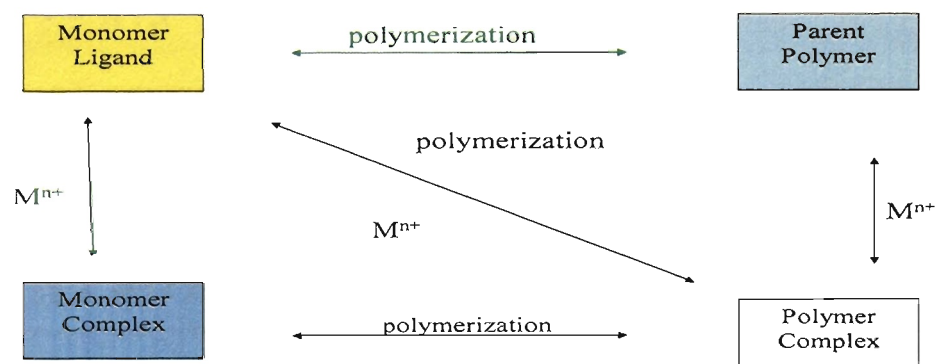
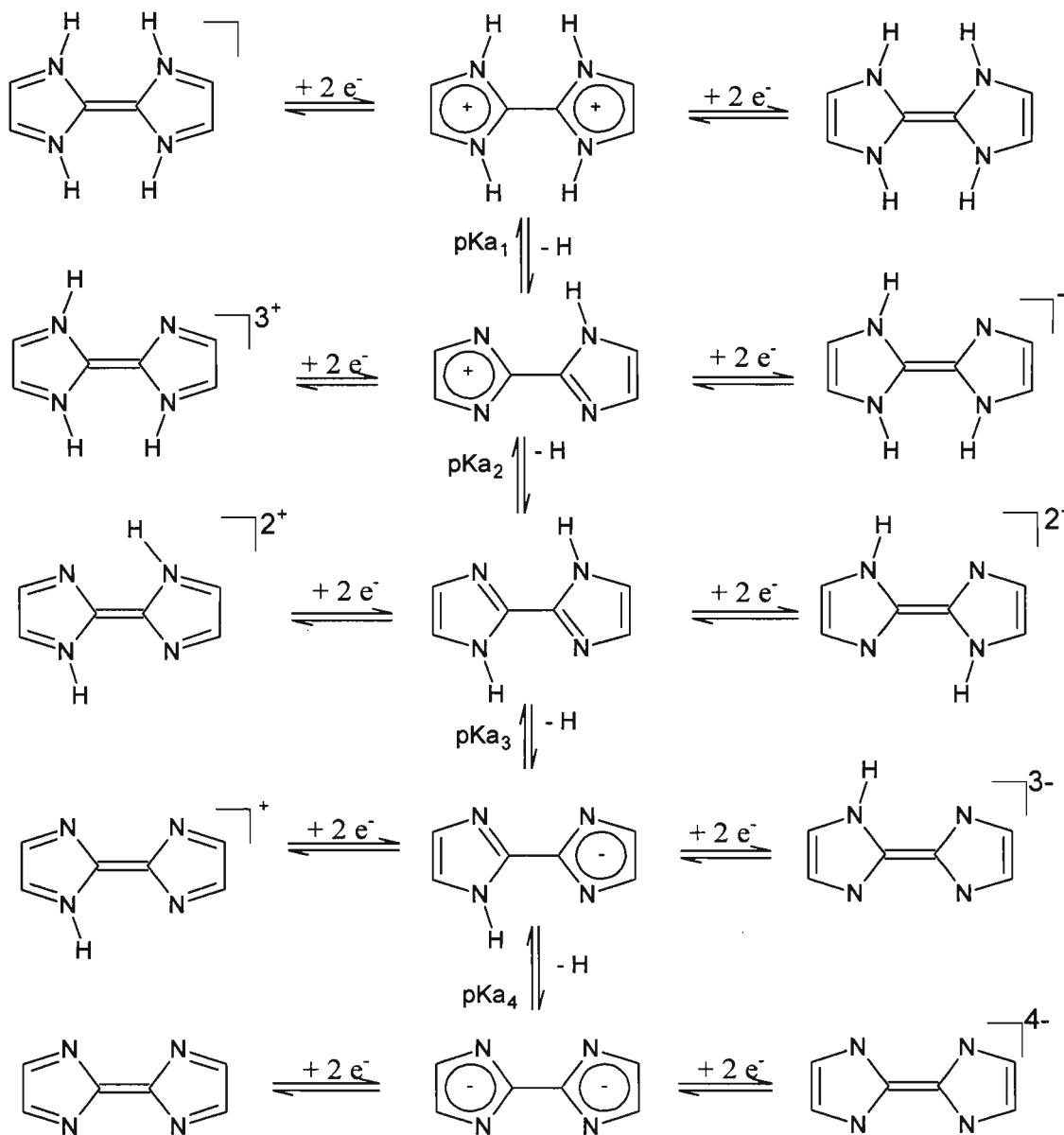


Figure 1.1. Strategic model for 2,2'-biimidazole-based esters.



R	pKa <sub>1</sub>	pKa <sub>2</sub>	pKa <sub>3</sub>	pKa <sub>4</sub>
Me	1.60	6.30	(14.15)	(18.17)
H	(-0.24)	4.60	(12.31)	(16.33)
Cl	(-5.52)	(-0.94)	7.45	11.40
Br	(-5.52)	(-0.94)	7.44	11.50
CN	(-9.68)	(-5.10)	2.99	7.60

( ) = estimated

Scheme 1.2. Protonation and deprotonation of 2,2'-biimidazole with redox pairs and corresponding pKas. [8, 9]

**1.2.1 Specificity.** The ultimate desire of this study is to understand the mechanism of metal binding in a macromolecular system. This understanding encompasses the selectivity of the compound to bind metals, the kinetics of metal binding, and the impact of metal complexation on monomer polymerization pathways. Metals can bind to a compound in one of four ways, illustrated in Figure 1.2, as a (1) pendant; (2) bridging; (3) non-pendant, non-bridging or an (4) associated metal salt.

The ability of 2,2'-biimidazole to protonate and deprotonate as illustrated in Scheme 1.2, results in a *cis* or *trans* effect about the central C2-C2' bond connecting the heterocyclic rings. Scheme 1.3 illustrates the preferred binding coordination of biimidazole with various metals. The size and charge of the metal ion along with the deprotonation and protonation of biimidazole display an interesting architecture in its preferred binding coordination geometry. To study the kinetics of metal ion binding, the resulting complex structure must be known so its formation can be spectroscopically monitored over time. When the biimidazole species is crystallized, a definite coordination compound structure can be established. Prior publications have reported 2,2'-biimidazole metal complexes to reveal heteronuclear metal binding as well as various morphology of homonuclear metal crystals. [10-20]

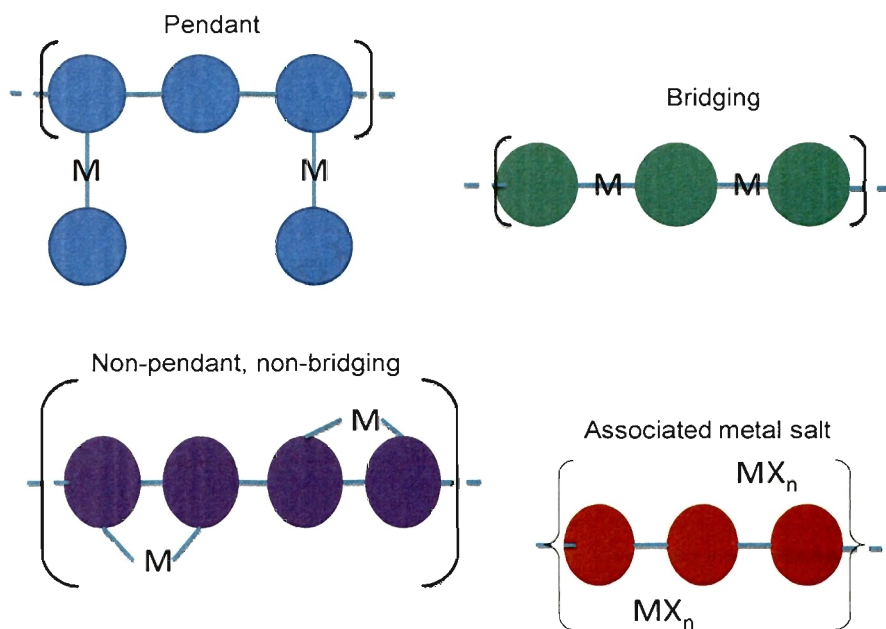
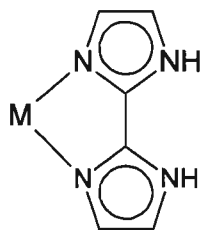
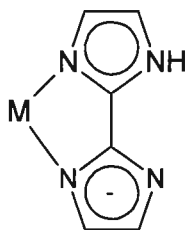


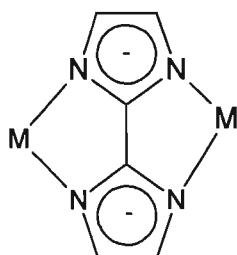
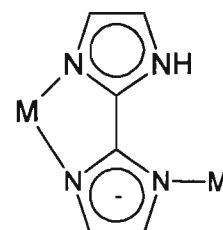
Figure 1.2. Macromolecular ligand-metal-ion binding models.



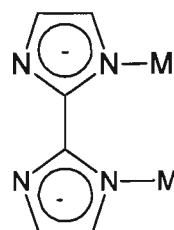
Cu(II), Fe(II), Fe(III), Ni(II),  
Co(II), Rh(I), Cd(II), Mo(II),  
Ru(II), and Au(III)



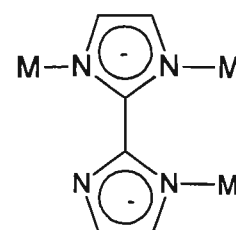
Rh(I)  
Ir(I)



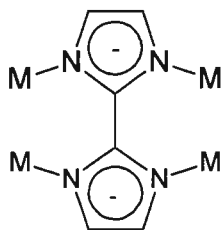
Cu(II), Ni(II), Co(II), Pd(II),  
Mo(II), Ru(II), Ti(III), Mn(II),  
Os(II), Rh(I), Au(III), and Ir(I)



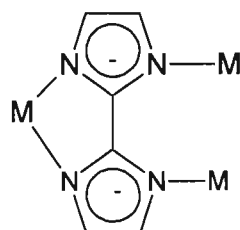
Au(I)



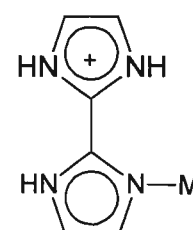
Au(I)



Au(I)



Rh(I), Pd(II), Au(I)



Cd(II), Ag(I)

Scheme 1.3. Metal complexes.



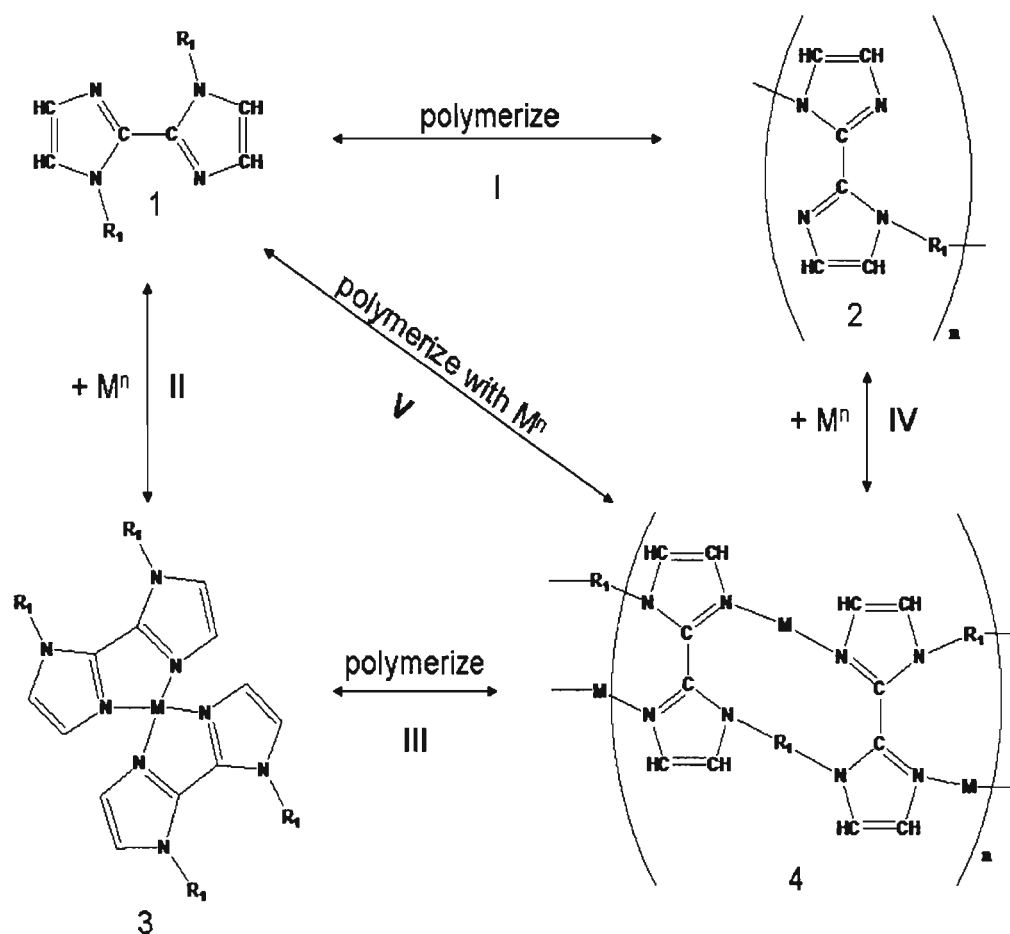
**1.2.2 Equilibrium Process.** The complete macroligand model can be simplified into five equilibrium processes. Each pathway is expressed with a Roman numeral in Scheme 1.3. The five reaction pathways display a generalized equilibrium reaction scheme. Pathway I expresses the polymerization of the starting monomer. Pathway II describes the metal complexation of the starting material. Pathway III illustrates the polymerization of the metal complexed 2,2'-biimidazole derivative. Pathway IV shows the polymer being complexed with a metal. Pathway V shows the monomer and metal ion together in a one-step polymerization process. Although Figure 1.1 is equivalent to Scheme 1.4, Scheme 1.4 is specific in showing 2,2'-biimidazole in a generalized representation.

Metal ion binding with the macroligand systems is expected to occur via equilibrium reactions. With these equilibrium processes, a kinetic study can lead to binding constant determination. Binding constants can then provide information on metal selectivity and role the ligand plays in metal ion binding.

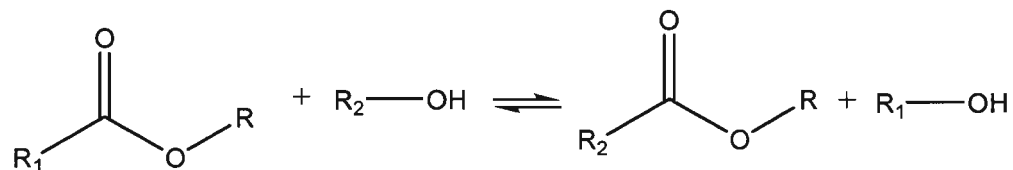
### 1.3 TRANSESTERIFICATION

Synthesis of 1,1'-di(methylacetato)-2,2'-biimidazole (DMAB), 1,1'-di(ethylacetato)-2,2'-biimidazole (DEAB), 1,1'-di(methylpropionato)-2,2'-biimidazole (DMPB), 1,1'-di(ethylpropionato)-2,2'-biimidazole (DEPB), 1,1'-di(methylacrylate)-2,2'-biimidazole (DMA\*B), 1,1'-di(ethylacrylate)-2,2'-biimidazole (DEA\*B), 1-hydroxyethyl-2,2'-biimidazole (mono-HEB), and 1,1'-di(hydroxyethyl)-2,2'-biimidazole (HEB) was the initial step in development of this study. The monomer was polymerized by a condensation process, transesterification, as described in Scheme 1.5. A transesterification reaction involves the reaction of an ester and an alcohol in an acid or

base-catalyzed environment resulting in a different ester and a different alcohol. Or simply stated, transesterification is a double displacement reaction. Acids tend to catalyze the reaction by donating a proton to the carbonyl group whereas bases catalyze the reaction by removing a proton from the alcohol. Since the focus of this study was polymers, the use of difunctional esters and difunctional alcohols provide more opportunity for the desired reaction, resulting in polymeric or at least oligomeric species as illustrated in Scheme 1.6.



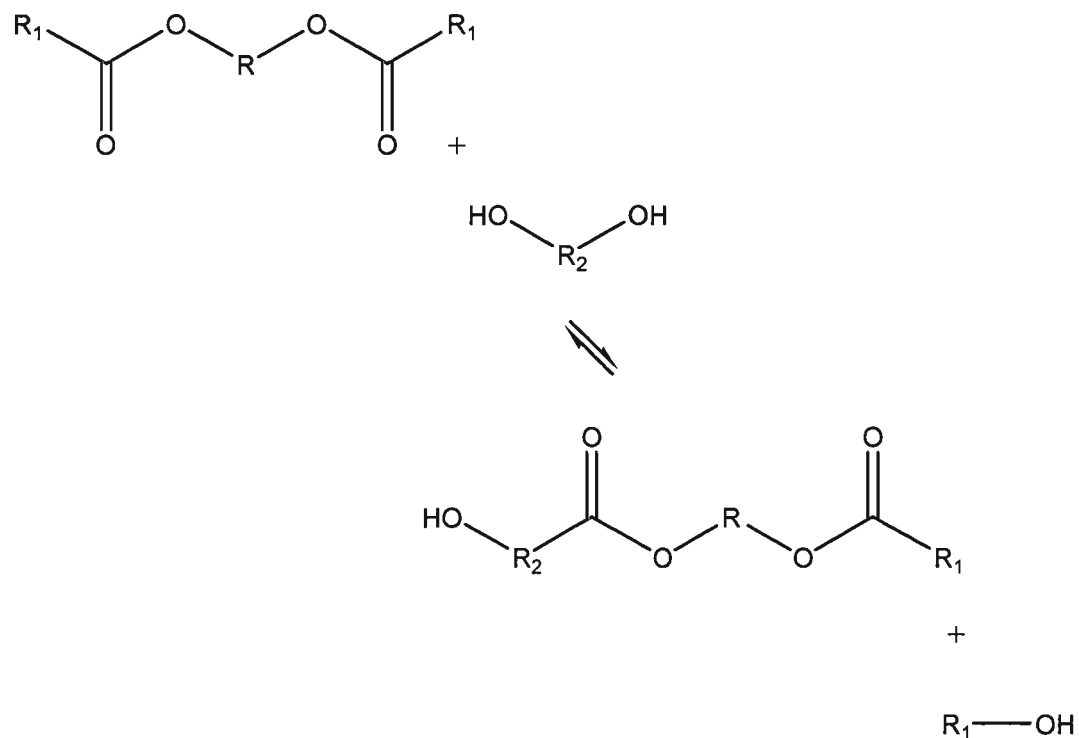
Scheme 1.4. General overview of synthetic pathways of a macromolecular coordination compound with 2,2'-biimidazole moiety.



Scheme 1.5. General transesterification reaction scheme.

Catalysts in transesterification reactions have been used extensively along with applying LeChâtelier's principle of collecting or removing the new alcohol to shift the reaction to the right to increase the yield of the new ester. The search for the perfect catalysts has been studied at length especially in the petroleum industry, particularly biodiesels, and with regard to green chemistry. General examples of catalysts are acids, alkaline metal hydroxides, alkoxides, carbonates, and enzymes. Schuchardt *et al.* used non-ionic bases such as amines, amidines, guanidines, and triamino(imino) phosphoranes. [21] Xiang *et al.* reported using a distannoxane catalyst in perfluorohexanes. [22] Additionally, Xiang lists four practical requirements for an ultimate transesterification reaction. These four requirements are 1) having the ester and alcohol reactants in a 1:1 ratio, 2) selecting a neutral catalyst that will readily separate from the reaction mixture, 3) being able to remove the liberated alcohol with no special technology, and 4) producing a yield and conversion rate of 100 %. [22]

Limited solubility is an issue when using 2,2'-biimidazole as a reactant. Most synthetic procedures call for use of dimethylformamide, DMF, and heat to solubilize 2,2'-biimidazole. The use of DMF in the reaction mixture makes isolation of the product unusually difficult when removing the solvent due to its high boiling point, which is due to its polarity.



Scheme 1.6. Transesterification reaction using diester and diol.

The reaction of metal salts with the 2,2'-biimidazole monomer and its diester and diol derivatives have been analyzed. This required the selection of a soluble 2,2'-biimidazole monomer that would allow the incorporation of the 2,2'-biimidazole moiety in the polymeric species.

## 2 2,2'-BIIMIDAZOLE

### 2.1 HISTORY OF 2,2'-BIIMIDAZOLE

First synthesized by Debus in 1858, the low yield preparation of 2,2'-biimidazole resulted from the mixing of equal volumes of glyoxal and ammonia. [1] Although there have been many reports to increase the yield up to 86% by modifying starting material [23-27], the procedure of mixing glyoxal with ammonia is simple. Yet, its purification to result in crystalline product remains tedious. In 1987, Cromer *et al.* reported on the crystal structure of 2,2'-biimidazole with a residual R-factor of 5.4% where the five atoms of the heterocycle were coplanar within 0.002 Å but the two rings had a dihedral angle of about 4.6° and a monoclinic  $P2_1/c$  space group. [7]

Applications of 2,2'-bimidazole run the gamut of increasing chemical and structural features utilization. The most logical avenues for applications are biological, since 2,2'-biimidazole contains the functionality of the amino acid histidine, but other applications include structural and electronic features all the way to its use to impart wrinkle-resistance to fabrics. [28-30]

The interest in biological-related investigations is due in large part to the correlation in structure to the amino acid histidine, formally named 2-amino-3-(3H-imidazol-4-yl)propanoic acid having D and L conformations. Derivatives of 2,2'-biimidazole have been sought for biologically specific treatments such as antiprotozoal [2, 31, 32], antibacterial and antiparasitic [33], cardiotonics [3] and antihypersensitives [4, 34], antimestatic and antitumor [35, 36], and antihistaminic [37] applications. Derivatives of 2,2'-biimidazole have even been found to retard the germination of barley [38] and to also have moderate herbicidal activity [39].

Noting the conjugation of 2,2'-biimidazole, interest in the investigation of charge transfer and proton transfer have also been studied. These properties [40] have been used in applications such as electroless copper plating [28], conducting film supports to assist in the electrostatograph film process [41], anisotropic conductor [42], along with photopolymerization processes as initiators [43-47]. In the case of a quinone-biimidazole hybrid, it was used for a dual response product as a leuco dye. [48] Hexaarylbiimidazole is used as a photoinitiator when combined with a leuco dye, commercial Dylux<sup>®</sup> from DuPont, producing instantly accessible colored images upon exposure to UV radiation [49].

Metal chelation and polymerization of 2,2'-biimidazole and its derivatives have also been studied. Polymerization research [50-52] has focused on methods to enhance the characteristics of the polymer through the incorporation of the heterocycles; and on the use of substituents on the rings in order to increase solubility. Another property which makes 2,2'-biimidazole significant is that since it can chelate metals [53-70], the addition of metal salts may also lead to a direct polymeric species [71-73]. This has conveniently led to some crystal engineering [10, 13, 15, 74-80]. Even with oligomeric species, this in turn has also led to macrocycles [81] and template effect [82] metal ion complex studies. Furthermore, its use in catalysis, as in the preparation of monacyl phosphine oxide [83], has been reported.

Information gained in a number of studies show the exact positioning of 2,2'-biimidazole and whether the rings remain planar in addition to *cis* or *trans* coordination about the C2-C2' bond connecting the imidazole rings. This insight can dramatically aid in template effects for constructing macrocyclic complexes along with crystal

engineering. In the case of a hydrothermal reaction resulting in a polymeric cadmium 2,2'-biimidazole species, the resulting crystal structure describes a right and left-helical three dimensional polymer [84].

Of the ten crystal structures [7, 85-91] three are of 2,2'-biimidazole, five are singly protonated, and two are doubly protonated. These crystals result in space groups of P-1, C2/m and P2<sub>1</sub> with additional properties. Results of these crystal structure determinations have been compiled in Table 2.1.

In the case of a diprotonated species, Belanger and Beauchamp reported an isolation by-product of rhenium(V)-oxo species with 2,2'-biimidazole. [91] They reported a dicationic species countered by chloride with the monoclinic space group C2/m having with  $a=9.500(2)$  Å,  $b=10.031(3)$  Å,  $c=4.910(2)$  Å,  $\beta=97.40(2)^\circ$ ,  $V=464.0(3)$  Å<sup>3</sup>, and  $Z=2$ . [91] Comparing geometries reported by Cromer [7] and Belanger and Beauchamp [91] protonation induces large variations in the geometry of 2,2'-biimidazole. The ring angle at the protonation site increases by  $3.7^\circ$ , the adjacent angles decrease by  $2.7^\circ$  and  $3.1^\circ$  while the remote angles undergo small increases of  $1.4^\circ$  and  $0.7^\circ$  in order to keep the ring planar.

Electrochemistry was used to determine the molar absorptivity of protonated radical of 2,2'-biimidazole by Lemke *et al.* [94] Although this species is stable during the reduction process, the neutral species generated by further reduction undergoes a subsequent unknown reaction in which an absorption spectrum cannot be recorded. [94] The potentials during a five minute reduction were listed as 0.0V, -1.10V, 1.15V, and 1.20V against a standard calomel electrode. [94]

Table 2.1. Crystal Structures of 2,2'-Biimidazole and Protonated 2,2'-Biimidazole

Compound	Space group and residual R-factor, (%)	Density (g/cm <sup>3</sup> ) counter ions	Ref
2,2'-biimidazole	P2 <sub>1</sub> /c 5.54	1.454 None	[7]
Tris(2,2'-bi-1H-imidazole) bis(2-(2-1H-imidazolyl)-1H-imidazolium) bis(iodide)	P2 <sub>1</sub> 5.28	1.68 Iodide	[85]
Bis(2-(2-1H-imidazolyl)-1H-imidazolium) bis(7,7,8,8-tetracyanoquinodimethane radical) 7,7,8,8-tetracyanoquinodimethane	P-1 8.38	1.408 7,7,8,8-tetracyanoquino- dimethane	[85]
Tris(2,2'-bi-1H-imidazole) bis(2-(2-1H-imidazolyl)-1H-imidazolium) bis(iodide)	P2 <sub>1</sub> /a 0	1.68 Iodide	[86]
2,2'-biimidazol-1-ium trichloroacetate	P2 <sub>1</sub> /c 5.54	1.679 Trichloroacetate	[87]
2-(2-1H-imidazolyl)-imidazolium chloride monohydrate	C2/m 5.04	1.427 chloride, water	[88]
2-(2-1H-imidazolyl)-1H-imidazolium chloride 4-aminobenzoic acid solvate	P2 <sub>1</sub> /n 4.26	1.433 chloride, 4-aminobenzoic acid	[89]
Bis(2,2'-bi-imidazol-1-ium) tetrachloro-iron(III)chloride	P2 <sub>1</sub> /c 8.5	1.692 tetrachloroferrate(III)	[90]
2,2'-bis(1H-imidazolium) dichloride	C2/m 4.3	1.482 Chloride	[91]
2,2'-bis(1H-imidazolium) dinitrate	P2 <sub>1</sub> 2 <sub>1</sub> 2 6.34	1.630 Nitrate	[92]
2-(1H-imidazol-2-yl)-1H-imidazol-3-ium nitrate	C2/c 4.66	1.498 Nitrate	[93]
2,2'-bis(1H-imidazolium) dibromide	P2 <sub>1</sub> /c 3.88	2.038 Bromide	[93]



In the case of dianionic 2,2'-biimidazole, specifically the ruthenium silver complex reported by Majumdar *et al.*, the biimidazolate chelates as a Type II tridentate bridge exhibiting low pKa values. [95, 96] When studying hybrid inorganic-organic materials, 2,2'-biimidazole and its monoanionic moiety have the ability to coordinate to metal centers and act as a donor in hydrogen bonding interactions. Metal centers, particularly  $\text{Co}^{2+}$  and  $\text{Ni}^{2+}$ , allow the formation of a distorted octahedral coordination environment with four nitrogen atoms of two  $\text{H}_2\text{biim}$  ligands arranged *trans* to each other, where water molecules help to maintain the 2D assembly. [97]

The significance of persistent carbocations has been well documented by Olah [98], whose research noted that without the realization of extremely strong superacids, the cationic species was a mere intermediate and not stable. In the case of organic dications, Lammertsma *et al.* [99] used mass spectrometry and computational studies to determine salient bonding features in small doubly-charged organic cations. The crystal structure of bis(1H-imidazolium) dinitrate illustrates the creation of a persistent 1,2-carbocation normally formed by superacids. [99]

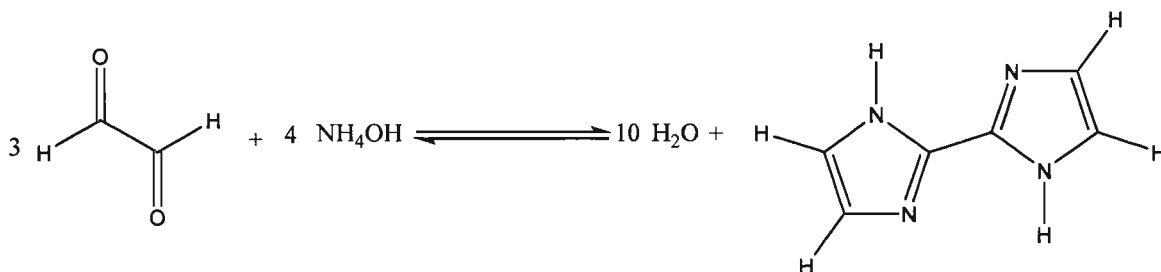
There are unusual and fascinating properties of monometallic transition metal complexes of 2,2'-biimidazole whereby oligomeric and polymeric species are formed. These occur due to the ability of 2,2'-biimidazole and its derivatives ability to enter into various modes of coordination. Fu *et al.* report on achiral 2,2'-biimidazole as having three characteristics: (1) coordination in the neutral form as bidentate, single anionic form as tridentate, and dianionic form as tetradentate; (2) twisting along the C2-C2' bond, particularly in the singly anionic form, shows higher prospects for helical structures; and (3) the nitrogen atoms tend to coordinate with metal ions leading to a five-membered ring

that can help to stabilize the metal-imino units. [84] Kamar *et al.* state the dianion base is bis-bidentate, however, it can also act as a bridge, allowing three metal centers to simultaneously attach, thus providing a platform for design and construction of polymetallic systems with unusual structural features. [100] In the case of the reaction between 2,2'-biimidazole and  $\text{Cu}_2\text{Cl}$ , a polymeric compound results with a *cis* conformation. [73] The bond distances were in agreement with that of Cromer *et al.* [7]; however, the interest lies in the manner in which the free ligand crystallizes [73]. The free ligand crystallizes in the *trans* conformation whereas the  $\text{H}_2\text{biim}$  ligand takes a *cis* conformation. [72] The dihedral angle also changes from *trans* ( $4.6^\circ$ ) to *cis* ( $2.3(4)^\circ$ ). [73]

## 2.2 SYNTHESIS OF 2,2'-BIIMIDAZOLE

Equal volumes, 1000 mL of ammonium hydroxide (28%  $\text{NH}_3$  by weight) and 1000 mL glyoxal, were poured into and mixed in a 5-gallon plastic bucket, adding ice and stirring while in the hood. Scheme 2.1 denotes the reaction scheme of the synthesis of 2,2'-biimidazole using ammonium hydroxide. Vigorous bubbling was observed along with a strong smell of ammonia and evolution of large amounts of heat. The precipitate was recovered by suction filtration and rinsed with distilled water three times. This product was light tan in color and fluffy in appearance. For a crystalline product, the fluffy product was placed in a 5-gallon plastic bucket along with distilled water. A steam coil was placed in the plastic bucket to allow the solution to boil. After boiling for approximately 30 minutes, a siphon tube was set up to extract the solution from the plastic steam bucket to another 5-gallon plastic bucket passing through funnel with a filter. This allowed the solubilized product to pass through the filter. The precipitate in

the filter was returned to the 5-gallon plastic steam bucket and heated in distilled water. Upon cooling, crystals were formed. These crystals were collected by gravity filtration and allowed to air dry. The crystalline product was dissolved in the plastic steam bucket and recrystallized by repeating the boiling, siphoning, and cooling process. The crystals were collected via gravity filtration and dried in an oven overnight.



Scheme 2.1. Reaction scheme for the synthesis of 2,2'-biimidazole.

Although improvements in the synthesis of 2,2'-biimidazole by changing the reactants were discussed earlier on page 12, using the less expensive glyoxal and ammonium hydroxide, a yield of 3.14% was obtained. Elemental analysis resulted in: 53.41 % C, 3.87 % H, 41.29 % N (theoretical 53.72 % C, 4.51 % H, 41.77 % N). FTIR confirmed peaks at: 3390  $\text{cm}^{-1}$  (N-H stretch); 3100  $\text{cm}^{-1}$  (C-H stretch); 3000  $\text{cm}^{-1}$  (Ar-H stretch); 2850, 2800  $\text{cm}^{-1}$  (C-H stretch); 1550, 1450  $\text{cm}^{-1}$  (N-H bend), 1100  $\text{cm}^{-1}$  (C-N bend). The IR was prepared as a KBr pellet and the spectrum is located in Appendix A.

### 2.3 SYNTHESIS OF 2,2-BIS(1H-IMIDAZOLIUM) DINITRATE

The synthesis of 2,2'-bis(1H-imidazolium) dinitrate was accomplished using 2,2'-biimidazole, silver nitrate, and nitric acid as reactants. The 2,2'-biimidazole was prepared according to published procedures [1], using equal portions of 40% glyoxal and

concentrated ammonium hydroxide (28-30%). Silver nitrate was used as received from Aldrich and concentrated nitric acid was diluted to 0.1 M.

The crystal growth of  $[\text{H}_2\text{biim}][\text{NO}_3]_2$  was achieved by the synthetic procedure reported by Hester *et al.* [71], using 0.1 M  $\text{HNO}_3$ . A mass of 1.343 g ( $1.001 \times 10^{-2}$  mol) 2,2'-biimidazole was dissolved in 15 mL of 0.1 M  $\text{HNO}_3$ . Silver nitrate (3.410 g,  $2.007 \times 10^{-2}$  mol) was then added to the solution as a solid. A precipitate formed upon mixing, and a few drops of 0.1 M  $\text{HNO}_3$  were added to resolubilize the precipitate. Golden crystals formed as the solution was allowed to slowly dry/evaporate over a period of several days.

Crystal structure determination of  $[\text{H}_2\text{biim}][\text{NO}_3]_2$  and collection and reduction of X-ray data was completed in the usual manner. Diffraction intensity data were collected with a Bruker Smart Apex I CCD diffractometer. The space group was determined from systematic absences. The structures were solved by direct methods and Fourier difference syntheses and refined by full-matrix least-squares procedures on peak intensities ( $F^2$ ). All non-hydrogen atoms were refined anisotropically. Hydrogen atoms were inserted in their calculated positions. Software and atomic scattering factors are contained in the SHELXTL program package [101].

The crystal structure has an orthorhombic  $P2_12_12$  space group. The five-membered rings are not exactly planar. The five atoms of one ring are out the plane by  $0.3\text{\AA}$  and the other ring by  $0.5\text{\AA}$ . These five member rings have a dihedral angle of  $30.5^\circ$ . The shortest distance from the oxygen on a nitrate to the nitrogen in the five-member ring is  $3.184\text{\AA}$ . The nitrate symmetry can be seen down the c-axis in Figure 2.4.

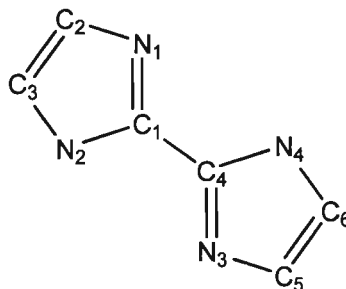
Comparing this structure to that of the monoclinic C2/m 2,2'-bis(1H-imidazolium) dichloride by Bélanger and Beauchamp [91], the imidazole rings are not as planar with respect to each other; the rings are only out of plane by 0.002Å and the chloride ions are out of plane by 0.42(6)Å. Noting the stabilizing influence of the counter ion and hydrogen bonding, the distance between the Cl···H-N is 3.067(2)Å, which is comparable to the O···H-N distance of 3.184Å. [91] However, the dibrominated species analyzed by Baughman [93] shows a similar trend with a fairly planar biimidazole. The dibrominated species crystallized in a P2<sub>1</sub>/c space group where the imidazole rings are rotated by about 0.34°. Bond lengths were comparable amongst the charged species and are listed in Table 2.2 using Scheme 2.2 for atom positions. Figure 2.1 illustrates the comparison of the diprotonated biimidazole species with bromide and chloride counter ions.

The Baughman group resolved a monoprotonated 2,2'-biimidazole species with a single nitrate counter ion along with a diprotonated 2,2'-biimidazole species with two nitrates. [93] Table 2.2 compiles select bond lengths and angles and Figure 2.2 illustrates the monoprotonated and diprotonated biimidazole species with the nitrate counter ions. The monoprotonated species crystallized in a monoclinic C2/c space group, whereas, the diprotonated species crystallized in an orthorhombic P2<sub>1</sub>2<sub>1</sub>2 space group. While the five-member rings for the monoprotonated 2,2'-biimidazole were rotated about 40.5°, the imidazole rings of the dicationic 2,2'-biimidazole species were rotated 30.4°.

Figure 2.3 displays the OR TEP diagram of 2,2'-bis(1H-imidazolium) dinitrate while Figure 2.4 presents the unit cell. Figure 2.7 allows an interesting view for symmetry elements. Details of the crystal data for [H<sub>2</sub>biim][NO<sub>3</sub>]<sub>2</sub> are provided in

Appendix B Table B.1. The absolute structure parameter listed for  $[\text{H}_2\text{biim}][\text{NO}_3]_2$  of 0.7(18) is not within the acceptable value of three standard deviations and warrants a matrix transformation. If the inversion does not allow the absolute structure parameter to converge to zero, the structure should be refined as a racemic twin. The atomic coordinates and equivalent isotropic displacement parameters are listed in Table B.2. The observed bond lengths, angles, and contacts are listed in Table B.3. Listed in Table B.4 are anisotropic displacement parameters. Table B.5 displays the hydrogen atoms along with isotropic displacement parameters.

See Appendix C, Figures C.1 and C.2 for graphs of proton and carbon NMR spectra in DMSO- $d_6$ :  $^1\text{H}$  NMR (theoretical) in DMSO,  $d_6$ :  $\delta$ 7.50, s ( $\delta$ 7.1, s) [C-H];  $\delta$ 8.44, broad ( $\delta$ 13.4, s) [N-H];  $^{13}\text{C}$  NMR (theoretical) in DMSO,  $d_6$ :  $\delta$ 39.5, m ( $\delta$ 127.8) [C-H]; ( $\delta$ 135.4) [C-C].

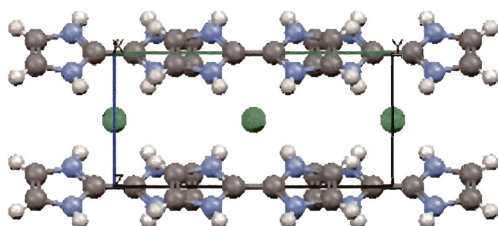


Scheme 2.2. Diagram of 2,2'-biimidazole for bond lengths.

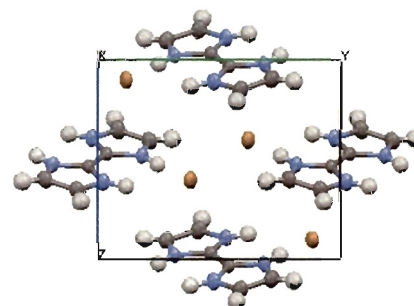
Table 2.2. Selected Bond Lengths for Protonated 2,2'-Biimidazole

Bond	2-(1H-imidazol-2-yl)-1H-imidazol-3-ium nitrate [93]	2,2'-bi(1H-imidazolium) dinitrate [92]	2,2'-bi(1H-imidazolium) dibromide [93]	2,2'-bi(1H-imidazolium) dichloride [91]
	Bond length, Å	Bond length, Å	Bond length, Å	Bond length, Å
C1-C4	1.44(1)	1.45(1)	1.43(3)	1.44(2)
C1-N1	1.33(0)	1.31(5)	1.31(9)	1.32(8)
C1-N2	1.32(7)	1.33(1)	1.34(2)	1.36(6)
N1-C2	1.36(3)	1.38(0)	1.37(2)	1.32(8)
N2-C3	1.36(3)	1.36(8)	1.37(7)	1.36(6)
C2-C3	1.34(4)	1.32(2)	1.34(6)	1.33(8)

## Diprotonated 2,2'-biimidazole



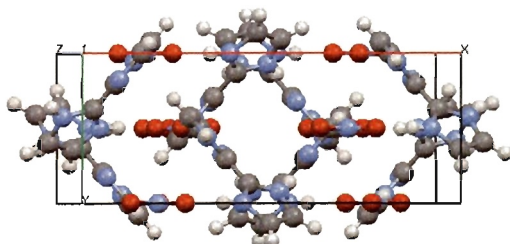
Bromide counter ion



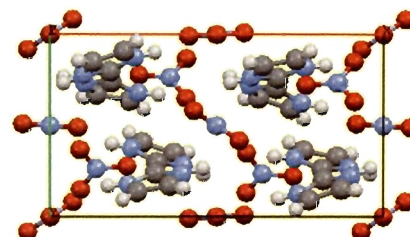
Chloride counter ion

Figure 2.1. Diprotonated 2,2'-biimidazole with bromide and chloride counter ions from the x-y plane.

## Nitrate Counter Ion



Monoprotonated



Diprotonated

Figure 2.2. Protonated 2,2'-biimidazole with nitrate counter ions.



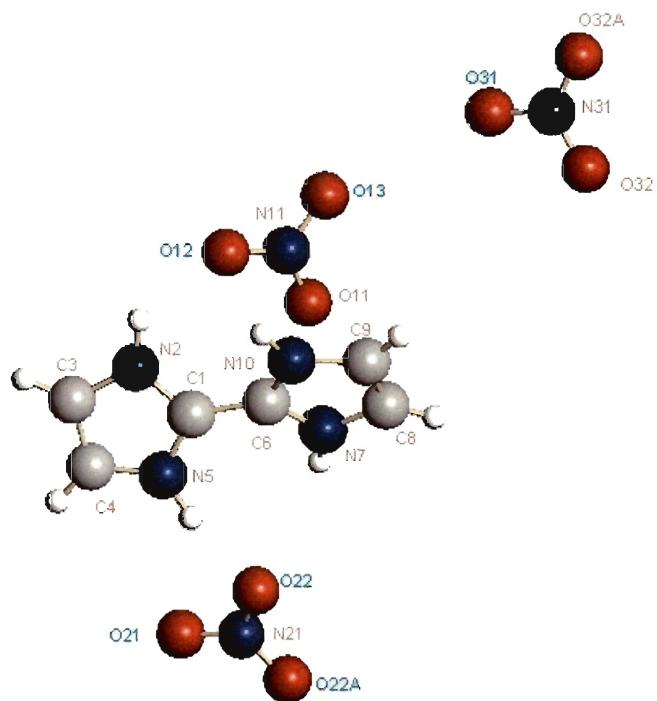


Figure 2.3. Asymmetric unit of [bimH<sub>2</sub>][NO<sub>3</sub>]<sub>2</sub>.

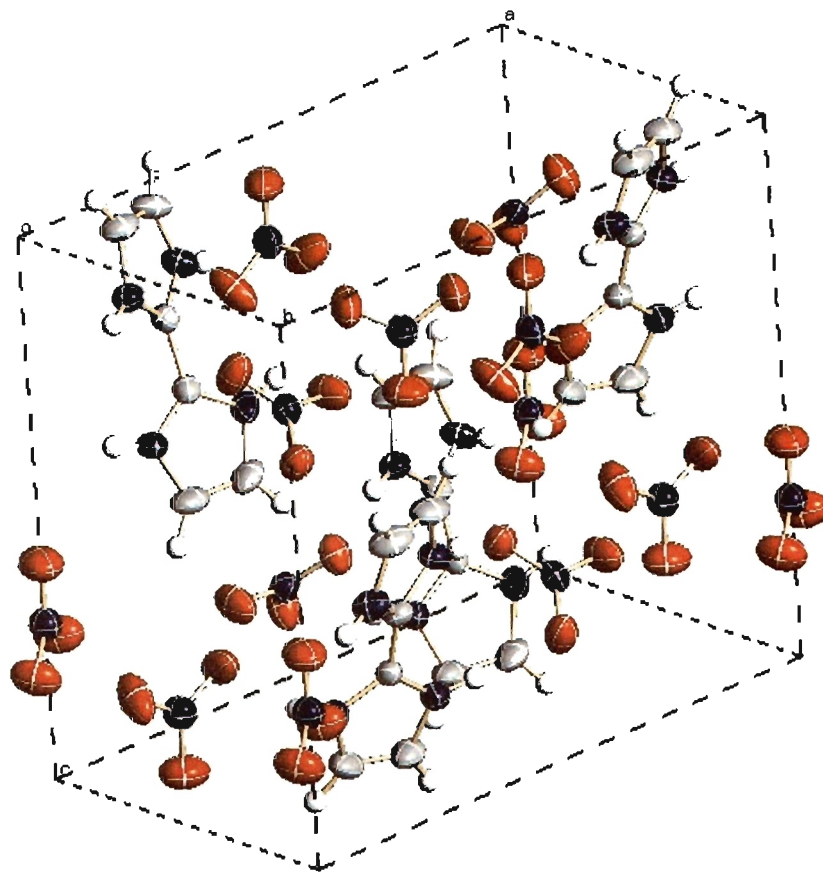


Figure 2.4. Unit cell of 2,2'-bis(1H-imidazolium) dinitrate.

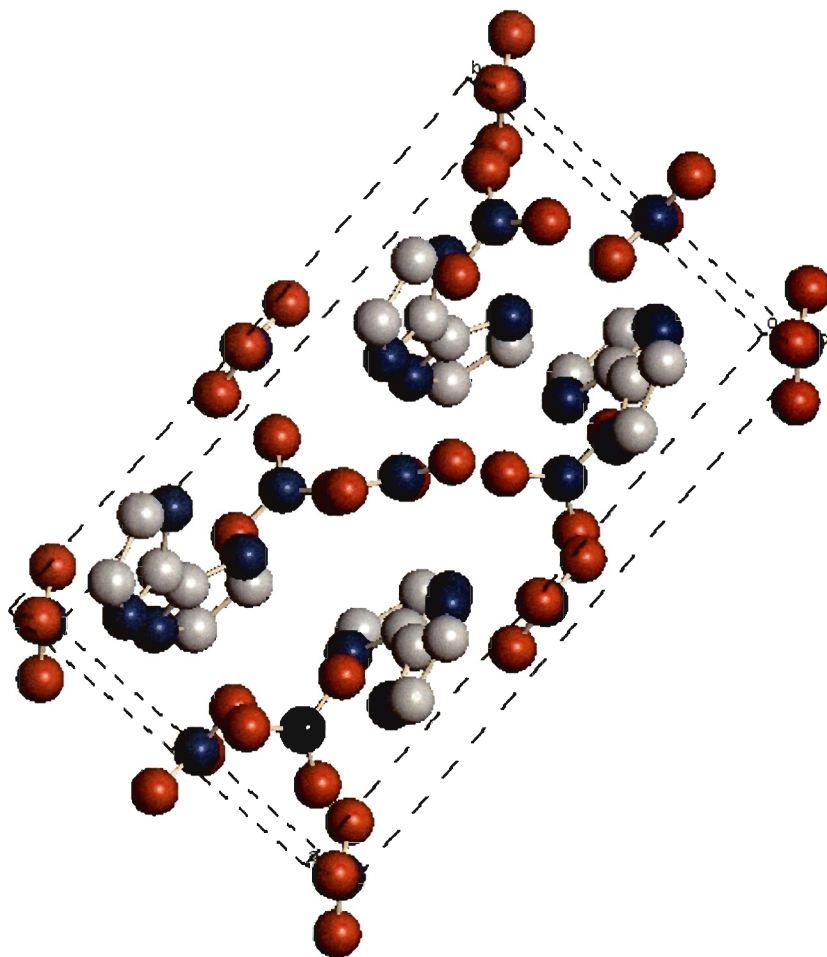


Figure 2.5. Unit cell of 2,2'-bis(1H-imidazolium) dinitrate.

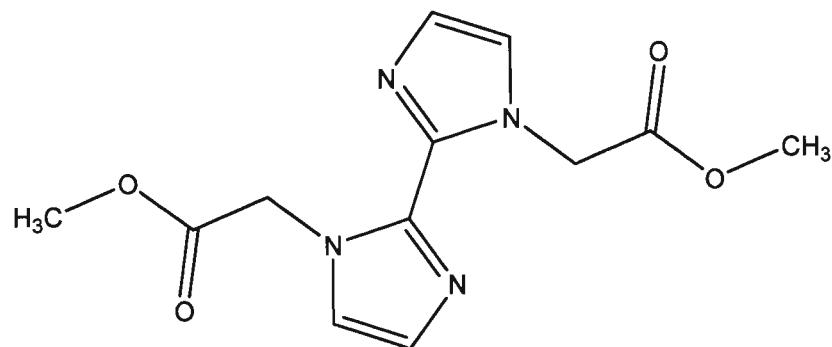
## 2.4 2,2'-BIIMIDAZOLE ESTER DERIVATIVES

Derivatives of 2,2'-biimidazole have been made to accommodate a variety of different chemical and physical properties of 2,2'-biimidazole, most notably its solubility. In making derivatives of specific functionality, routes to form polymeric species with metal complexation ability became a focus of study. Methyl derivatives studied by Deady [102] investigated the substituent effect on the heterocycle. Rasmussen *et al.* [103] synthesized tetracyano derivatives, described as colorless, and reported the derivatives were usually dianionic and readily chelated as a bidentate ligand or

quadridentate bridging ligand between pairs of metal ions. The Collier research group [104-108] has published syntheses and characterizations of difunctional ester derivatives noting their ability as a macromolecular precursor [107].

**2.4.1 Previously reported 1,1'-diesters of 2,2'-biimidazole.** The diesters previously reported include 1,1'-di(methylacetato)-2,2'-biimidazole [104, 107], 1,1'-di(methylpropionato)-2,2'-biimidazole [106, 108, 109], 1,1'-di(ethylpropionato)-2,2'-biimidazole [104, 105], and 1,1'-di(ethylacrylate)-2,2'-biimidazole [106, 108, 109].

**2.4.1.1 1,1'-Di(methylacetato)-2,2'-Biimidazole, DMAB.** Synthesis of 1,1'-di(methylacetato)-2,2'-biimidazole, dimethyl 2,2'-(2,2'-bi(1H-imidazole)-1,1'-diyl)diacetate, structural drawing given in Scheme 2.3, was performed using the technique reported by Barnett *et al.* whereby a multi-step process was employed adding the ligand in two separate steps of one equivalent portions to 2,2'-biimidazole. [104] Following Barnett's procedure, a mass of 12.696 g 2,2'-biimidazole ( $9.475 \times 10^{-2}$  mol) was added to a 1000 mL round bottom flask equipped with a condenser, 700 mL DMF, and a magnetic stir bar. The mixture was heated to 50°C, then 18.0 mL 6 M NaOH (0.108 mol) was added. While the solution continued to be heated, 9.0 mL methyl monochloroacetate (0.102 mol) was added. As the solution continued to be heated, it turned dark green. The solution was heated for an additional 30 minutes, then 14.0 mL 6 M NaOH (0.084 mol) was added. The solution was heated an additional 20 minutes before adding an equivalent of methyl monochloroacetate, 8.0 mL (0.090 mol). The solution was heated and stirred for 2 hours.



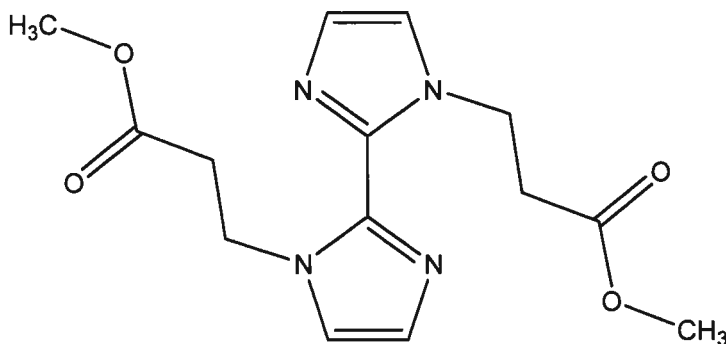
Scheme 2.3. Structure of 1,1'-di(methylacetato)-2,2'-biimidazole.

The reaction mixture was then vacuum distilled to remove DMF. Approximately 500 mL of refluxing acetone was added and then the product was rotoevaporated to dryness. The product was cooled and washed with a small amount of methanol. The product was recrystallized in 300 mL methanol to yield 9%.

The FTIR spectrum of the product confirmed synthesis of 1,1'-di(methylacetato)-2,2'-biimidazole, dimethyl 2,2'-(2,2'-bi(1H-imidazole)-1,1'-diyl)diacetate with peaks at: 3480, 3150  $\text{cm}^{-1}$  (N-H stretch); 3100  $\text{cm}^{-1}$  (C-H stretch); 3000  $\text{cm}^{-1}$  (Ar-H stretch); 2900, 2800  $\text{cm}^{-1}$  (C-H stretch); 1620  $\text{cm}^{-1}$  (C=O stretch); 1600  $\text{cm}^{-1}$  (C=N stretch); 1400  $\text{cm}^{-1}$  (C-H bend); 1125  $\text{cm}^{-1}$  (C-O stretch). The IR was prepared as a KBr pellet and the spectrum is given in Appendix A. Barnett *et al.* previously reported the crystal structure of DMAB, dimethyl 2,2'-(2,2'-bi(1H-imidazole)-1,1'-diyl)diacetate synthesized by this method. [107]

**2.4.1.2 1,1'-Di(methylpropionato)-2,2'-Biimidazole, DMPB.** Synthesis of 1,1'-di(methylpropionato)-2,2'-biimidazole, dimethyl 3,3'-(2,2'-bi(1H-imidazole)-1,1'-diyl)dipropionate (structural drawing in Scheme 2.4) was performed using the technique reported by He. [106] Using the Michael addition approach by He, a mass of 4.791 g 2,2'-biimidazole ( $3.575 \times 10^{-2}$  mol) was added to a 50 mL round bottom flask containing

10.0 mL DMF, a stir bar, and condenser. The solution was heated at 120°C for 15 minutes. A mass of 0.5 g tetramethylammonium hydroxide pentahydrate ( $5.49 \times 10^{-3}$  mol) was added and the solution was heated an additional 10 minutes. While the solution was being heated, 6.5 mL methyl acrylate ( $7.146 \times 10^{-2}$  mol) was added dropwise.

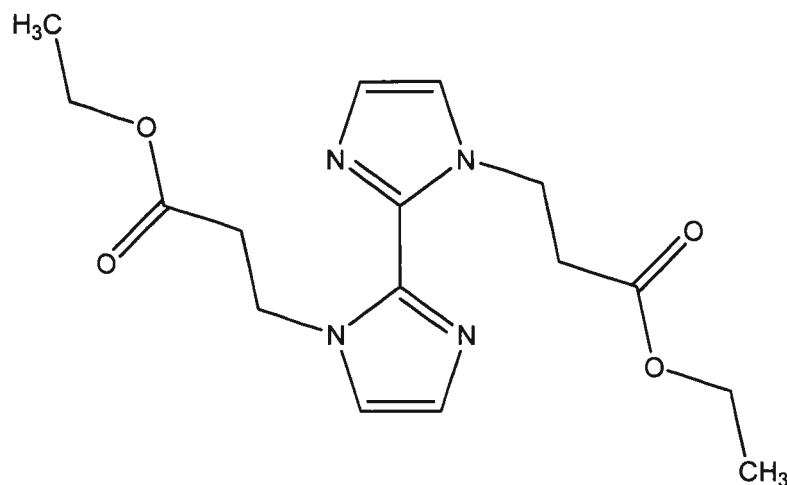


Scheme 2.4. Structure of 1,1'-di(methylpropionato)-2,2'-biimidazole.

The solution was refluxed for 12 hours at 120°C. DMF was vacuum distilled and several drops of distilled water were added. The product was purified by recrystallization in acetone to yield 6.164 g product or 56.3%. The melting point range was 91-93°C. Elemental analysis resulted in 55.11 % C, 5.39 % H, 18.34 % N, 21.16 % O (Theoretical 54.89 % C, 5.92 % H, 18.29 % N, 20.89 % O). The crystal structure of DMPB was previously reported by He. [106]

**2.4.1.3 1,1'-Di(ethylpropionato)-2,2'-Biimidazole, DEPB.** Synthesis of 1,1'-di(ethylpropionato)-2,2'-biimidazole, diethyl 3,3'-(2,2'-bi(1H-imidazole)-1,1'-diyl)dipropionate (structural drawing given in Scheme 2.5), was prepared using a modified technique reported by Barnett *et al.* [105] A mass of 2.818 g 2,2'-biimidazole ( $2.103 \times 10^{-2}$  mol) was added to a 500 mL round bottom flask with a magnetic stir bar

and condenser. A volume of 200 mL DMF was added and the mixture was heated to 50°C. Once the temperature of 50°C was reached, 2.0 mL 1 N NaOH was added. The solution was heated for approximately 20 minutes before the gradual drop-wise addition of 4.6 mL ethyl acrylate ( $4.203 \times 10^{-2}$  mol). The solution was heated for 4 hours and then rotovapped in a hot water bath to remove DMF. It was then filtered and the solution was chilled in an ice bath for approximately 10 minutes. Approximately 10 mL chilled ethanol was added and the product was allowed to crystallize in the refrigerator overnight. The product was recovered using glass frit suction filter and aspirator. This resulted in 2.503 g product with a 35.6% yield and melting point range of 69-70°C. Elemental analysis resulted in 57.44 % C, 5.84 % H, 16.75 % N, 19.97 % O (Theoretical 57.47 % C, 6.63 % H, 16.76 % N, 19.14 % O).

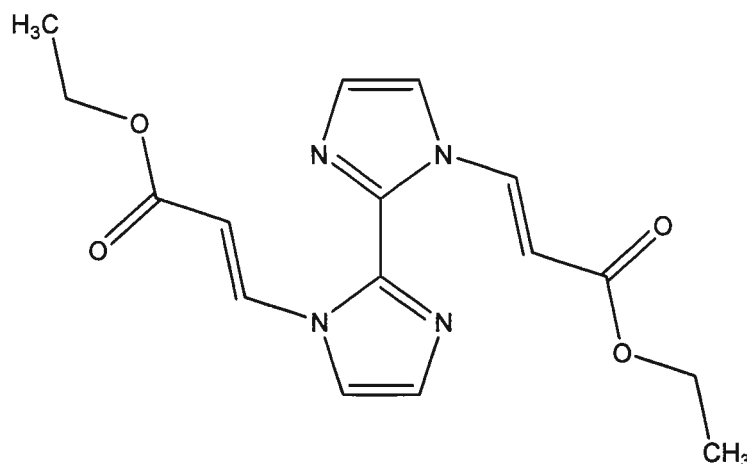


Scheme 2.5. Structure of 1,1'-di(ethylpropionato)-2,2'-biimidazole.

The FTIR spectrum revealed peaks at: 3450, 3140  $\text{cm}^{-1}$  (N-H stretch); 3120  $\text{cm}^{-1}$  (C-H stretch); 2990  $\text{cm}^{-1}$  (Ar-H stretch); 2950, 2900  $\text{cm}^{-1}$  (C-H stretch); 1740  $\text{cm}^{-1}$  (C=O stretch); 1440  $\text{cm}^{-1}$  (C=N stretch); 1375, 1370  $\text{cm}^{-1}$  (C-H bend);

1240  $\text{cm}^{-1}$  (C-O stretch). The IR was prepared as a KBr pellet and the spectrum is located in Appendix A.

**2.4.1.4 1,1'-Di(ethylacrylate)-2,2'-Biimidazole, DEA\*B.** The synthesis of 1,1'-di(ethylacrylate)-2,2'-biimidazole, (2E,2'E)-diethyl 3,3'-(2,2'-bi(1H-imidazole)-1,1'-diyl)diacrylate (structural drawing in Scheme 2.6), was prepared using the technique reported by He. [106] A mass of 2.682 g 2,2'-biimidazole ( $2.001 \times 10^{-2}$  mol) was added to a 25 mL round bottom flask equipped with a stir bar and condenser and containing 10 mL DMF. After the solution was heated to  $100^{\circ}\text{C}$ , 0.800 g tetramethylammonium hydroxide was added. The solution was heated for 20 minutes before a gradual drop-wise addition of 5.2 mL ethyl propiolate ( $5.08 \times 10^{-2}$  mol) over a period of 15 minutes. The solution became homogeneous and dark in color. The solution was heated and refluxed at  $120^{\circ}\text{C}$  for 12 hours. The precipitate was filtered and washed with acetone until the filtrate became clear. An off-yellow powdered product was obtained recrystallized in acetone. The product had a melting point range of  $178\text{-}180^{\circ}\text{C}$  and a 48 % yield. Theoretical composition for this compound: 58.17 % C, 5.49 % H, 16.96 % N, 19.37 % O.

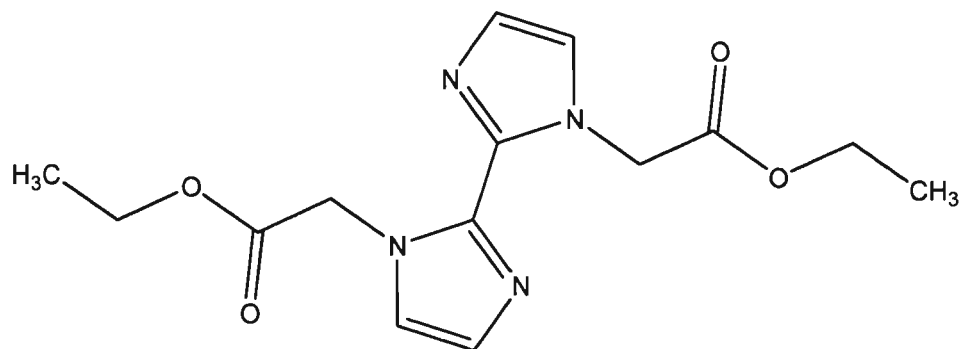


Scheme 2.6. Structure of 1,1'-di(ethylacrylate)-2,2'-biimidazole.

The FTIR spectrum confirmed peaks at: 3400, 3120  $\text{cm}^{-1}$  (N-H stretch); 3100, 3090  $\text{cm}^{-1}$  (C-H stretch); 3000  $\text{cm}^{-1}$  (Ar-H stretch); 2980  $\text{cm}^{-1}$  (C-H stretch); 1740  $\text{cm}^{-1}$  (C=O stretch); 1700  $\text{cm}^{-1}$  (C=C stretch); 1400  $\text{cm}^{-1}$  (C=N stretch); 1350  $\text{cm}^{-1}$  (C-H bend); 1260, 1240  $\text{cm}^{-1}$  (C-O stretch); 1200, 1010  $\text{cm}^{-1}$  (C-O stretch). The IR was prepared as a KBr pellet and the spectrum is located in Appendix A.

**2.4.2 New 2,2'-biimidazole diesters synthesized.** In an effort to have similar linkage, two additional diesters were synthesized and characterized. They are 1,1'-di(ethylacetato)-2,2'-biimidazole and 1,1'-di(methylacrylate)-2,2'-biimidazole.

**2.4.2.1 1,1'-Di(ethylacetato)-2,2'-Biimidazole, DEAB.** The synthesis of 1,1'-di(ethylacetato)-2,2'-biimidazole (DEAB), diethyl 2,2'-(2,2'-bi(1H-imidazole)-1,1'-diyl)diacetate (structural drawing in Scheme 2.7), has not yet been reported. Synthesis of DEAB was performed using a modified technique reported by Barnett *et al.* whereby a multi-step process was used to add ligand in two-one equivalent portions. [104]



Scheme 2.7. Structure of 1,1'-di(ethylacetato)-2,2'-biimidazole.

A mass of 10.295 g 2,2'-biimidazole ( $7.6828 \times 10^{-2}$  mol) was added to a 1000 mL round bottom flask equipped with a condenser, 700 mL DMF, and a magnetic stir bar. The mixture was heated to 50°C, then 13.0 mL 6 M NaOH ( $7.80 \times 10^{-2}$  mol) was added. While the solution continued to be heated, 8.2 mL ethyl monochloroacetate



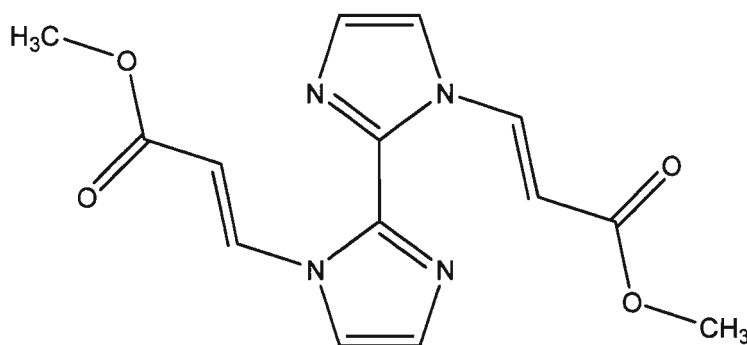
( $7.7 \times 10^{-2}$  mol) was added. As the solution continued to be heated, it turned dark green. The solution was heated for an additional 30 minutes, then 12.6 mL 6 M NaOH ( $7.56 \times 10^{-2}$  mol) was added. The solution was heated an additional 20 minutes before adding an equivalent of ethyl monochloroacetate, 8.2 mL ( $7.7 \times 10^{-2}$  mol). The solution was heated and stirred for 2 hours.

The reaction mixture was then vacuum distilled to remove DMF. Approximately 500 mL of refluxing acetone was added and then the product was rotoevaporated to dryness. The product was cooled and washed with a small amount of methanol. The product was recrystallized in 300 mL methanol to yield 11%.

The FTIR spectrum of the product confirmed synthesis of 1,1'-di(ethylacetato)-2,2'-biimidazole, with peaks at: 3480, 3150  $\text{cm}^{-1}$  (N-H stretch); 3100  $\text{cm}^{-1}$  (C-H stretch); 3000  $\text{cm}^{-1}$  (Ar-H stretch); 2900, 2800  $\text{cm}^{-1}$  (C-H stretch); 1620  $\text{cm}^{-1}$  (C=O stretch); 1600  $\text{cm}^{-1}$  (C=N stretch); 1400  $\text{cm}^{-1}$  (C-H bend); 1125  $\text{cm}^{-1}$  (C-O stretch). The IR was prepared as a KBr pellet and the spectrum is given in Appendix A. Theoretical properties of this compound yield 54.89 % C, 5.92 % H, 18.29 % N, 20.89 % O. Elemental analysis resulted in 55.11 % C, 5.39 % H, 18.34 % N, 21.16 % O.

**2.4.2.2 1,1'-Di(methylacrylate)-2,2'-Biimidazole, DMA\*B.** Synthesis of 1,1'-di(methylacrylate)-2,2'-biimidazole, (2E,2'E)-dimethyl 3,3'-(2,2'-bi(1H-imidazole)-1,1'-diyl)diacrylate (structural drawing in Scheme 2.8), was attempted modifying the procedure of He [106]. A quantity of 2.207 g 2,2'-biimidazole, ( $1.647 \times 10^{-2}$  mol) was added to a round bottom flask containing 15 mL DMF and equipped with a stir bar and condenser. A mass of 1.5 g NaOH ( $3.75 \times 10^{-2}$  mol) was dissolved with a minimal amount of distilled water and added to the 2,2'-biimidazole DMF solution. The solution

was heated to 100°C for about 30 minutes. After this time, 3.5 mL methyl propiolate ( $4.146 \times 10^{-2}$  mol) was added slowly drop-wise. The solution was heated to 120°C and allowed to reflux for 12 hours. A yellow precipitate resulted after gravity filtration. The precipitate was washed in a small amount of acetone and resulted in 3.665 g of an off-yellow powder, 73.61% yield. The product's melting point was 243°C. The theoretical composition for this compound is 55.63 % C, 4.67 % H, 18.53 % N, 21.17 % O, although no elemental analysis was performed.



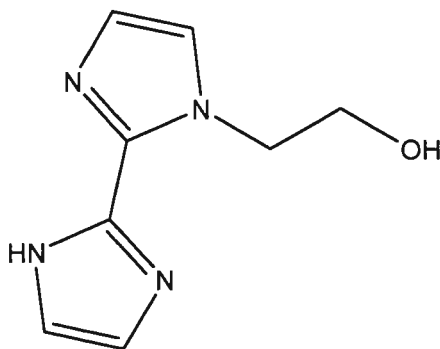
Scheme 2.8. Structure of 1,1'-di(methylacrylate)-2,2'-biimidazole.

## 2.5 ALCOHOLS

In an effort to polymerize the 2,2'-biimidazole moiety, alcohols were needed for the transesterification process. The three alcohols were chosen. Although two of the alcohols contain the 2,2'-biimidazole moiety, the third was chosen for convenience, availability and similar carbon chain length.

**2.5.1 1-Hydroxyethyl-2,2'-Biimidazole, mono-HEB.** Synthesis of 1-hydroxyethyl-2,2'-biimidazole, 2-(2,2'-bi(1H-imidazol)-1-yl)ethanol (structural drawing in Scheme 2.9), was conducted using a modified procedure reported by Lin [110, 111] and Lister [112]. In a 1 L round bottom flask equipped with a stir bar, condenser, and

addition funnel, 11.365 g 2,2'-biimidazole ( $8.481 \times 10^{-2}$  mol) was added to 450 mL of absolute ethanol. The solution was heated to  $80^{\circ}\text{C}$  before the addition of 3.595 g NaOH ( $8.986 \times 10^{-2}$  mol) dissolved in approximately 20 mL of distilled water. The solution was heated at  $80^{\circ}\text{C}$ . The solution turned reddish brown and there were no visible signs of 2,2'-biimidazole. While the solution was heated at  $80^{\circ}\text{C}$ , 6.0 mL 2-chloroethanol ( $8.950 \times 10^{-2}$  mol) suspended in  $\sim 50$  mL absolute ethanol was slowly added drop-wise from the addition funnel. The red solution turned cloudy with a salt like precipitate. The reaction was allowed to proceed for 30 minutes. After which, 3.235 g NaOH ( $8.088 \times 10^{-2}$  mol) dissolved in  $\sim 20$  mL distilled water was added to the flask and allowed to react for 45 minutes. After the 45 minutes, 5.6 mL 2-chloroethanol ( $8.347 \times 10^{-2}$  mol) suspended in 50 mL absolute ethanol was added to the flask via addition funnel. The temperature was maintained at  $80^{\circ}\text{C}$  for 18 hours. The reaction was filtered with fritted funnel.



Scheme 2.9. Structure of 1-hydroxyethyl-2,2'-biimidazole.

The filtrate was rotoevaporated until no other liquid appeared to come off. Approximately 200 mL chloroform was added to the residue. There were particles that did not dissolve completely. The solution was filtered. Distilled water was added to the filtrate and the solution was poured into a separatory funnel. The top aqueous layer was

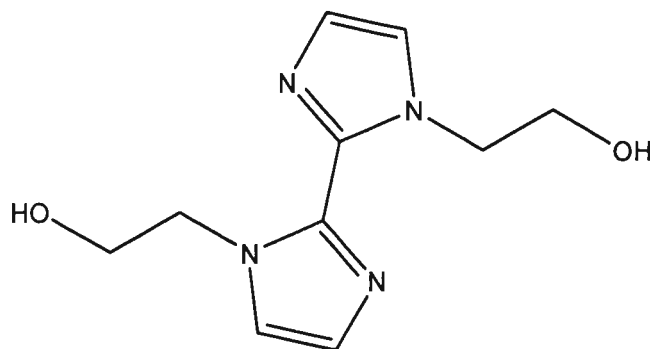
retrieved by pipette and put into the refrigerator. The bottom layer, chloroform portion, was added to ~200 mL hot distilled water. The solution bubbled and some foam formed. This solution was poured into a separatory funnel and allowed to cool at room temperature overnight.

Needles formed in the filtrate left overnight in the refrigerator. A mass of 0.113 g was recovered with a fritted funnel. The solution left in the separatory funnel to cool visually separated. The top portion was again removed by pipette and chilled four hours in a refrigerator. A mass of 0.954 g of product was recovered via fritted funnel.

The crystal structure showing a *trans* configuration of 1-hydroxyethyl-2,2'-biimidazole, 2-(2,2'-bi(1H-imidazol)-1-yl)ethanol was reported by Lin [112]. The product's melting point was measured at 139°C. Elemental analysis resulted in 54.04 % C, 6.63 % H, 26.21 % N, 13.12 % O (Theoretical 53.92 % C, 5.66 % H, 31.44 % N, and 8.98 % O). FTIR spectrum confirmed peaks at: 3370 cm<sup>-1</sup> (O-H stretch); 3130 cm<sup>-1</sup> (N-H stretch); 3125 cm<sup>-1</sup> (Ar-H stretch); 2990, 2940 cm<sup>-1</sup> (C-H stretch); 1700 cm<sup>-1</sup> (C=N stretch); 1550 cm<sup>-1</sup> (N-H bend); 1400 cm<sup>-1</sup> (O-H bend). The IR was prepared as a KBr pellet and the spectrum is located in Appendix A.

**2.5.2 1,1'-Di(hydroxyethyl)-2,2'-Biimidazole, HEB.** The synthesis of 1,1'-di(hydroxyethyl)-2,2'-biimidazole, 2,2'-(2,2'-bi(1H-imidazole)-1,1'-diyl)diethanol (structural drawing in Scheme 2.10), was prepared using a modified technique reported by Lin [111] and Lister [112] and using the exact procedure listed previously for mono-HEB. By using this approach, flash column chromatography was eliminated. In a 1 L round bottom flask equipped with a stir bar, condenser, and addition funnel, 11.365 g 2,2'-biimidazole ( $8.481 \times 10^{-2}$  mol) was added to 450 mL of absolute ethanol. The

solution was heated to 80°C before the addition of 3.595 g NaOH ( $8.986 \times 10^{-2}$  mol) dissolved in approximately 20 mL of distilled water. The solution was heated at 80°C. The solution turned reddish brown and there were no visible signs of 2,2'-biimidazole. While the solution was heated at 80°C, 6.0 mL 2-chloroethanol ( $8.950 \times 10^{-2}$  mol) suspended in ~50 mL absolute ethanol was slowly added drop-wise from the addition funnel. The red solution turned cloudy with a salt like precipitate. The reaction was allowed to proceed for 30 minutes. After which, 3.235 g NaOH ( $8.088 \times 10^{-2}$  mol) dissolved in ~20 mL distilled water was added to the flask and allowed to react for 45 minutes. After the 45 minutes, 5.6 mL 2-chloroethanol ( $8.347 \times 10^{-2}$  mol) suspended in 50 mL absolute ethanol was added to the flask via addition funnel. The temperature was maintained at 80°C for 18 hours. The reaction was filtered with fritted funnel.



Scheme 2.10. Structure of 1,1'-di(hydroxyethyl)-2,2'-biimidazole.

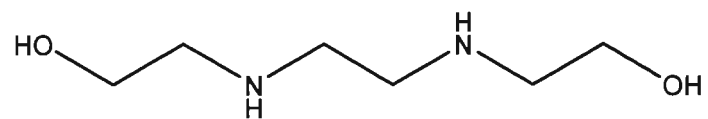
The filtrate was rotoevaporated until no other liquid appeared to come off. Approximately 200 mL chloroform was added to the residue. There were particles that did not dissolve completely. The solution was filtered. Distilled water was added to the filtrate and the solution was poured into a separatory funnel. The top layer, water portion, was retrieved by pipette and put into the refrigerator. The bottom layer,

chloroform portion, was added to ~200 mL hot distilled water. The solution bubbled and had some foam formed. This solution was poured into a separatory funnel and allowed to cool overnight.

Needles formed in the filtrate left overnight in the refrigerator. A mass of 0.113 g was recovered with a fritted funnel. The solution left in the separatory funnel to cool visually separated. The top portion was again removed by pipette and chilled four hours in a refrigerator. A mass of 0.954 g of product was recovered via fritted funnel.

The residue recovered from the first separation was golden brown in color. Chloroform was added and the solution was filtered again. The residue had a mass of 12.728 g but seemed to decrease over time due to solvent evaporation. This product recovery resulted in a 67.6 % yield. Elemental analysis resulted in 43.08 % C, 4.80 % H, 21.69 % N, 30.43 % O (Theoretical 54.04 % C, 6.35 % H, 25.21 % N, 14.40 % O). FTIR confirmed peaks at: 3438  $\text{cm}^{-1}$  (O-H stretch); 3167  $\text{cm}^{-1}$  (N-H stretch); 3065, 3000  $\text{cm}^{-1}$  (Ar-H stretch); 2875, 2780  $\text{cm}^{-1}$  (C-H stretch); 1430  $\text{cm}^{-1}$  (O-H bend); 1125  $\text{cm}^{-1}$  (C-N stretch). The IR spectrum was prepared as a smear on a KBr plate and is located in Appendix A.

**2.5.3 N, N'- Bis(2-hydroxyethyl)ethylenediamine, mock-HEB.** The diol N,N'-bis(2-hydroxyethyl)ethylenediamine, 1,1'-(ethane-1,2-diylbis(azanediyl))diethanol (structural drawing in Scheme 2.11), was purchased from Aldrich and used as received. This compound was chosen because it was commercially available and similar in linkage to 1,1'-di(hydroxyethyl)-2,2'-biimidazole when comparing Schemes 2.10 and 2.11. The elemental composition consists of 48.63 % C, 10.88 % H, 18.90 % N, 21.59 % O with a melting point of 98-100°C. This compound will be referred to as mock-HEB.



Scheme 2.11. Structure of N,N'-bis(2-hydroxyethyl)ethylenediamine.

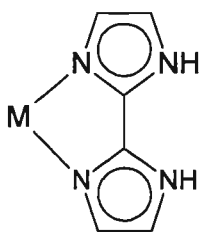
### 3 METAL COMPLEXES OF 2,2'-BIIMIDAZOLE

#### 3.1 METAL COMPLEXES OF 2,2'-BIIMIDAZOLE

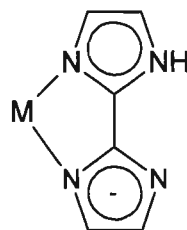
Metal chelation and complexation of 2,2'-biimidazole and its derivatives have been studied for reasons of crystal engineering [10, 13, 15, 74-80] and mimicking enzymes [113, 114]. Crystallographic studies reveal information on the exact positioning of 2,2'-biimidazole and whether the rings remain planar along with *cis* or *trans* coordination. This information can lead to insight which can dramatically aid in template effects for constructing macrocyclic complexes in addition to crystal engineering. In general, the coordination properties of the metal ion, to include coordination number and geometry, are matched to the donor properties of the ligands. The interaction between the two defines the organic-inorganic ensemble, like discrete polygons or polyhedra, one-, two-, or three-dimensional coordination networks [115]. Scheme 3.1 shows 2,2'-biimidazole and various metals.

A review of metal complexes of 2,2'-biimidazole have yielded 130 crystal structures. The first reported crystal structure was that of diaquobis (2,2'-biimidazole)nickel(II) dinitrate by Mighell *et. al* in 1969 [116]. These crystal structures are grouped by metals and listed in Table 3.1.

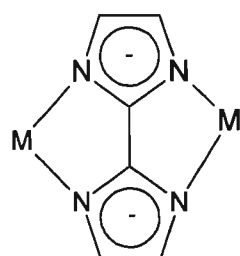
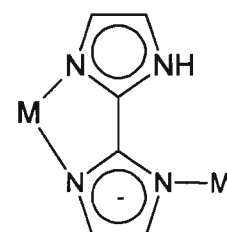




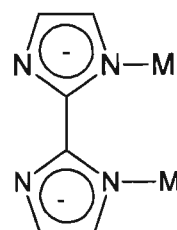
Cu(II), Fe(II), Fe(III), Ni(II),  
Co(II), Rh(I), Cd(II), Mo(II),  
Ru(II), and Au(III)



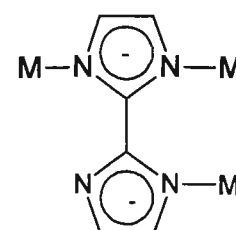
Rh(I)  
Ir(I)



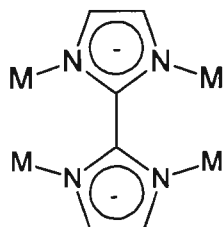
Cu(II), Ni(II), Co(II), Pd(II),  
Mo(II), Ru(II), Ti(III), Mn(II),  
Os(II), Rh(I), Au(III), and Ir(I)



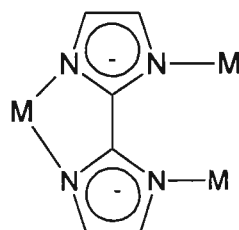
Au(I)



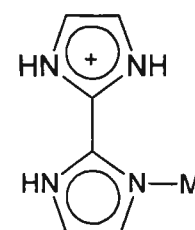
Au(I)



Au(I)



Rh(I), Pd(II), Au(I)



Cd(II), Ag(I)

Scheme 3.1. Metal complexes.

Table 3.1. Crystal Information for Various Metal - 2,2'-Biimidazole Compounds

Metal	Coordination	Space Group	Reference
Ag	5 3 2	P-1, P3 <sub>2</sub> , P3 <sub>2</sub> 1 <sub>2</sub> , Pnna, Cc	[71, 95, 117-120]
Cd	6	P-1, P2 <sub>1</sub> /n, P2 <sub>1</sub> /c, C2/c, R-3, Pna2 <sub>1</sub> , Pbcn, P3 <sub>2</sub> 1 <sub>2</sub>	[72, 84, 121-128]
Co	6 5 4	P2 <sub>1</sub> , P2 <sub>1</sub> /c, P2 <sub>1</sub> /n P2 <sub>1</sub> 2 <sub>1</sub> 2 <sub>1</sub> , P-1, R-3c, C2/c, C2/m, Ccc2	[10, 19, 97, 121, 126, 129-135]
Cr	6	I4 <sub>1</sub> , C2/m, P4 <sub>2</sub> /n, P-3 <sub>1</sub> , R-3c	[136, 137]
Cu	6 5 4	P-1, P2 <sub>1</sub> , P2 <sub>1</sub> /n, C2/c, Fdd2	[14, 18, 127, 138-144]
Fe	6	P2 <sub>1</sub> /c, P2 <sub>1</sub> /n, I4 <sub>1</sub>	[61, 145]
Ir	4	P2 <sub>1</sub> 2 <sub>1</sub> 2 <sub>1</sub>	[146]
Mn	5	Pna2 <sub>1</sub>	[147]
Mo	5	P-1	[148, 149]
Ni	6	P-1, P-3, P4 <sub>2</sub> 1 <sub>2</sub> 1 <sub>2</sub> , P2 <sub>1</sub> /c, P2 <sub>1</sub> /n, Pccn, Pbca, Pca2 <sub>1</sub> , C2/m, C2/c, Ccc2, Ccca,	[10, 11, 16, 79, 80, 97, 116, 135, 150, 151]
Os	6	P-1	[152-154]
Re	6	P-1, P2 <sub>1</sub> /c, Pca2 <sub>1</sub> , Fdd2, I4/m	[155-157]
Ru	6 4	Pbca, P-1, P2 <sub>1</sub> C2/c, Cc, Pnna	[10, 96, 158, 159]
V	6	P2 <sub>1</sub> /n	[160, 161]
Zn	6 5 4	Pbca, C2/c, P2 <sub>1</sub> /c, P2 <sub>1</sub> /n, P-1, I4 <sub>1</sub>	[121, 124, 125, 127, 133, 139, 162, 163]

**3.1.1 Silver Complexes.** The general characteristics and properties of silver include an oxidation state of one, a crystal structure of face centered cubic. Of the seven reported crystal structures of silver complexed with 2,2'-biimidazole compounds, five exhibit a catena structure and the other two are bis. Silver usually has a coordination geometry of 2, however, when complexed, the crystal structures show a coordination geometry of 3 and 5. [71, 95, 117-119] Constable reports the reemergence of interest in silver-containing coordination polymers stating its variable coordination numbers and geometries, combinations of metal-ligand and other supramolecular interactions, silver-silver interactions, and photophysical, electronic, and biomedical applications. [115].

**3.1.2 Cadmium Complexes.** The general characteristics and properties of cadmium metal include an oxidation state of two, a crystal structure of hexagonal close-packed. Of the twenty-one reported crystal structures, six coordination geometries of cadmium 2,2'-biimidazole compound complexes, having either +2 or +1 charge, were predominately exhibited with the exception of a five coordination geometry with that of the counter clock-wise crystal structure. [72, 84, 121-128]

**3.1.3 Cobalt Complexes.** The general characteristics and properties of cobalt include oxidation states of two and three with two being the most stable, a crystal structure of face-centered cubic. Eighteen coordination compounds of cobalt complexed with 2,2'-biimidazole or its derivatives, having charges of either +2 or +3, have been reported. [97, 121, 126, 129-135] All but two of geometries are six coordination, whereby one has a coordination number of five and the other one a coordination geometry of four. Three of these structures are of the exact same compound, having different resolutions with data collection at different temperatures. [97,121,126,129-135]

**3.1.4 Chromium Complexes.** The general characteristics and properties of chromium include oxidation states of two, three, and six with three listed as the most stable, a crystal structure of body-centered cubic. All of the six reported crystal structures of chromium complexed with 2,2'-biimidazole compounds exhibited six coordination geometry. [136, 137]

**3.1.5 Copper Complexes.** The general characteristics and properties of copper include oxidation states of one and two with two being the most stable, a crystal structure of face-centered cubic. The thirteen reported crystal structures of copper, all of copper(II) with 2,2'-biimidazole compounds, had varying coordination geometries of four to six. [127, 138-144]

**3.1.6 Iron Complexes.** The general characteristics and properties of iron include oxidation states of two and three with three listed as the most stable, a crystal structure of body-centered cubic. All five crystal structures of iron complexed with 2,2'-biimidazole or its derivatives, four of iron(II) and one iron(III), exhibited six coordination geometry. [61, 145]

**3.1.7 Iridium Complexes.** The general characteristics and properties of iridium include oxidation states of two, three, four, and six with four listed as the most stable, a crystal structure of face-centered cubic. The only reported iridium compound complexed with 2,2'-biimidazole has a coordination geometry of four, charge of +3 and space group of  $P2_12_12_1$ . [146]

**3.1.8 Manganese Complexes.** The general characteristics and properties of manganese include oxidation states of two, three, four, six, and seven with two listed as the most stable, a crystal structure of cubic. The lone crystal structure of manganese

complexed with 2,2'-biimidazole, with +2 charge, exhibited a coordination geometry of five and a space group of  $Pna2_1$ . [147]

**3.1.9 Molybdenum Complexes.** The general characteristics and properties of molybdenum include oxidation states of two, three, four, five, and six with six listed as the most stable, a crystal structure of body-centered cubic. The two reported crystal structures of molybdenum complexed with 2,2'-biimidazole compounds have P-1 space groups and a coordination geometry of five, with one of the crystal structures also containing rhenium. [148, 164]

**3.1.10 Nickel Complexes.** The general characteristics and properties of nickel include oxidation states of two and three, with two listed as the most stable, a crystal structure of face-centered cubic. There are twenty reported crystals structures of nickel 2,2'-biimidazole complexes, all performed at room temperature, eight of which have structures containing nickel(II), and all having a coordination geometry of six. [79, 97, 116, 135, 150, 151, 165]

**3.1.11 Osmium Complexes.** The general characteristics and properties of osmium include oxidation states of two, three, four, six, and eight with four listed as the most stable, a crystal structure of hexagonal close-packed. The four crystal structures of osmium compounds, with osmium(III) complexed with 2,2'-biimidazole compounds, exhibited a coordination geometry of six and P-1 space group. The x-ray determination of the osmium complexes was performed at 173K; the crystal measurements of all other metal 2,2'-biimidazole compound complexes listed in Table 3.1 were taken at room temperature. [153]

**3.1.12 Rhenium Complexes.** The general characteristics and properties of rhenium include oxidation states of negative one, two, four, six, and seven, with seven listed as the most stable, a crystal structure of hexagonal close-packed. From the nine reported crystal structures of rhenium 2,2'-biimidazole compound complexes, six were of rhenium(III) and three were of rhenium(V), all of which exhibited a coordination geometry of six and were performed at room temperature. [155-157]

**3.1.13 Ruthenium Complexes.** The general characteristics and properties of ruthenium include oxidation states of two, three, four, six, and eight with four listed as the most stable, a crystal structure of hexagonal close-packed. Of the seven reported crystal structures of ruthenium complexes with 2,2'-biimidazole or its derivatives, five of the compounds had a coordination geometry of six, primarily for ruthenium(IV), and two had a coordination geometry of four. [159]

**3.1.14 Vanadium Complexes.** The general characteristics and properties of vanadium include oxidation states of two, three, four, and five, with five listed as the most stable, a crystal structure of hexagonal body-centered. The two reported crystal structures of vanadium-biimidazole complexes consisted of vanadium(IV), a coordination geometry of six and  $P2_1/n$  space group. [160, 161]

**3.1.15 Zinc Complexes.** The general characteristics and properties of zinc include an oxidation state of two, the crystal structure of hexagonal close-packed. Out of the fourteen reported crystal structures of zinc 2,2'-biimidazole compound complexes, one has a coordination geometry of four, five have a coordination of five, and eight have the typical coordination geometry of six. [121, 124, 125, 127, 133, 139, 162, 163]

### 3.2 SILVER BIS(1H-IMIDAZOLIUM) TRINITRATE

Synthesis of silver bis(1H-imidazolium) trinitrate,  $[\text{Ag}(\text{biimH})_2(\text{NO}_3)_3]$ , was prepared by using the same technique as that for the creation of 2,2'-bis(1H-imidazolium) dinitrate [71], employing a 1:2 mole ratio for 2,2'-biimidazole and silver nitrate respectively. The synthesis of  $[\text{Ag}(\text{biimH})_2(\text{NO}_3)_3]$  was accomplished using 2,2'-biimidazole, silver nitrate, and nitric acid as starting materials. The 2,2'-biimidazole was prepared according to published procedures [1], using equal portions of 40% glyoxal and concentrated ammonium hydroxide (28-30%). Silver nitrate, A.C.S. grade, was used as received from Aldrich and concentrated nitric acid was diluted to 0.1 M.

The crystal growth of  $[\text{Ag}(\text{biimH})_2(\text{NO}_3)_3]$  was achieved by the synthetic procedure reported by Hester *et al.* [71], using 0.1 M  $\text{HNO}_3$ . A mass of 0.222 g ( $1.65 \times 10^{-3}$  mol) 2,2'-biimidazole was dissolved by the drop-wise addition of 0.1 M  $\text{HNO}_3$ . Silver nitrate (0.586 g,  $3.45 \times 10^{-3}$  mol) was then added to the solution as a solid. The solution became cloudy. A few more drops of 0.1 M  $\text{HNO}_3$  were added to the vial and the solution was stirred. After 24 hours, the solution had a pink hue with a visible precipitate. Crystals formed as the solution was allowed to slowly dry/evaporate over a period of several days.

Crystal structure determination of  $[\text{Ag}(\text{biimH})_2(\text{NO}_3)_3]$  and collection and reduction of X-ray data was completed in the usual manner. Diffraction intensity data were collected with a Bruker Smart Apex CCD diffractometer. The space group was determined from systematic absences. The structures were solved by direct methods and Fourier difference syntheses and refined by full-matrix least-squares procedures on peak intensities ( $F^2$ ). All non-hydrogen atoms were refined anisotropically. Hydrogen atoms

were inserted in their calculated positions. Software and atomic scattering factors are contained in the SHELXTL program package [101].

The enhanced crystallographic information file (CIF) revealed that the silver bis(1H-imidazolium) trinitrate  $[\text{Ag}(\text{biimH})_2(\text{NO}_3)_3]$  product has a monoclinic crystal system with Cc space group and a residual R-factor of 4.72 % with refinement. Figure 3.1 gives a diagram of  $[\text{Ag}(\text{biimH})_2(\text{NO}_3)_3]$  and Figure 3.2 is a unit cell representation of  $[\text{Ag}(\text{biimH})_2(\text{NO}_3)_3]$  along the x-y face. Details of the crystal data for  $[\text{Ag}(\text{biimH})_2(\text{NO}_3)_3]$  are provided in Appendix B.6. The atomic coordinates and equivalent isotropic displacement parameters are listed in Appendix B.7. The observed bond lengths, angles, and contacts are listed in Appendix B.8. Listed in Appendix B.9 are anisotropic displacement parameters. Appendix B.10 displays the coordinates of the hydrogen atoms along with isotropic displacement parameters. Appendix B.11 lists the torsion angles.

On the resolved structure, the Ag atom is weakly bonded or semi-coordinated to N on two different 2,2'-biimidazole entities with a distance of 2.11(8) Å. The nearest contact with O from a nitrate group is 3.07(0) Å. The other nitrate is hydrogen bonded to the other side of the uncoordinated ring of 2,2'-biimidazole. The rings semi-coordinated to Ag have a dihedral angle of 6.1° whereas the dihedral angle on the imidazole rings of 2,2'-biimidazole averages 32.1°. This differs from the other silver complexed 2,2'-biimidazole crystal reported by Hester *et al.* [71]

Deviations from the helical shape obtained by Hester include coordination of the ligand with biimidazole as a bidentate ligand when complexed or bonded to same metal ion, rings seem to be 'forced' to a somewhat planar geometry with N-Ag-N "semi-bond"



angle of  $6.1^\circ$ , and the non-bonded heterocycle on the same side of the other non-bonded heterocycle.

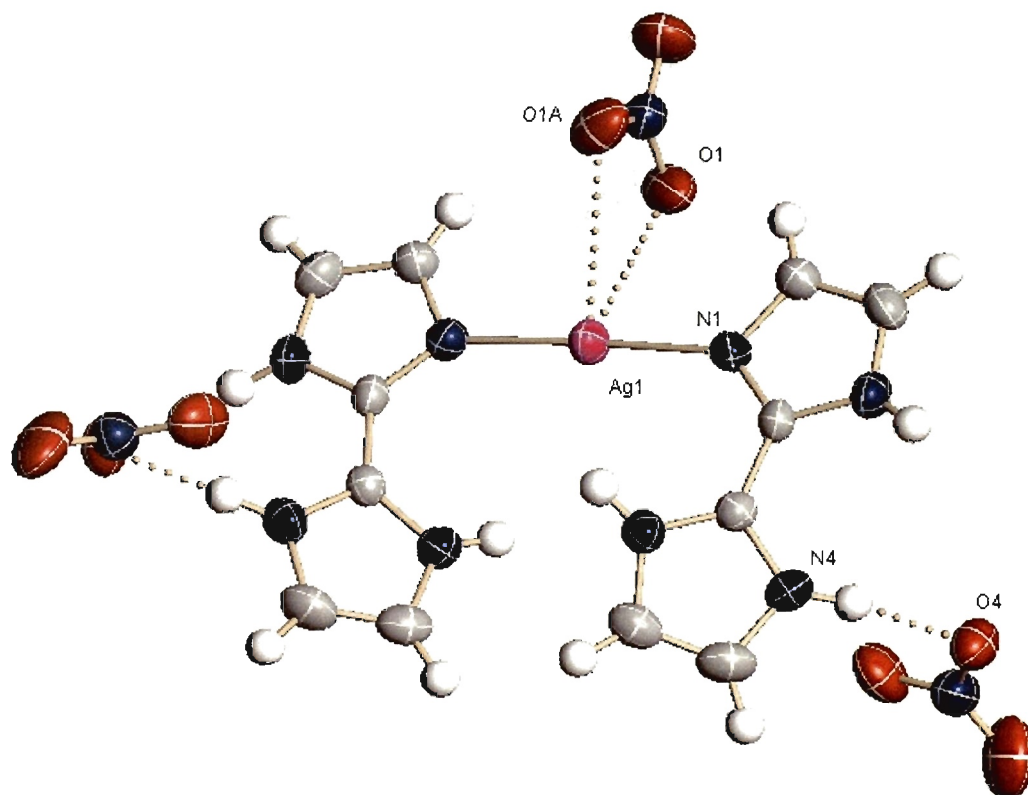


Figure 3.1. Ellipsoid / OR TEP diagram of silver 2,2-bis(1H-imidazolium) trinitrate.

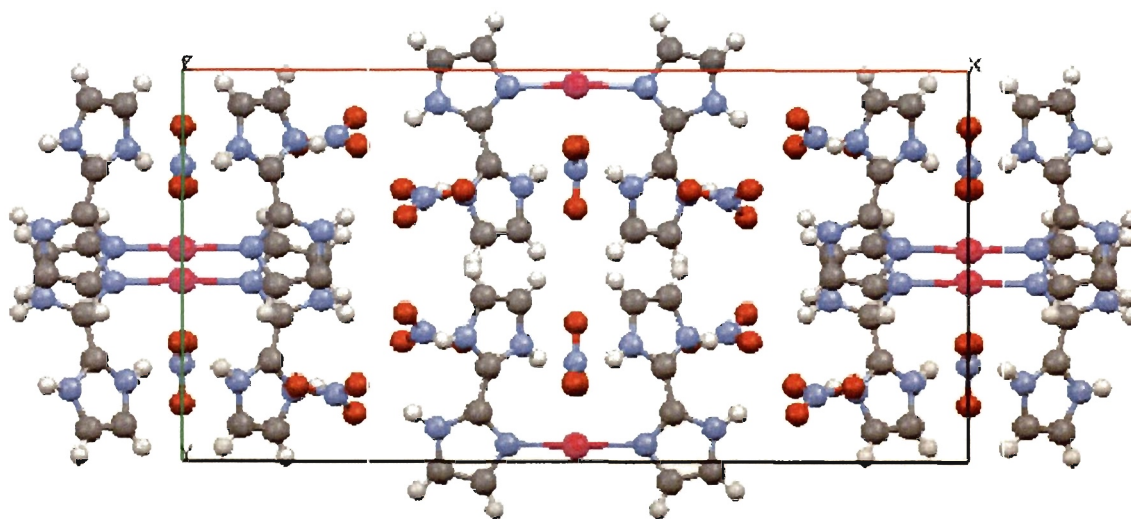


Figure 3.2. Unit cell silver bis(1H-imidazolium) trinitrate along x-y face.

### 3.3 METAL COMPLEXATION OF 2,2'-BIIMIDAZOLE DERIVATIVES

In reviewing the Cambridge crystallographic database [166], there was a plethora of crystal structures that incorporated the 2,2'-biimidazole somewhere within the molecular structure. By focusing on those compounds in which “biimidazole” appeared explicitly in the name, only three types of derivatives have been crystallized with a metal. The crystal structures reported included the tetramethyl, tetracyano, and bibenzimidazole derivatives [167-173] which have been compiled in Table 3.2.

Bernarducci *et al.* [167] examined the tetramethyl derivative and reported on the copper (II) and zinc complexes. The Rasmussen group reported on the tetracyano derivatives [169-173], and Uson *et al.* on the bibenzimidazole [65-67, 168].

Table 3.2. Crystal Structures of Metals with 2,2'-Biimidazole Derivatives

Metal	Derivative	Space Group(s)	Reference
Cu	Tetramethyl	$P\bar{1}$	[167]
	Tetracyano	$P\bar{1}$	[169]
Ir	Tetracyano	$P2_12_12_1$	[172]
		Pnmm	
		$P\bar{1}$	
Mo	Tetracyano	$P2_1/n$	[173]
Pd	Tetramethyl	$P\bar{1}$	[171]
	Bibenzimidazole	$P\bar{1}$	[168]
Pt	Tetracyano	$P\bar{1}$	[170]
Rh	Tetracyano	$P\bar{1}$	[172]
	Bibenzimidazole	$P\bar{1}$	[168]
Zn	Tetramethyl	$P\bar{1}$	[167]

Figure 3.3 shows crystallographic evidence of a partially resolved structure of silver nitrate with 1,1'-di(ethylpropionato)-2,2'-biimidazole which was determined at the Missouri University of Science and Technology. From the image, silver nitrate is bound to nitrogen on the imidazole ring, however, precise bond lengths cannot be given at this time. Also, the diester does not act as a bidentate ligand to the same silver atom since the bottom portion of the illustration shows a complete 1,1'-di(ethylpropionato)-2,2'-biimidazole molecule and the silver atom is connected to a different nitrogen atom from a separate diester.

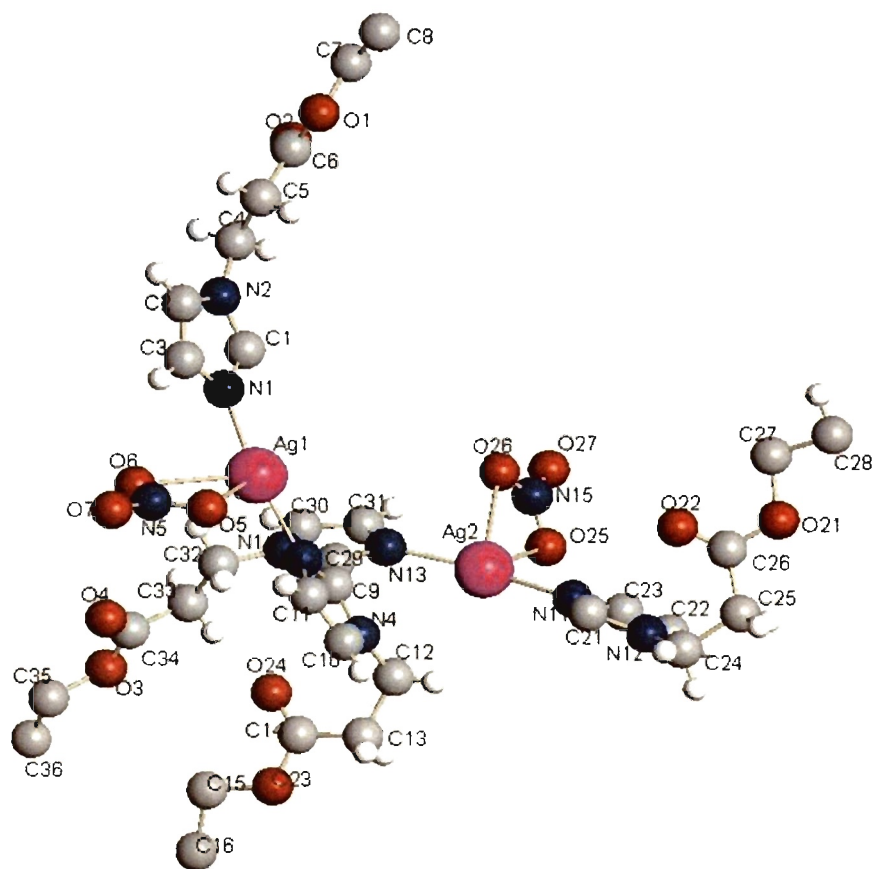


Figure 3.3. Preliminary crystallographic determination of silver nitrate with 1,1'-di(ethylpropionato)-2,2'-biimidazole.

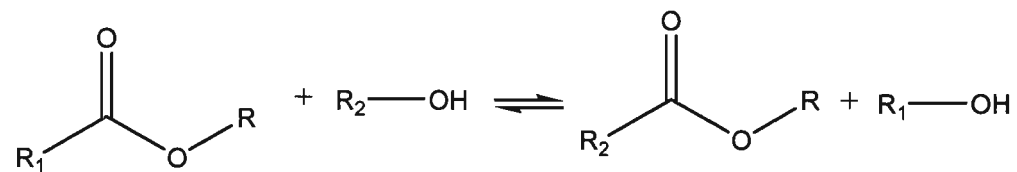
## 4 POLYMERIZATION OF 2,2'-BIIMIDAZOLE AND DERIVATIVES

### 4.1 BACKGROUND ON POLYMERS OF 2,2'-BIIMIDAZOLE

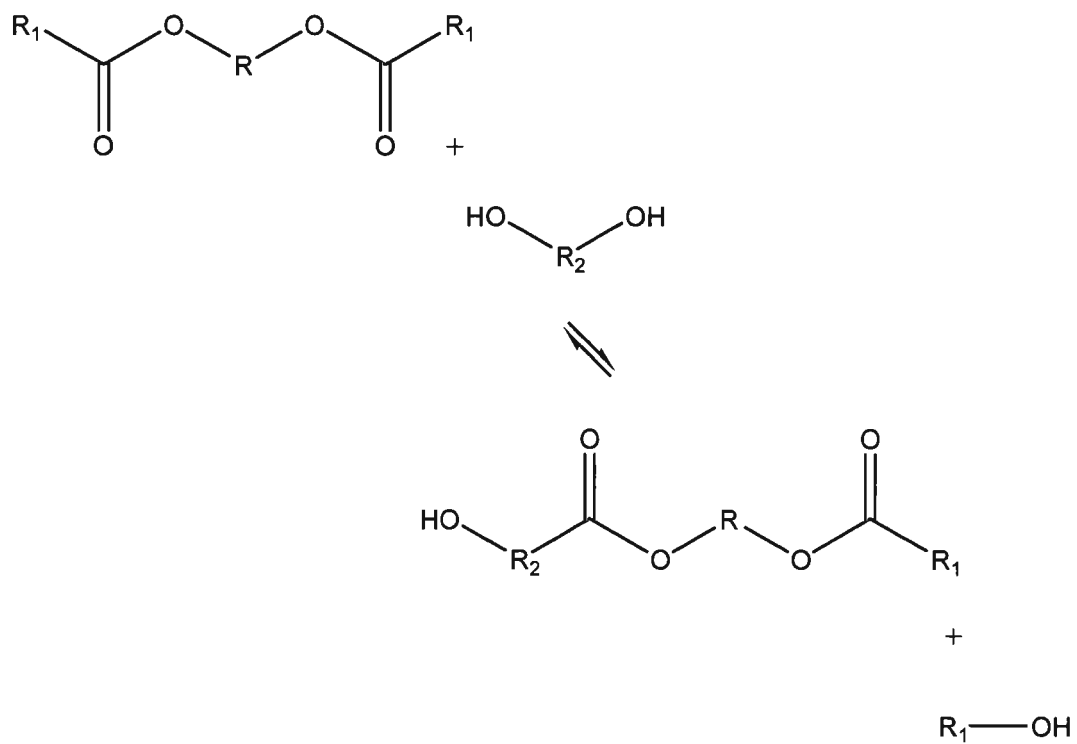
A SciFinder search [174] on polymers with the 2,2'-biimidazole moiety yields few published reports on these materials. Most of the reported literature reveals block-like polymers of biimidazole. Yamamoto *et al.* reported on  $\pi$ -conjugated poly(imidazole) synthesized in a nitrogen environment by dehalogenation of halogenated imidazole derivatives using a zero valent nickel complex and recovered a brown powder with electrochemically active properties. [175]. Forster reported the 2,2'-biimidazole moiety as a pendant group [176] and studied charge transport dynamics and its potential as an enzyme-based biosensor and a biofuel cell.

### 4.2 TRANSESTERIFICATION

Transesterification is typically defined by the reaction of an ester and an alcohol. Scheme 4.1 depicts a general transesterification reaction while Scheme 4.2 illustrates a difunctional alcohol and ester. There is a simple exchange of R groups from the ester and alcohol. With the end goal being a polymer containing the 2,2'-biimidazole moiety, diesters and diols containing this molecular component were chosen as the logical reactants for this desired product. The transesterification process requires the use of a catalyst for the reaction to proceed. Generally, the reaction is catalyzed by an acid or base. However, enzymes like lipase also have this ability.



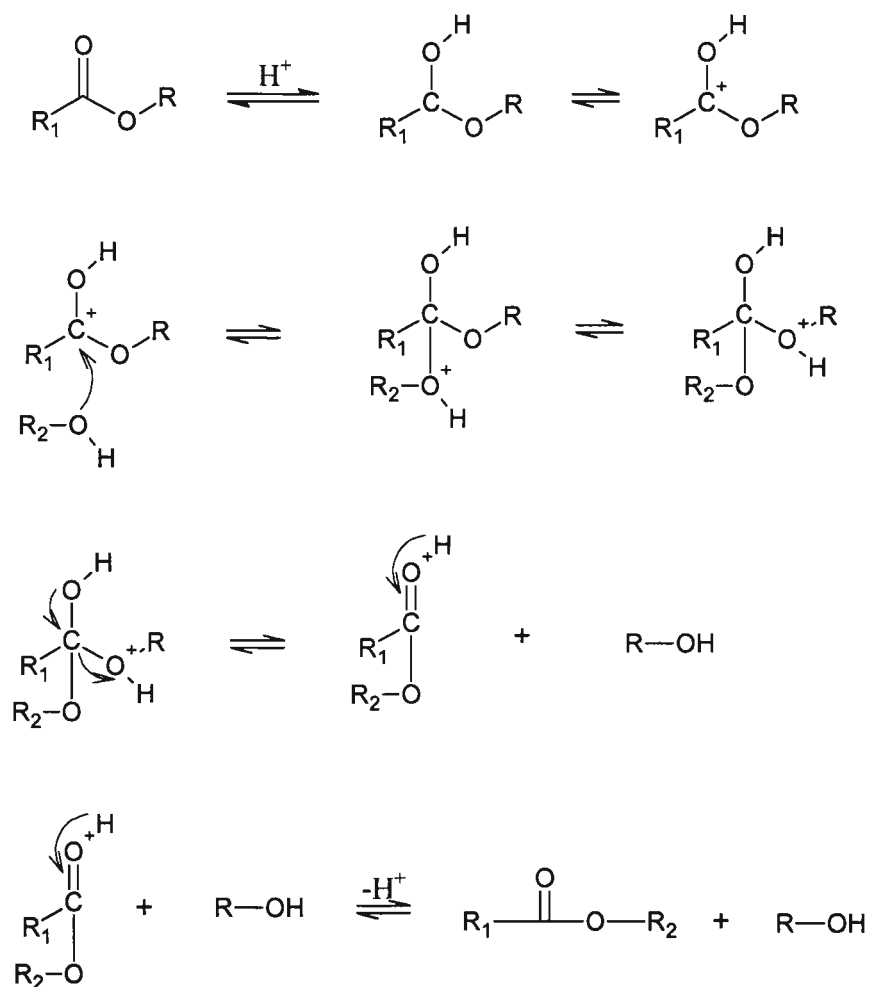
Scheme 4.1. General transesterification reaction scheme.



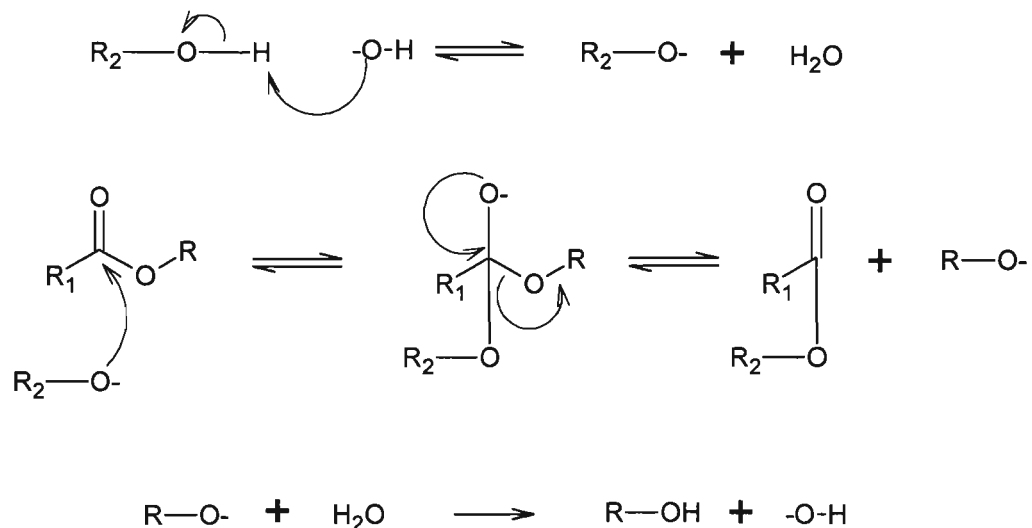
Scheme 4.2. Transesterification reaction using diester and diol.

**4.2.1 Acid vs. Base Catalyzed.** In an acid-catalyzed reaction, the acid donates a proton to the carbonyl group to promote a nucleophilic attack from the alcohol, illustrated in Scheme 4.3 [177]. Although high yields are reported in alkyl esters, the reactions are slow and require temperatures above 100°C. It should also be noted that this is an equilibrium process and the reaction can be shifted.

In a base-catalyzed reaction, the base removes a proton from the alcohol creating a nucleophile. This process requires the absence of water since its presence gives rise to hydrolysis or saponification which ultimately reduces ester yields. The base-catalyzed transesterification reaction is illustrated in Scheme 4.4 [177].



Scheme 4.3. Acid-catalyzed transesterification mechanism. [178]



Scheme 4.4. Base-catalyzed transesterification mechanism. [178]

**4.2.2 Enzyme Catalyzed.** Enzymes are used as catalysts because they are reasonably stable, readily available, and are easy to handle. Typically, the reaction conditions must be optimized to establish suitable conditions for the enzyme, *e.g.*, solvent, temperature, and pH. Although enzymes possess great potential for regioselective synthesis, reaction yields and reaction times are not as good as that of a base-catalyzed reaction system [21].

**4.2.3 Viscometry.** Viscometry is a relative method to determine molecular weight. Because of the inherent nature of a molecule's interaction, particularly a polymer, with a solvent, the viscosity of the two combined is greater than that of the solvent alone. Although determining relative and reduced viscosity using a capillary viscometer is inexpensive, it is quite time consuming and factors are specific for solvent systems at specified temperatures.

Several relationships need to be defined eventually to determine intrinsic viscosity. The equations involved can be found in a fundamental polymer text by Painter.

[178] Relative viscosity,  $\eta_{rel}$ , is the ratio of the solution viscosity to the solvent viscosity, defined by Equation 4.1. Whereby the solution viscosity is defined as  $\eta$  and the solvent viscosity is defined as  $\eta_o$ . Equation 4.2 defines the specific viscosity,  $\eta_{sp}$ , as the ratio of the difference of the solution viscosity and solvent viscosity to the solvent viscosity. The reduced viscosity,  $\eta_{red}$ , is the ratio of the specific viscosity to the concentration,  $c$ , in terms of mass per deciliter, defined in Equation 4.3. Inherent viscosity (Equation 4.4) is defined as the natural log of the ratio of the solution viscosity to solvent viscosity. The intrinsic viscosity (Equation 4.5),  $[\eta]$ , is described as the limit of the reduced viscosity as the polymer solute concentration approaches zero or the limit of the inherent viscosity as the solution polymer concentration approaches zero.

$$\eta_{rel} = \frac{\eta}{\eta_o} \quad \text{Equation 4.1}$$

$$\eta_{sp} = \frac{\eta - \eta_o}{\eta_o} \quad \text{Equation 4.2}$$

$$\eta_{red} = \frac{\eta_{sp}}{c} \quad \text{Equation 4.3}$$

$$\eta_{inh} = \ln \frac{\eta}{\eta_o} \quad \text{Equation 4.4}$$

$$[\eta] = \lim_{c \rightarrow 0} \frac{\eta_{sp}}{c} = \lim_{c \rightarrow 0} \ln \frac{\eta}{\eta_o} \quad \text{Equation 4.5}$$



The Huggins equation, Equation 4.6, shows that the intrinsic viscosity is proportional to the reduced viscosity. The graph of reduced viscosity versus concentration should exhibit a linear positive slope which equals that of  $k'[\eta]^2$  and the y-intercept equals the intrinsic viscosity. Kraemer uses a similar relationship using inherent viscosity, where the graph of  $\ln(\eta / \eta_0)$  versus concentration exhibits a negative linear slope and the y intercept is indicative of the intrinsic viscosity. The negative slope is equal to  $k''[\eta]^2$ . See equation 4.7. The difference between  $k'$  and  $k''$  should have a value of five tenths on the same graph to indicate the process was done correctly. The Mark-Houwink-Sakurada relationship, Equation 4.8, states that the intrinsic viscosity is proportional to the molecular weight of the polymer, where  $M$  is the viscosity average molecular weight, with  $K$  and  $a$  as constants specific for solvent and polymer systems. The idealized relationship between the Huggins and Kraemer equations are shown in Figure 4.1. Extrapolation of both the Huggins equation and the Kraemer equation to zero concentration denotes the Mark-Houwink-Sakurada definition of intrinsic viscosity. For the ideal representation to occur, interaction between the polymer and the solvent does not occur.

$$\eta_{red} = k'[\eta]^2c + [\eta] \quad \text{Huggins Equation} \quad \text{Equation 4.6}$$

$$\eta_{inh} = k''[\eta]^2c + [\eta] \quad \text{Kraemer Equation} \quad \text{Equation 4.7}$$

$$[\eta] = KM^a \quad \text{Mark-Houwink-Sakurada Equation} \quad \text{Equation 4.8}$$

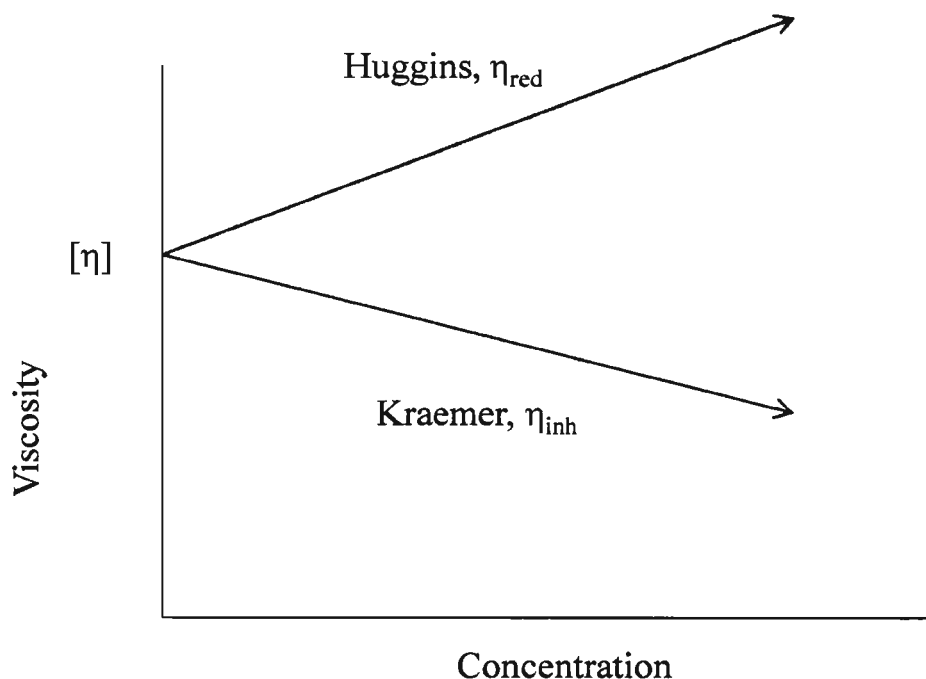


Figure 4.1. The ideal Huggins, Kraemer, and Mark-Houwink-Sakurada relationships.  
[180]

In the case of 2,2'-biimidazole polymers, the proportionality constants used in the Huggins, Kraemer, and Mark-Houwink-Sakurada equations are as yet undefined. However, by plotting the reduced and inherent viscosities versus concentration and using the Huggins and Kraemer equations, insight into intermolecular attractions can be gained for the systems studied. The relationship is not always a linear function, as when the solvent and polymer have strong intermolecular interactions. It should also be noted that although extrapolation to zero concentration leads to intrinsic viscosity, there are serious limitations and this region is generally where the greatest error in measurement occurs. [178] Large errors specifically occur with systems containing strong intermolecular interactions between solvent and polymer, with extreme examples of polyelectrolytes and ionic polymers. [178]

**4.2.4 Experimental.** The procedure used by the author for the synthesis of the polymeric species was a similar process for the following reactions and typical for polymerization syntheses. All systems were prepared by adding a 1:1 molar ratio of diester and diol. A distillation apparatus was also employed.

Reaction I -- HEB:DMPB: The ester alcohol system of 1,1'-di(methylpropionato)-2,2'-biimidazole (DEPB) and 1,1-di(hydroxyethyl)-2,2'-biimidazole (HEB) was prepared by using a 1:1 molar ratio of diester and diol. In a 25 mL round bottom flask equipped with a condenser and magnetic stir bar, 2.687 g HEB ( $1.210 \times 10^{-2}$  mol) and 4.001 g DMPB ( $1.197 \times 10^{-2}$  mol) were added. The two components were allowed to mix while weighing 0.051 g tetramethylammonium hydroxide (TMAH). The TMAH was added to the flask. Approximately 5 mL of water and 5 mL of ethanol were added to the flask. The materials were heated at 80°C for 4 hours.

Reaction II -- HEB:DEPB: The ester alcohol system of 1,1'-di(ethylpropionato)-2,2'-biimidazole (DEPB) and 1,1-di(hydroxyethyl)-2,2'-biimidazole (HEB) was prepared by using a 1:1 molar ratio of diester and diol. The addition of lipase was also used in this system as a catalyst. In a 25 mL round bottom flask equipped with a condenser and magnetic stir bar, 2.764 g HEB ( $1.244 \times 10^{-2}$  mol) and 4.016 g DEPB ( $1.201 \times 10^{-2}$  mol) were added along with 0.05 g lipase. The materials were heated at 80°C for 4 hours.

Reaction III -- DEPB:mock-HEB with EtOH: The ester alcohol system of 1,1'-di(ethylpropionato)-2,2'-biimidazole (DEPB) and N,N'-bis(2-hydroxyethyl)-ethylenediamine (mock-HEB) was prepared by using a 1:1 molar ratio of diester and diol. In a 25 mL round bottom flask equipped with a condenser and magnetic stir bar, 1.531 g

mock-HEB ( $1.033 \times 10^{-2}$  mol), 3.014 g DEPB ( $9.014 \times 10^{-3}$  mol), and 5 mL ethanol (EtOH) were added. The materials were heated at 100°C for 5 hours.

Reaction IV -- DEPB:mock-HEB with H<sub>2</sub>O: The ester alcohol system of 1,1'-di(ethylpropionato)-2,2'-biimidazole (DEPB) and N,N'-bis(2-hydroxyethyl)-ethylenediamine (mock-HEB) was prepared by using a 1:1 molar ratio of diester and diol. In a 25 mL round bottom flask equipped with a condenser and magnetic stir bar, 3.197 g DEPB ( $9.564 \times 10^{-3}$  mol), 1.505 g mock-HEB ( $1.016 \times 10^{-2}$  mol), and 5 mL water were added. The materials were heated at 100°C for 5 hours.

**4.2.5 Results and Discussion.** Viscosity measurements were taken on four systems in dimethylformamide at 25°C to determine intrinsic viscosity, establish polymer size and establish constants for the Mark-Houwink-Sarakuda relationship pertaining to 2,2'-biimidazole polyesters. TGA measurements were taken to determine degradation temperatures and characteristics for the 2,2'-biimidazole ester products. With DSC, the melting and crystallization temperatures were sought. Initial TGA measurements were taken using a Perkin-Elmer TG/S/2 thermographic analyzer with output to an XY plotter. Subsequent measurements were performed at the Materials Research Center at the Missouri University of Science and Technology using a NETZSCH and a TA-DSC using Al<sub>2</sub>O<sub>3</sub> as reference.

**4.2.5.1 Reaction I – HEB:DMPB.** The viscosity plot of the HEB-DMPB reaction, Figure 4.2, is not a classic example of an ideal polymer and solvent representation of the Huggins and Kraemer equations. To determine molecular weight average, the plotted points are forced into a linear relationship. The forced linear equations of the reduced and inherent viscosity have a good fit when considering the correlation coefficient.

However, extrapolation to zero concentration does not exhibit a viable intrinsic viscosity value. Since the polyester biimidazole system has yet to be fully documented and reported, it is probable that there may be a small range where the concentration is particularly suitable to fit the extrapolation of the Huggins and Kraemer equations to determine the Mark-Houwink-Sakurada relationship. Although in the single crystal study of DMPB there was evidence of non-aromatic rings [106], the hydrogen bonding would indicate interaction with the solvent which would lead to non-linear fitting of viscometry measurements.

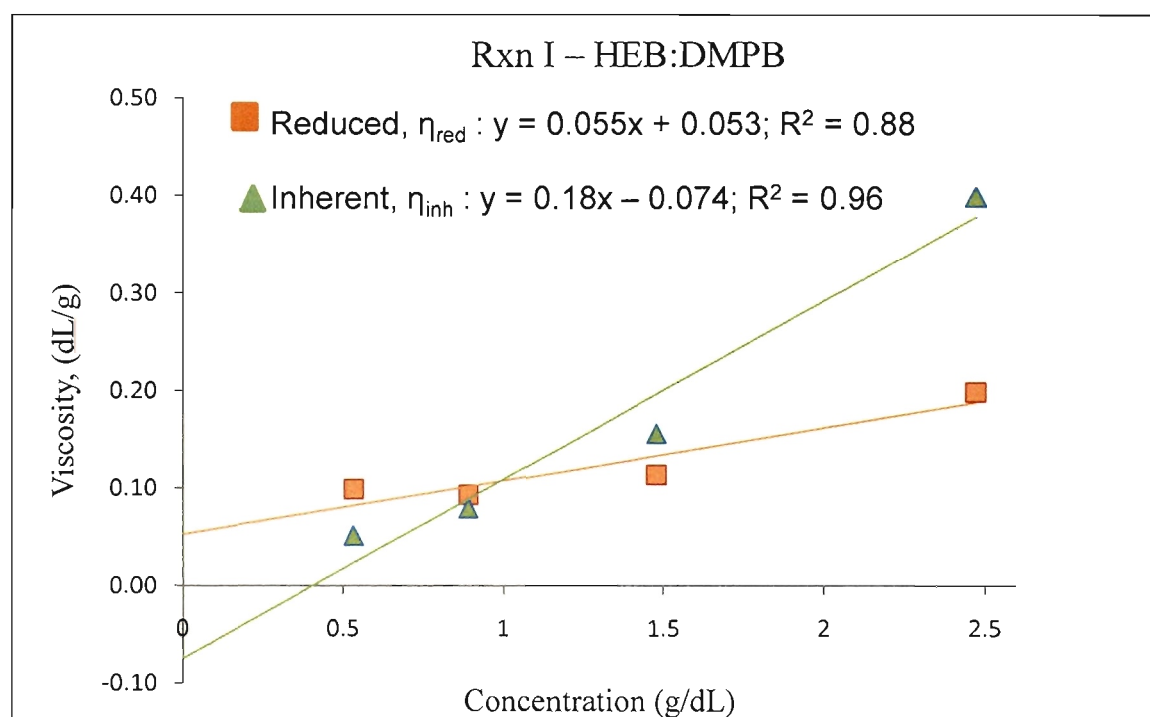


Figure 4.2. Plot of  $\eta_{red}$  and  $\eta_{inh}$  versus concentration of HEB:DMPB in DMF at 25°C.

The DSC overlay of the spectra of HEB, DMPB and the HEB:DMPB product (Figure 4.3) show exothermic transitions for the HEB:DMPB system occurring at lower

temperatures than the initial diol, HEB, and diester, DMPB, alone. The first major transition occurs around 60°C for HEB, at 75°C for the blend, and at 90°C for DMPB. Spectra for TGA and IR were done as a comparison of the four reaction systems and displayed over the same coordinates. However, the individual IR spectrum can be found in Appendix A. It is not unusual to have broader transitions for mixtures relative to the individual components. With these exothermic transitions, consideration should also be taken that the distribution and completion of the reaction are quite different.

**4.2.5.2 Reaction II – HEB:DEPB.** The reaction of HEB with DEPB produced the viscosity plot in Figure 4.4 is not typical of a classic example of the Huggins and Kraemer equations. To use the Huggins and Kraemer equations, the reduced and inherent viscosity were linearly fit and the difference between the forced linear slopes is 0.26. Although the reduced viscosity has a nice fit with a correlation factor around 0.97, the linear representation of the inherent viscosity does not fit well. Depending on the distribution of products, there could be an ideal range in which a linear representation of both the reduced and inherent viscosity exists. However, it should also be noted that there could be strong intermolecular interactions between the products and solvent and thus make a non-linear fit more applicable.

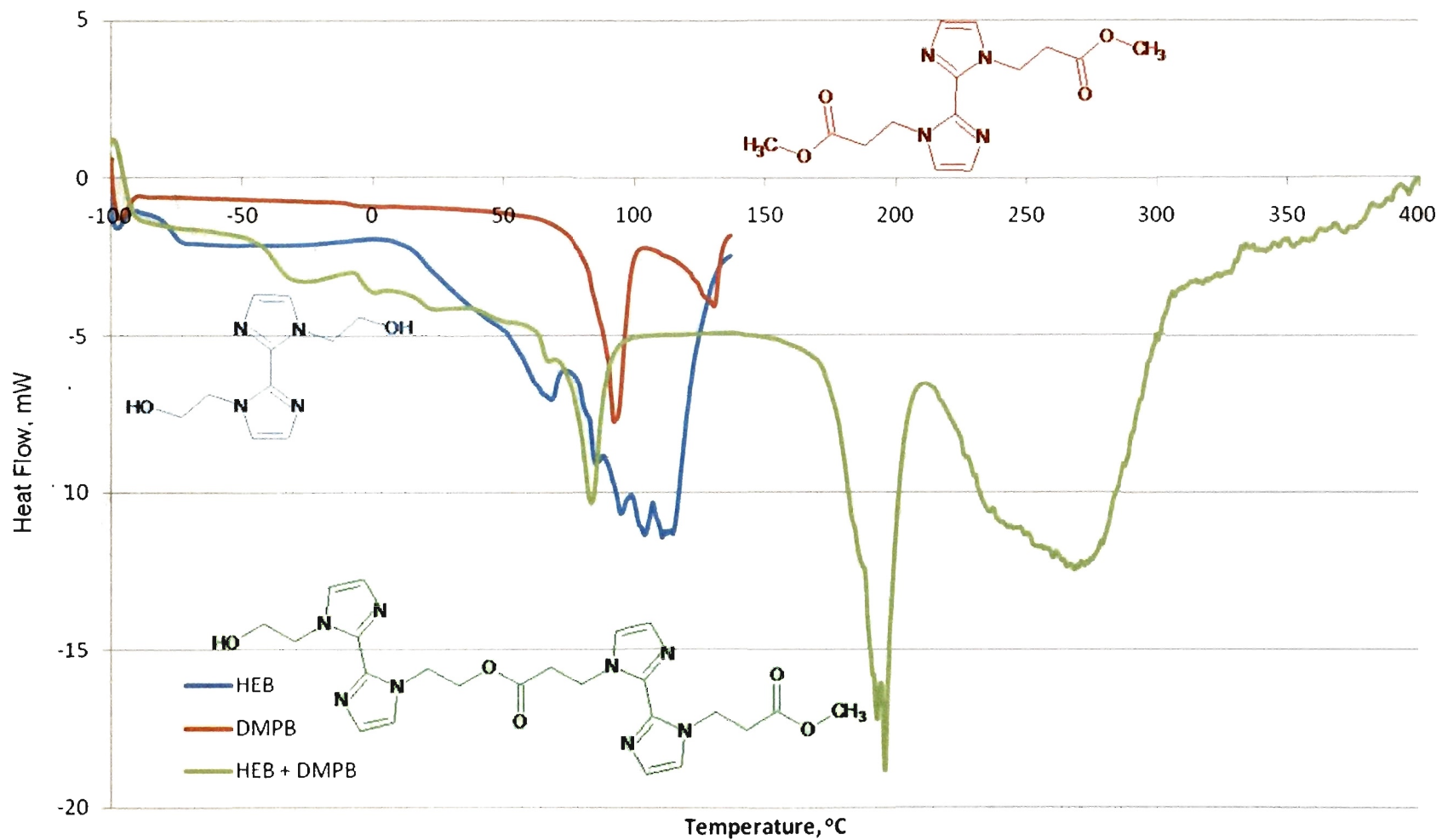


Figure 4.3. DSC overlay of HEB, DMPB, and HEB:DMPB product.

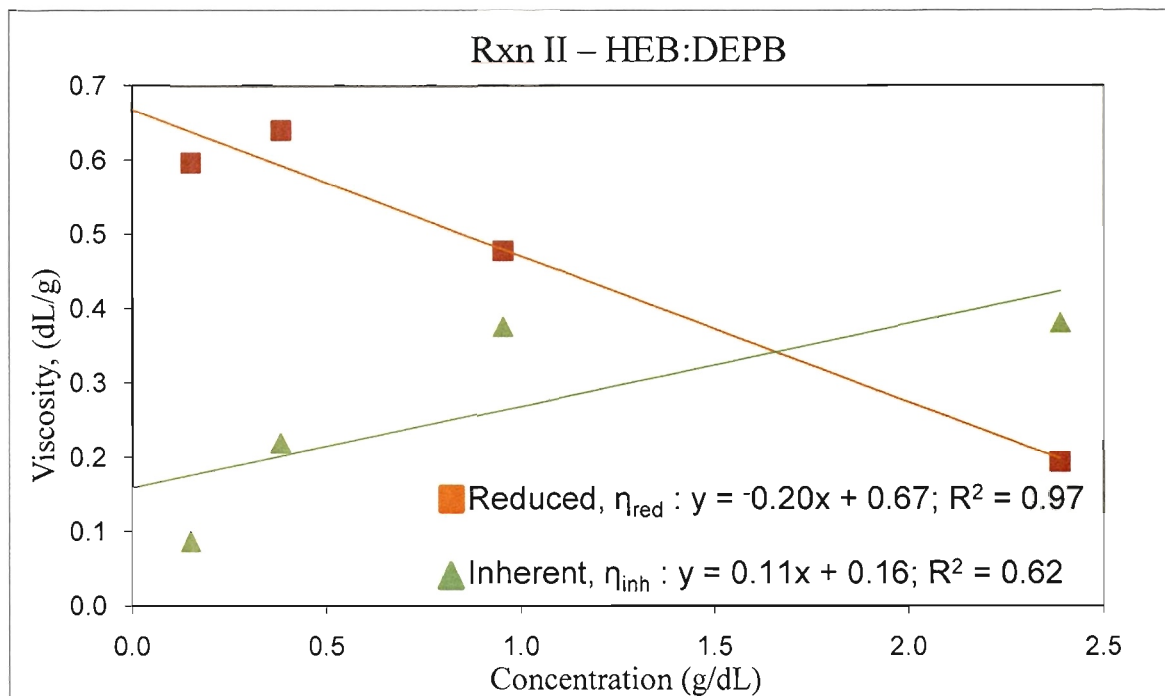


Figure 4.4. Plot of  $\eta_{red}$  and  $\eta_{inh}$  versus concentration of HEB:DEPB in DMF at 25°C.

In Figure 4.5, the DSC spectrum displays exothermic transitions for the HEB:DEPB system occurring at a lower temperature than the reactants of diol, HEB, and diester, DMPB, alone. The first major transition occurs around 55°C for HEB:DEPB, at 65°C for the blend, and around 75°C for DEPBB. The IR and TGA spectra are illustrated in comparison to the other three reaction systems on the same coordinates. However, the individual IR spectrum can be found in Appendix A. It is not unusual to have broader transitions for mixtures relative to the individual components. It appears that this reaction product is more uniform and exhibits a smooth transition.



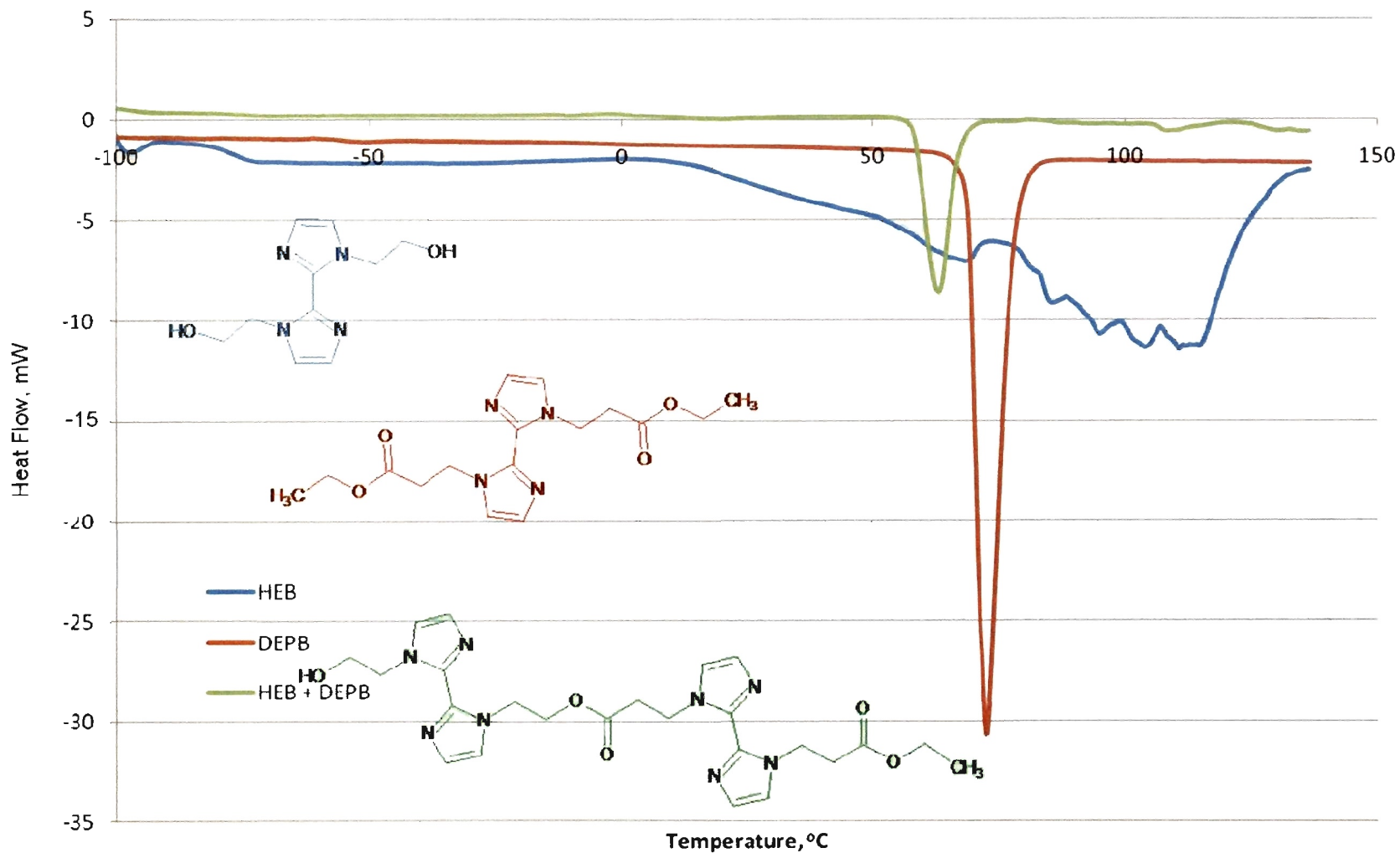


Figure 4.5. DSC Overlay of HEB, DEP, and HEB:DEP product.

**4.2.5.3 Reaction III – DEPb:mock-HEB with EtOH.** Viscometry measurements were taken for the reaction of DEPb and mock-HEB to determine reduced, inherent, and intrinsic viscosity. To establish the Huggins and Kraemer equations for reduced and inherent viscosity, a linear expression is required. The viscosity plot of the DEPb – mock-HEB reaction, Figure 4.6, does not represent an ideal system. Neither the reduced nor the inherent viscosity expression exhibits a linear fit since the correlation factor is far less than 0.50. Again, the linear Huggins and Kraemer relationships may not be suited for the 2,2'-biimidazole derivative system due to its inherent amphoteric nature and strong intermolecular interactions. The possibility of a more dilute concentration range might also lead to a classic type fit.

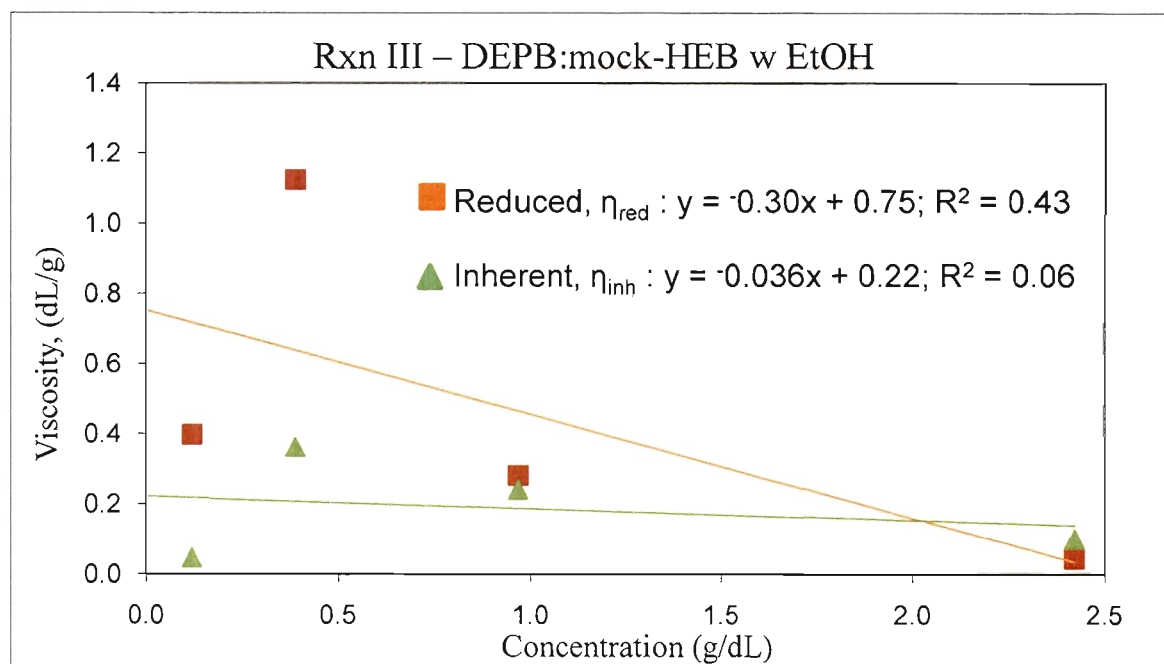


Figure 4.6. Plot of  $\eta_{red}$  and  $\eta_{inh}$  versus concentration of DEPb:mock-HEB with ethanol in DMF at 25°C.

The DSC spectrum, Figure 4.7, shows exothermic transitions for both of the DEPb:mock-HEB systems. The system in ethanol, DEPb + mock-HEB EtOH curve,

appears to just degrade after 65°C since there are no clear transitions, whereas, the water system has three exothermic transitions with the most drastic occurring at 200°C. The reactants of DEPB and mock-HEB had initial transitions occur around 70°C and 85°C respectively. IR and TGA spectra were displayed over the same coordinates for comparison, however, the individual IR spectra can be found in Appendix A. It appears that this reaction product is broad and difficult to define.

**4.2.5.4 Reaction IV – DEPB:mock-HEB with H<sub>2</sub>O.** The viscosity plot in Figure 4.8 is not typical of a classic example of the Huggins and Kraemer equations. To determine intrinsic viscosity, linear expressions for the reduced and inherent viscosities are used. By making the measurements fit a linear relationship, it is clear by the correlation factors for reduced viscosity line and the inherent viscosity line that a non-linear fit would be more appropriate. A non-linear fit would definitely give a better resolution and indicate strong intermolecular interactions of the components in DMF. However it must also be noted that a particular range of concentrations could exhibit a classic Huggins Kraemer relationship where an intrinsic viscosity could be determined and an average molecular weight calculated.

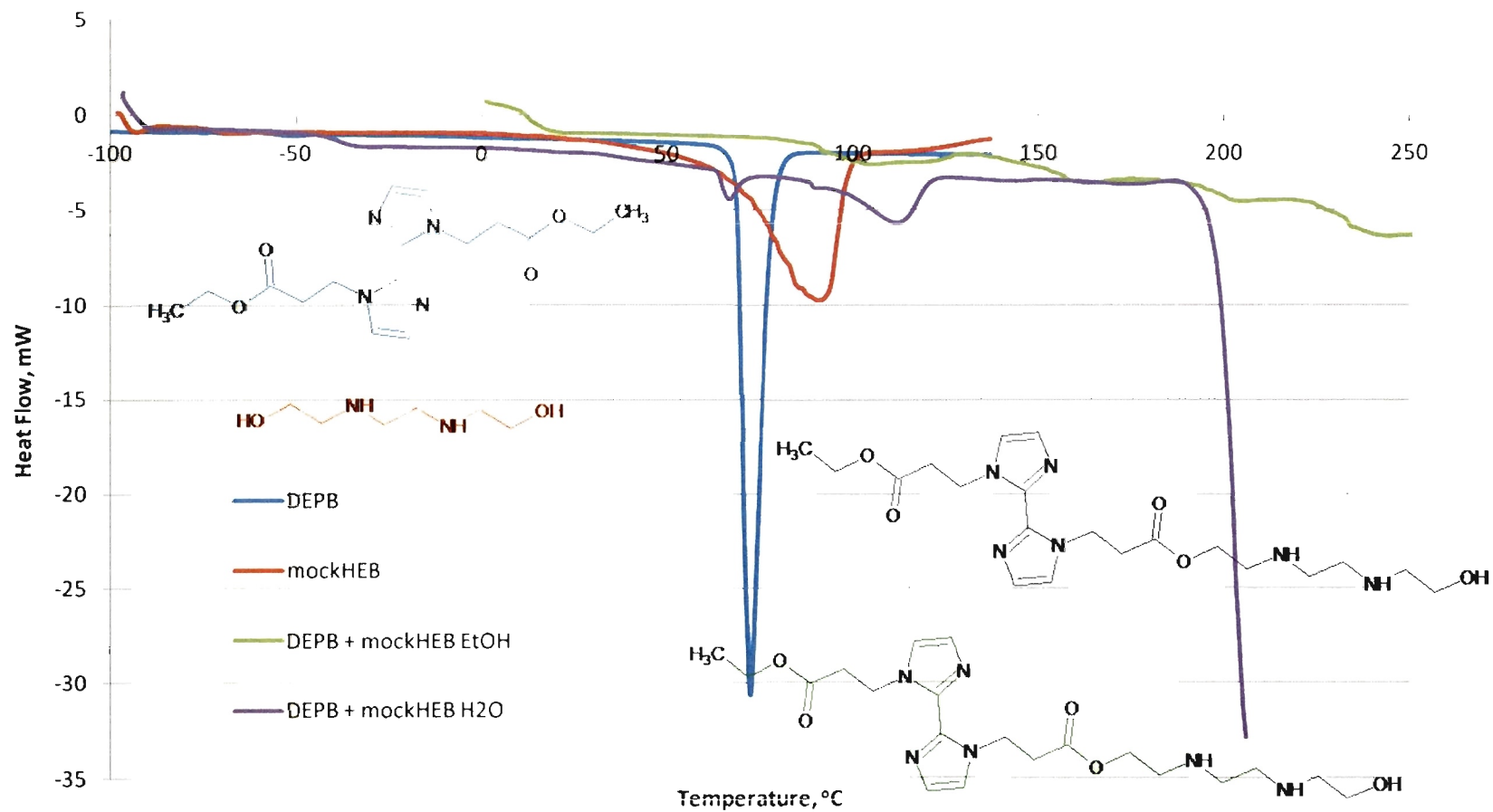


Figure 4.7. DSC overlay of DEPBB, mock-HEB, DEPBB:mock-HEB w EtOH, and DEPBB:mock-HEB w H<sub>2</sub>O.

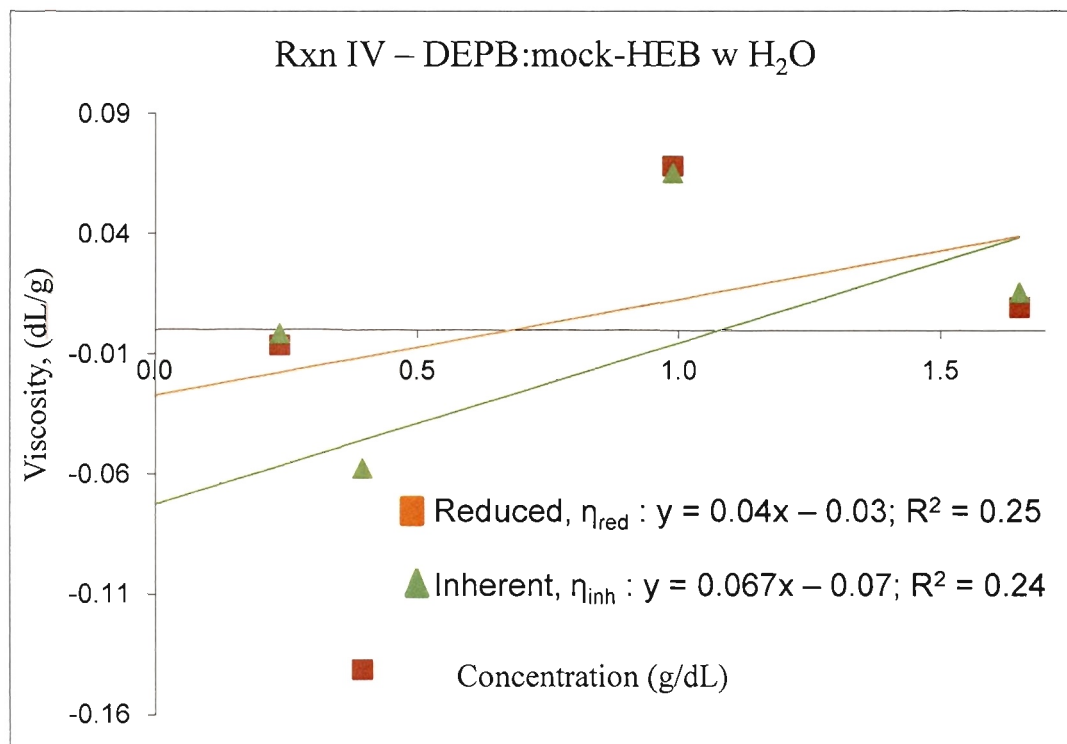


Figure 4.8. Plot of  $\eta_{red}$  and  $\eta_{inh}$  versus concentration of DEPB:mock-HEB with water using DMF at 25°C.

The TGA analysis of the compounds show stability temperatures at 10% of 270°C for 2,2'-biimidazole, 145°C for mock-HEB, 175°C for DEPB, and 215°C for the reaction of DEPB and mock-HEB at a scan rate of 5 degrees/minute. The stability temperatures, usually reported at 10% mass loss, along with the temperatures for 50% mass loss is listed in Table 4.1. In the case of reaction IV, the scan rate increase indicated a change in the mass reduction occurring at least 50°C later. This could indicate the intermolecular forces versus intramolecular forces exhibited within the product.

The DSC spectrum, Figure 4.7, shows exothermic transitions for both of the DEPB:mock-HEB systems. The system in ethanol does not exhibit clear transitions and appears to just degrade, whereas, the water system has three exothermic transitions with the most drastic occurring at 200°C. The reactants of DEPB and mock-HEB had initial

transitions occur around 70°C and 85°C respectively. IR and TGA spectra were displayed over the same coordinates for comparison, however, the individual IR spectra can be found in Appendix A.

Table 4.1. TGA Values of 2,2'-Biimidazole, mock-HEB, DEPBP and Reaction Product

Compound	10 %	50 %	Scan rate (deg/min)
2,2'-Biimidazole	270oC	310oC	5
Mock-HEB	145oC	225oC	5
DEPBP	175oC	243oC	5
DEPBP + mock-HEB	215oC	255oC	5
DEPBP + mock-HEB	265oC	310oC	20

**4.2.5.5 Comparison of Reactions.** The IR spectra were obtained by spreading a thin film of the viscous compound over a KBr plate. When plotting IR spectra over the same coordinates for the four transesterification reaction, similar characteristic bands are evident, illustrated in Figure 4.9. It is interesting to note that the ethanol system had a broader OH band than that of the same components but with water.

The TGA analysis of the compounds demonstrate stability at around 90% mass or 10% mass loss. For the transesterification products, the stability temperatures were around 240°C for the HEB:DMPBP product, 260°C for the HEB:DEPBP product, 200°C for the DEPBP:mock-HEB with ethanol product, and 210°C for DEPBP:mock-HEB with water product listed in Table 4.2 with the spectra given in Figure 4.10. At 50% mass loss, the temperatures are 390°C, 290°C, 405°C, and 425°C correspondingly. These products could be exhibiting intramolecular and intermolecular interactions.

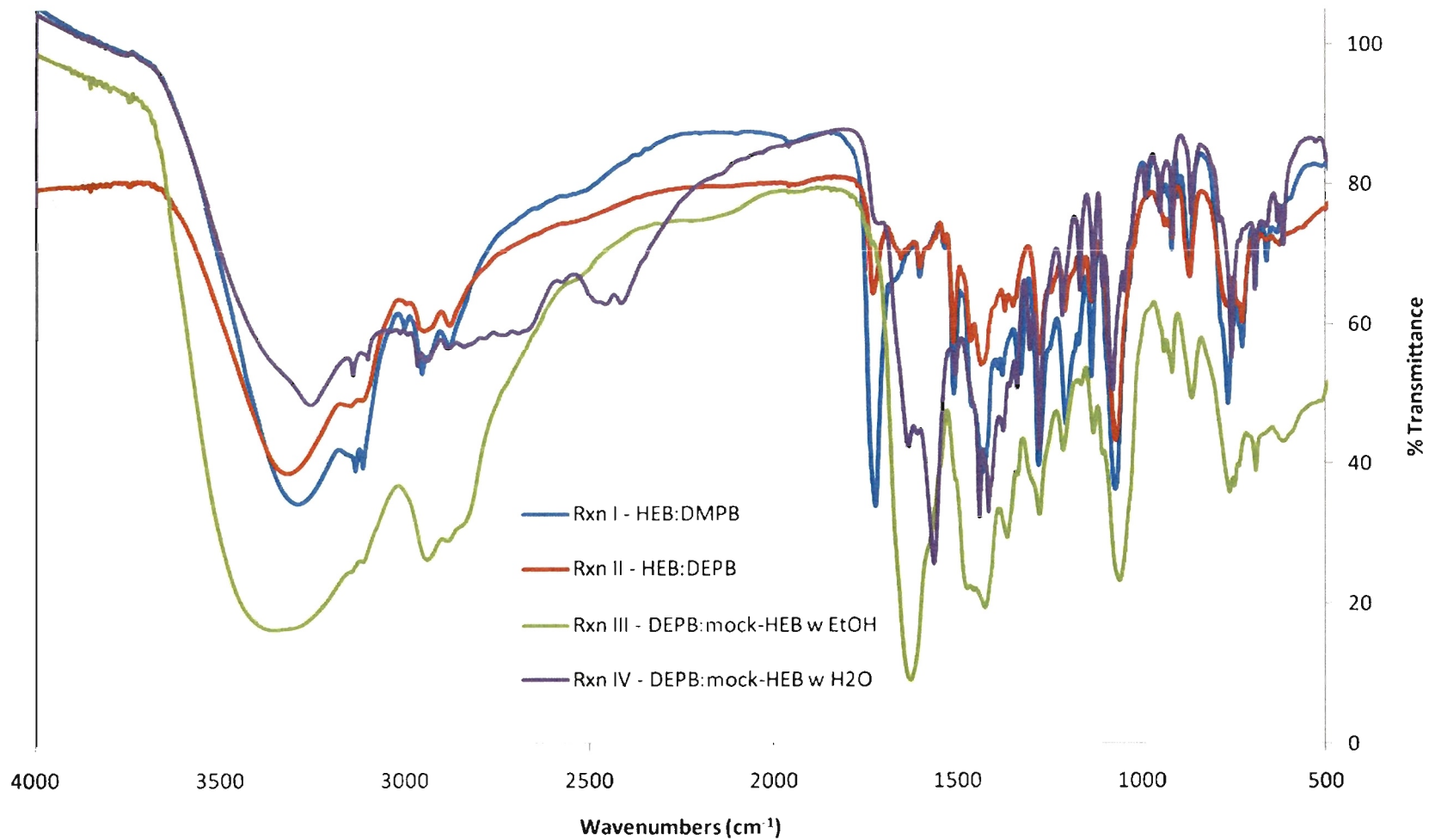


Figure 4.9. IR overlay of HEB:DMPB, HEB:DEPB, DEPB:mock-HEB w EtOH, and DEPB:mock-HEB w H<sub>2</sub>O

Table 4.2. TGA Values of Reaction Products

Reaction Product	10 %	50 %
HEB:DMPB	240oC	390oC
HEB:DEPB	260oC	290oC
DEPB:mock-HEB w EtOH	200oC	405oC
DEPB:mock-HEB w H2O	210oC	425oC

The compilation of DSC spectra, illustrated Figure 4.11, shows exothermic transitions for all the transesterification products. The system in ethanol appears to just degrade, whereas, the water system has three exothermic transitions with the most drastic occurring at 200°C. All the systems have different transitions and may reflect a skewed distribution in condensation of the ester and alcohol.



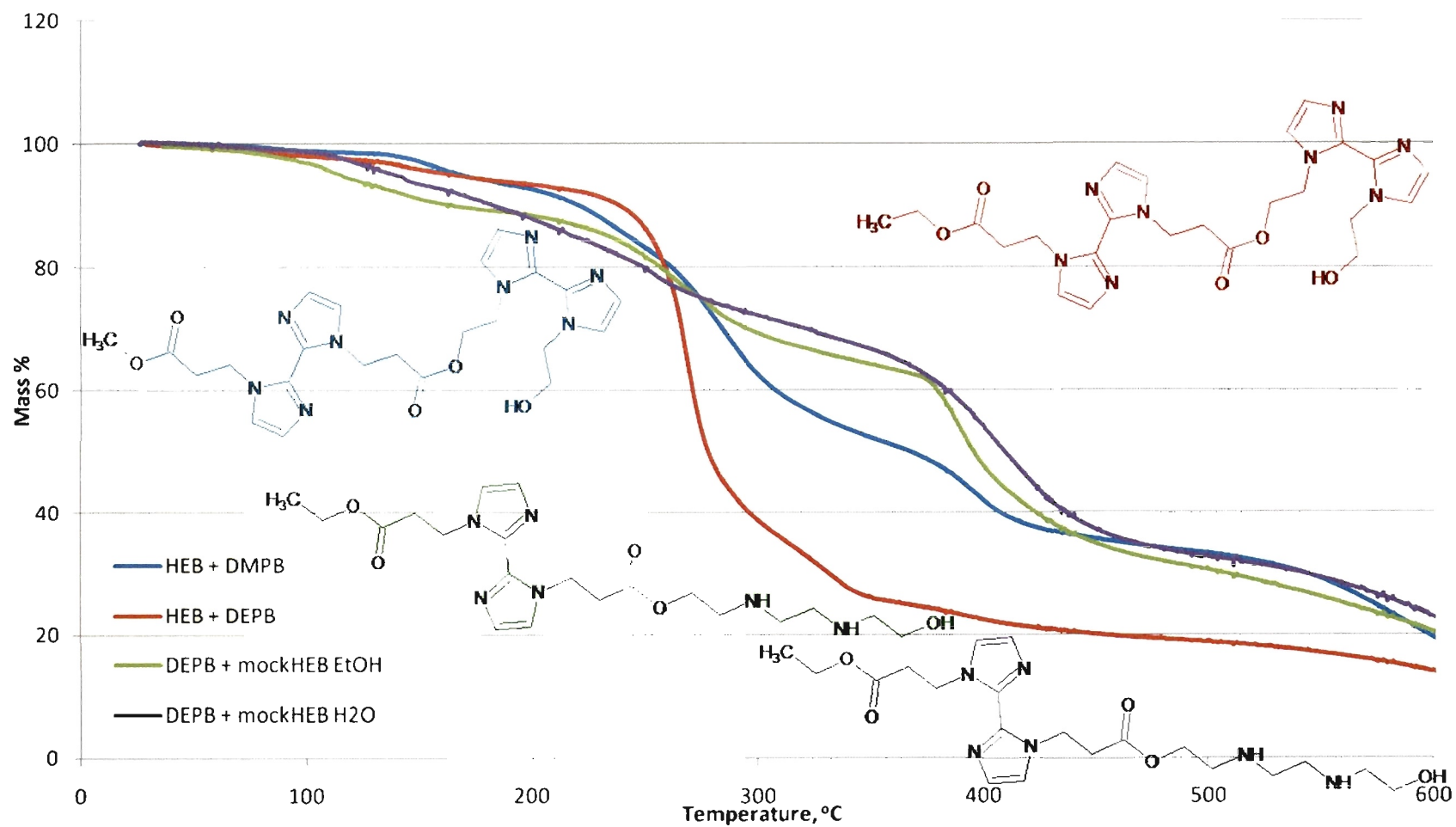


Figure 4.10. TGA overlay of HEB:DMPB, HEB:DEPBB, DEPBB:mock-HEB w EtOH, DEPBB:mock-HEB w H<sub>2</sub>O.

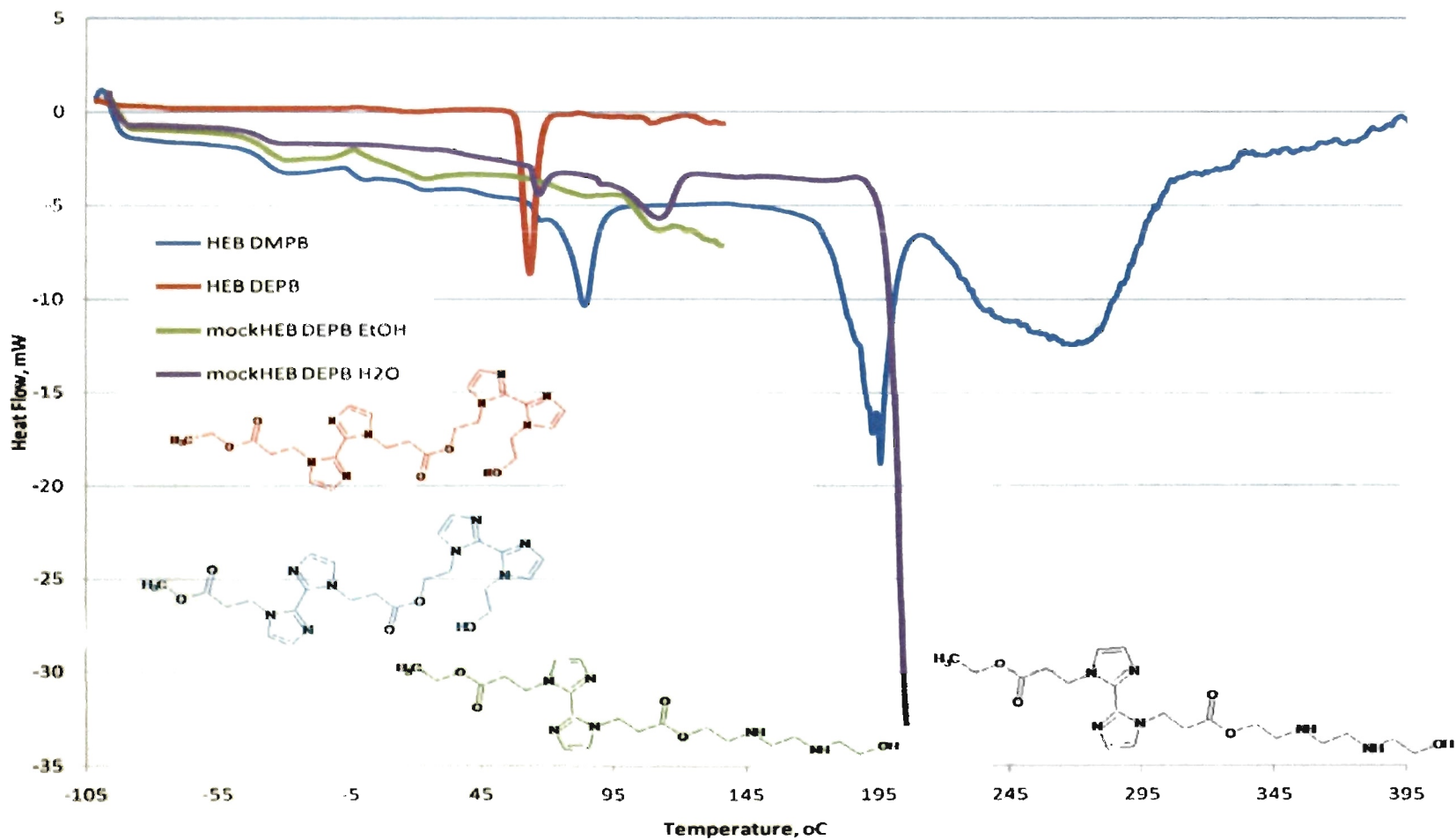


Figure 4.11. DSC overlay of HEB:DMPB, HEB:DEPB, DEPBB:mock-HEB w EtOH, DEPBB:mock-HEB w H<sub>2</sub>O.

**4.2.6 Molecular Weight Determination.** The use of boiling point elevation was used to determine molecular weight. The relationship is defined in Equation 4.9. Using the weight of the solute,  $W_2$ , and weight of the solvent,  $W_1$ , along with the boiling point constant for the solvent, ethanol,  $K_b$ , and the change in temperature,  $\Delta T$ , the molecular weight,  $M$ , can be calculated. Table 4.3 shows the average molecular weight and then the number of mers in the particular system. The mers were calculated by dividing the average molecular weight as calculated from the change in temperature, by the sum of the alcohol and ester molecular weights, Equation 4.10.

$$M = K_b \frac{1000 W_2}{\Delta T W_1} \quad \text{Equation 4.9}$$

$$Mer = \frac{Average}{MW_{alcohol} + MW_{ester}} \quad \text{Equation 4.10}$$

Table 4.3 shows the average molecular weight determination and then the number of mers in the particular system. The resulting data shows that oligomeric and not polymeric species were formed, ranging from about two to five mers.

Table 4.3. Molecular Weight and Mer Determination

Reaction	Alcohol	MW	Ester	MW	Avg	Mer
HEB:DMPB	HEB	222.24	DMPB	306.32	$1.6 \times 10^2$	3.0
HEB:DEPB	HEB	222.24	DEPB	334.37	$2.6 \times 10^2$	4.7
DEPB:mock-HEB wEtOH	mockHEB	148.20	DEPB	334.37	$1.2 \times 10^2$	2.4
DEPB:mock-HEB wH2O	mockHEB	148.20	DEPB	334.37	$8.6 \times 10^2$	1.8

## 5 METAL COMPLEXATION OF POLYMERIC 2,2'-BIIMIDAZOLE AND DERIVATIVES

### 5.1 METAL COMPLEX POLYMERIZED

From the general overview diagram, illustrated in Figure 5.1, this section represents the monomer complex undergoing polymerization resulting in a polymer complex. However, noting the metal complexes listed in Table 3.1 and Table 3.2 (Section 3) possible metal ion candidates can be determined. There are currently no reported crystal structures of metal complexes of any ester derivatives of 2,2'-biimidazole, although a crystal structure of silver nitrate with 1,1'-di(ethylpropionato)-2,2'-biimidazole was partially resolved at Missouri University of Science and Technology, Figure 3.8.

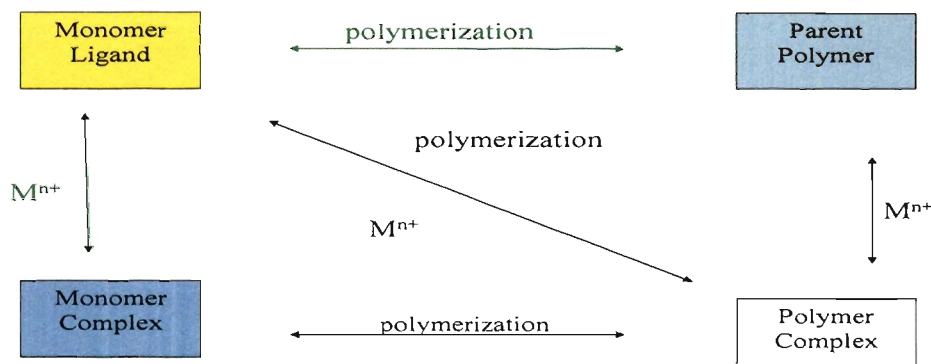


Figure 5.1. Strategic model for 2,2'-biimidazole-based esters.

## 5.2 POLYMER CHELATED BY A METAL

Figure 5.1 also shows the general reaction pathway of the parent polymer in the top right corner reacting with a metal ion to produce a macromolecular coordination compound with 2,2'-biimidazole moiety. Lister [112] and Lister and Collier [116] reported on the metal ion binding of copper with polyester containing 2,2'-biimidazole. However no crystal structure was reported.

## 5.3 2,2'-BIIMIDAZOLE OR 2,2'-BIIMIDAZOLE DERIVATIVE DIRECTLY POLYMERIZED BY A METAL SALT

The pathway in Figure 5.1 from the monomer going diagonally to the polymer complex also represents a viable route for a macromolecular metal complex of 2,2'-biimidazole. In an effort to get metal complexed esters of 2,2'-biimidazole, copper(II) acetate was combined with 2,2'-biimidazole and esters of 2,2'-biimidazole. As a result, some metal complexed polymeric species were produced. Currently, the example for this process is the helical silver biimidazole structure reported by Hester *et al.* [71].

## 5.4 EXPERIMENTAL – SYNTHESIS OF LIGAND WITH COPPER(II) ACETATE

Into a 10 mL Erlenmeyer flask, 1.257 g  $\text{Cu}(\text{CH}_3\text{COO})_2 \cdot \text{H}_2\text{O}$  were added along with 2 mL hot distilled  $\text{H}_2\text{O}$ . The flask was gently agitated. To this flask, 1.0 mL hot ethanol was added. The flask was placed in a sand bath for 5 minutes.

In a 10 mL Erlenmeyer flask,  $3.856 \times 10^{-1}$  g pink ester ligand were added along with 1.0 mL hot distilled  $\text{H}_2\text{O}$ . The flask was gently agitated and placed in the sand bath for 3 minutes.

The ester/ligand solution was added to the copper(II) acetate solution dropwise and gently agitated. After the flask was cool enough to touch, the flask was then placed in an ice bath for 15 minutes.


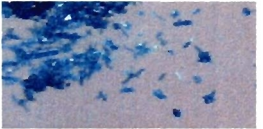


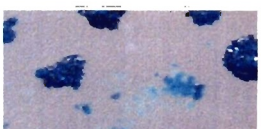
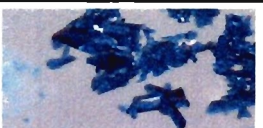
See Table 5.1 for amounts used for the ligand copper acetate syntheses.

Table 5.1. Amounts of Copper(II) Acetate and Ligands Used and Mixture Recovered

g Cu(CH <sub>3</sub> COO) <sub>2</sub> ·H <sub>2</sub> O	g Ligand	Amount recovered
1.257 g	0.3856 g DEAB	1.011 g
0.9366 g	0.3895 g DEPB	0.589 g
1.0448 g	0.50678 g DMPB	0.5888 g
1.01870 g	0.33931 g DEA*B	0.9275 g
1.35115 g	0.14010 g HEB:DMPB	1.0433 g
0.96137 g	0.23568 g DMAB	0.5582 g

Table 5.2 indicates the elemental analysis for the ligand copper acetate mixtures and their relative ratios to one another. These relationships are more indicative of an associated metal salt as opposed to a single crystal or metal ligand adduct. However the products did not undergo a second recrystallization.

Table 5.2. Elemental Analysis of Copper(II) Acetate and Ligand Recovered with Metal Ligand Ratios

Ligand	Analyzed %C, %H, %N	Theoretical %C, %H, %N	M:L	Product image at 10X magnification*
DEAB	24.89, 2.89, 0.70	27.74, 3.47, 0.70	42:1	
DEPB	24.21, 2.41, 0.23	26.87, 3.38, 0.23	130:1	
DMPB	24.20, 2.86, 0.27	26.86, 3.37, 0.27	112:1	
DEA*B	35.63, 3.47, 5.86	34.87, 4.10, 5.43	4:1	
HEB:DMPB	24.09, 2.80, 0.12	26.60, 3.35, 0.12	500: (1:1)	
DMAB	24.22, 3.05, 0.22	26.71, 3.35, 0.22	140:1	
Cu-acetate		26.44, 3.33, 0		

\*Products were not recrystallized.

## 6 SUMMARY

### 6.1 OUTCOMES

This investigation of the preliminary model development of the complex formation of a macroligand system with multi-metal binding sites of 2,2'-biimidazole can be viewed through five pathways. Figure 6.1 illustrates the general model. The results will be grouped by focusing on a specific portion of the strategic model.

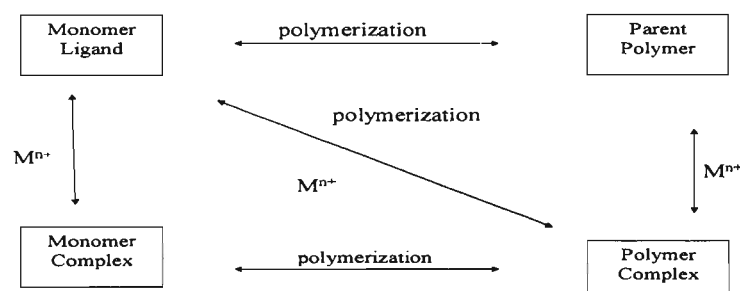


Figure 6.1. Strategic model for 2,2'-biimidazole-based esters.

No biological activity was tested, however, given the background on anti-protozoal, anti-fungal, and anti-parasitic activity, the ester derivatives should be studied for effectiveness and possible applications as such.

**6.1.1 Monomer Ligand.** Selection of monomers included those suitable for transesterification, esters and alcohols. The monomers chosen were those previously reported by the Collier group along with two additional diesters. [104-108] Figure 6.2 represents the general global schematic with the monomer ligand highlighted.



The synthesis of 1,1'-di(methylacetato)-2,2'-biimidazole (DMAB), 1,1'-di(methylpropionato)-2,2'-biimidazole (DMPB), 1,1'-di(ethylpropionato)-2,2'-biimidazole (DEPB), 1,1'-di(methylacrylate)-2,2'-biimidazole (DMA\*B), 1-hydroxyethyl-2,2'-biimidazole (mono-HEB), and 1,1'-di(hydroxyethyl)-2,2'-biimidazole (HEB) were previously reported and successfully reproduced. In addition, the synthesis of 1,1'-di(ethylacetato)-2,2'-biimidazole (DEAB) and 1,1'-di(ethylacrylate)-2,2'-biimidazole (DEA\*B) were added along with the use of N,N'-bis(2-hydroxyethyl)ethylenediamine, which is commercially available.

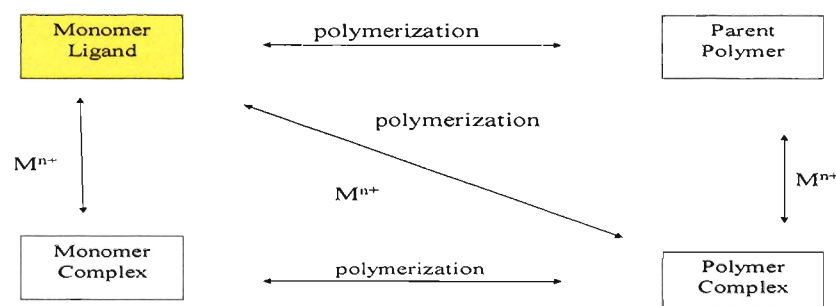


Figure 6.2. Strategic model for 2,2'-biimidazole-based esters with focus on monomer.

The crystal structure determination of two single crystals, 2,2'-bis(1H-imidazolium) dinitrate and silver bis(1H-imidazolium) trinitrate along with the crystal data from the Baughman group of 2,2'-bis(1H-imidazolium) dibromide and 2-(1H-imidazol-2-yl)-1H-imidazol-3-ium nitrate reveal stability of the cationic biimidazole and the effect of the acid and counter anion. [93] Based on the higher electronegative counter anion, the rings become more planar and may lead to a less sterically hindered polymerization process of the imine nitrogen of the imidazole ring.

### 6.1.2 Parent Polymer. Polymerization was performed via transesterification.

Figure 6.3 illustrates the general global schematic with the parent polymer highlighted.

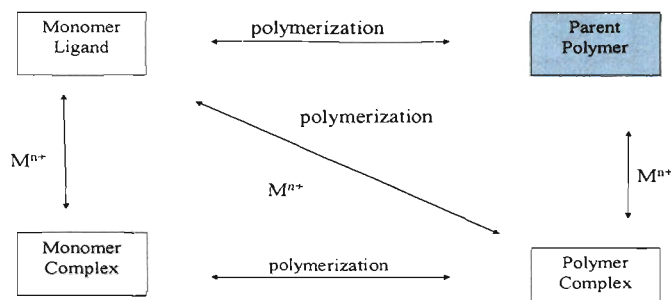


Figure 6.3. Strategic model for 2,2'-biimidazole-based esters with focus on parent polymer.

Polymer synthesis and determination via the Huggins and Kraemer equations is not conclusive or typical of an ideal and well defined polymer system. Since there are no constants for the 2,2'-biimidazole ester system, it is possible that a more dilute concentration range may be needed or studied. However, due to the amphoteric nature of biimidazole, it is highly likely that a linear fit will not define the solvent polymer system. Multiple trials should be employed to establish and determine Mark-Houwink-Sakurada parameters for this unknown system. Additional experimentation should be performed using different catalysts to determine efficiency, reaction rates, and polymer size.

DSC curves of all four systems exhibited exothermic transitions. Molecular weight determinations based on the colligative property of boiling point elevation revealed oligomeric systems ranging from two mers to five mers.

**6.1.3 Monomer Complex.** Figure 6.4 highlights the monomer complex. Metal complexation experiments of monomers were studied resulting in some viable crystals that were not reported here. The cobalt complexes seemed to form readily and did not exhibit polymeric species, but the biimidazole ligand showed bidentate binding.

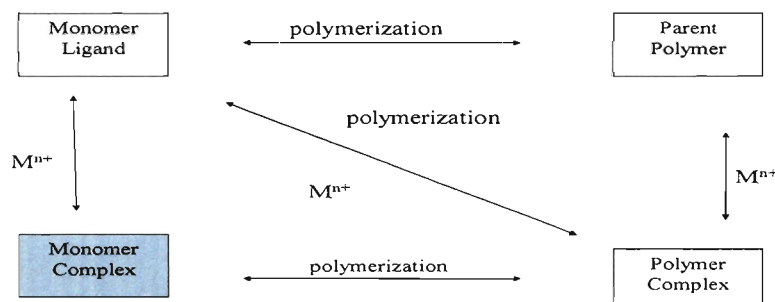


Figure 6.4. Strategic model for 2,2'-biimidazole-based esters with focus on monomer complex.

Simple reactions with metal salts revealed crystalline products. These products were associated within the crystalline matrix of the metal salt and not directly bound to the metal. However a crystal structure was partially resolved in the case of silver nitrate with 1,1'-di(ethylpropionato)-2,2'-biimidazole.

No biological activity was tested, however, given the background on anti-protozoal, anti-fungal, and anti-parasitic activity, the ester derivatives should be studied for effectiveness and possible applications as such.

**6.1.4 Polymer Complex.** The last stage of the model system focuses on the polymer complex, highlighted in Figure 6.5. This illustration shows that there are three possible routes.

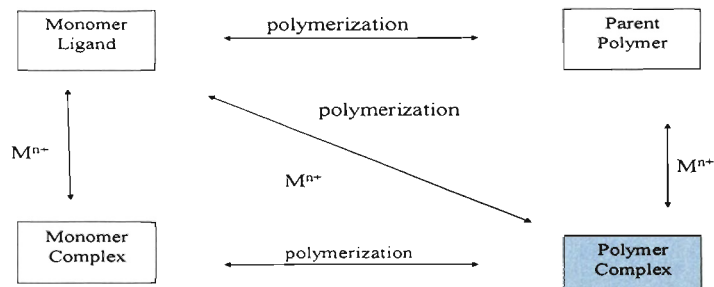


Figure 6.5. Strategic model for 2,2'-biimidazole-based esters with focus on polymer complex.

The copper(II) acetate reactions with the esters of 2,2'-biimidazole had relative ratios of metal to ligand from 1:4 to 1:500 revealing a mixture. These relationships are more indicative of an associated metal salt as opposed to a single crystal or metal ligand adduct. However, multiple recrystallizations were not conducted.

## 6.2 FURTHER STUDY

The ability to understand and determine the rate of formation is quite desirable. Once the metal complexed derivatives can be completely characterized, the specified parameters can be monitored to determine kinetic information. This could possibly lead to morphological differences and design based targets, engineering a specific binding geometry or particular linkage. Moreover, given the amphoteric nature of 2,2'-biimidazole potentiostatic and galvanic studies as a function of pH can aid in the determination of structure property relationship, and further describe its polymorphic ability.

Derivatives of 2,2'-biimidazole should be viewed in terms of polymerization. Other derivatives, like a vinyl or carboxylate, may have interesting properties to easily polymerize and effectively determine rate and distribution of polymerization. These polymer systems may be easier to study. Additionally, the ability to differentiate between 2,2'-biimidazole, 4,4'-biimidazole, and bisimidazole systems would assist in metal selection.

APPENDIX A

INFRARED SPECTRA

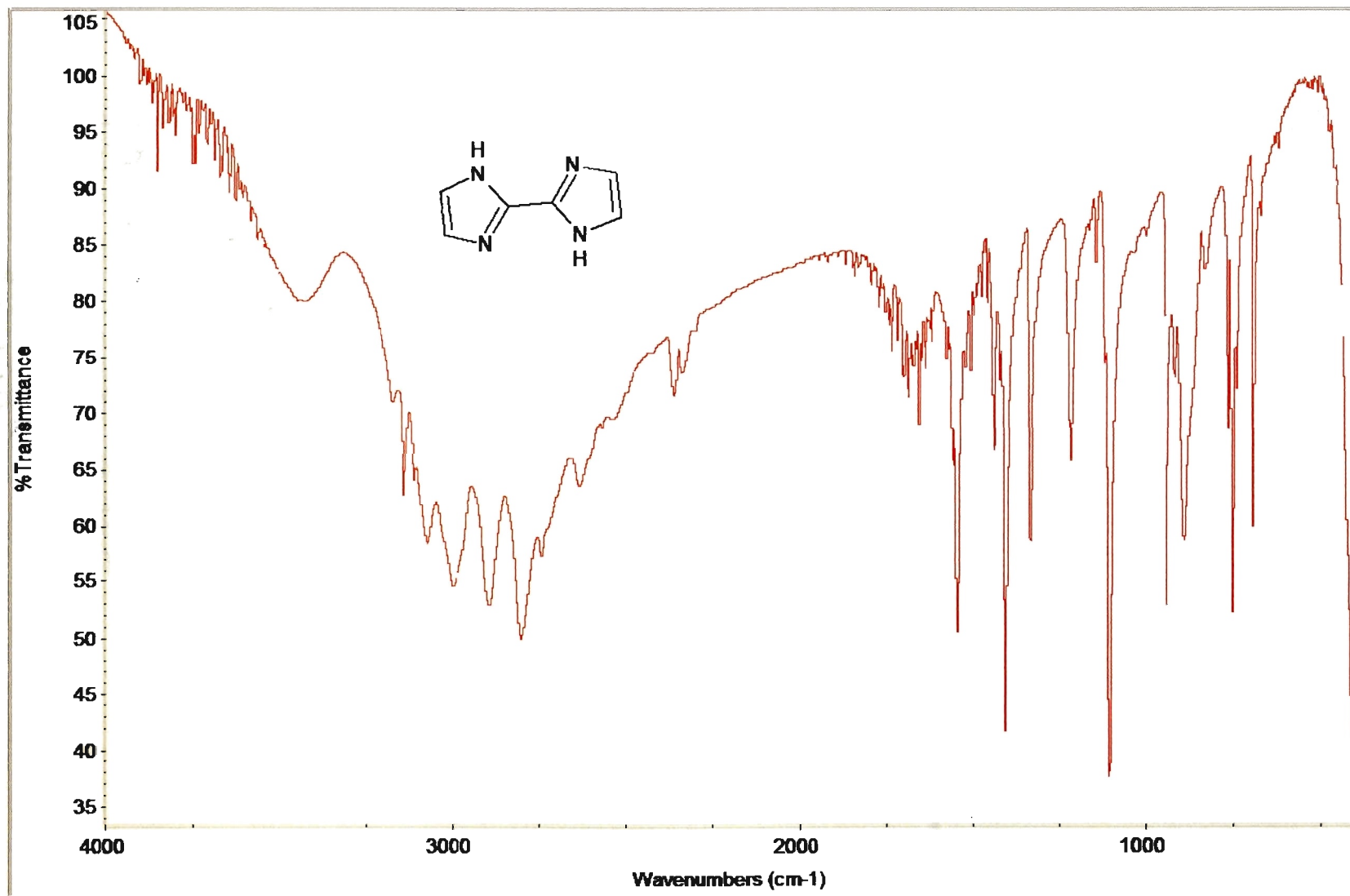


Figure A.1. Infrared spectrum of 2,2'-biimidazole.

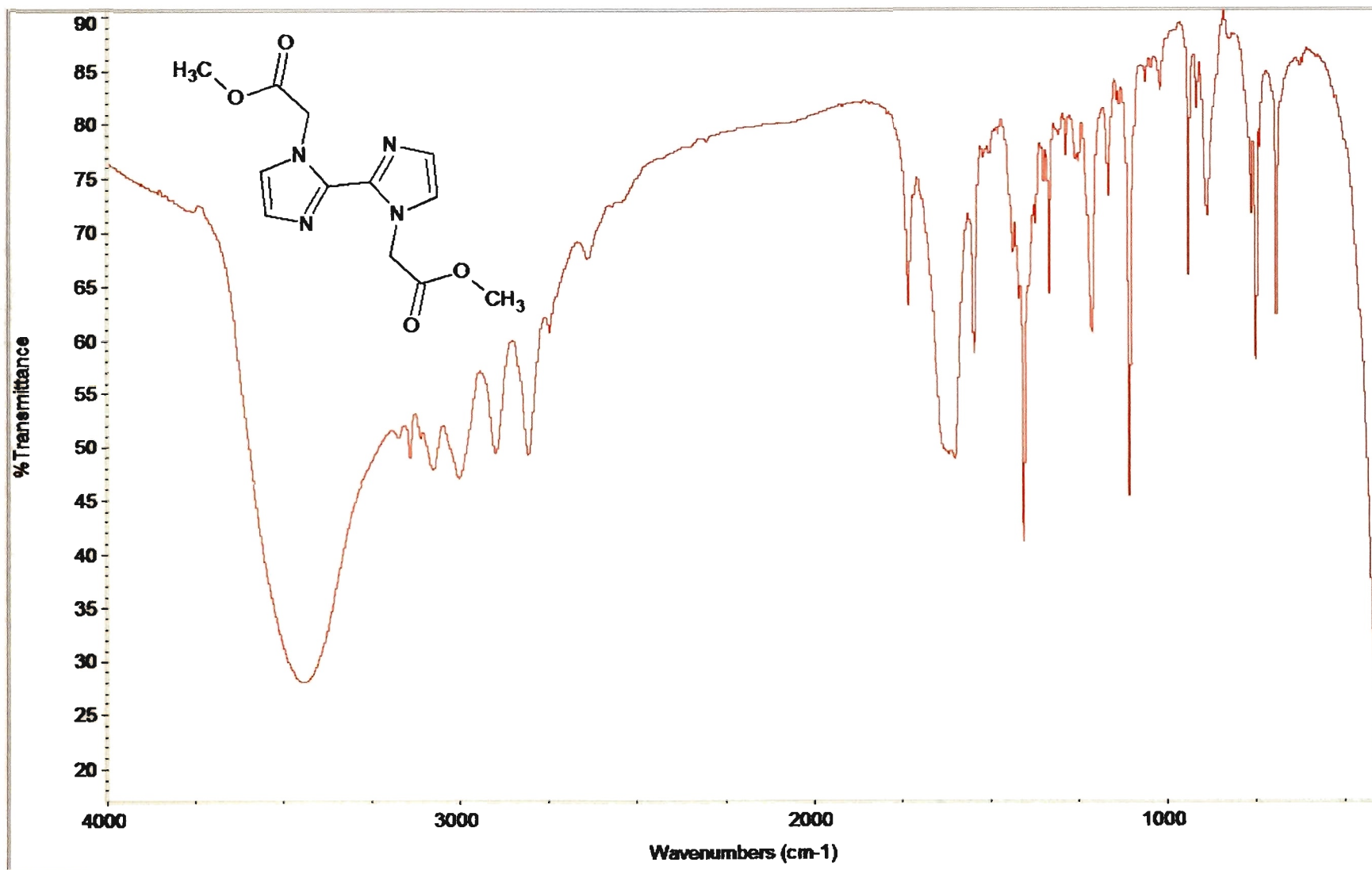


Figure A.2. Infrared spectrum of 1,1'-di(methylacetato)-2,2'-biimidazole.



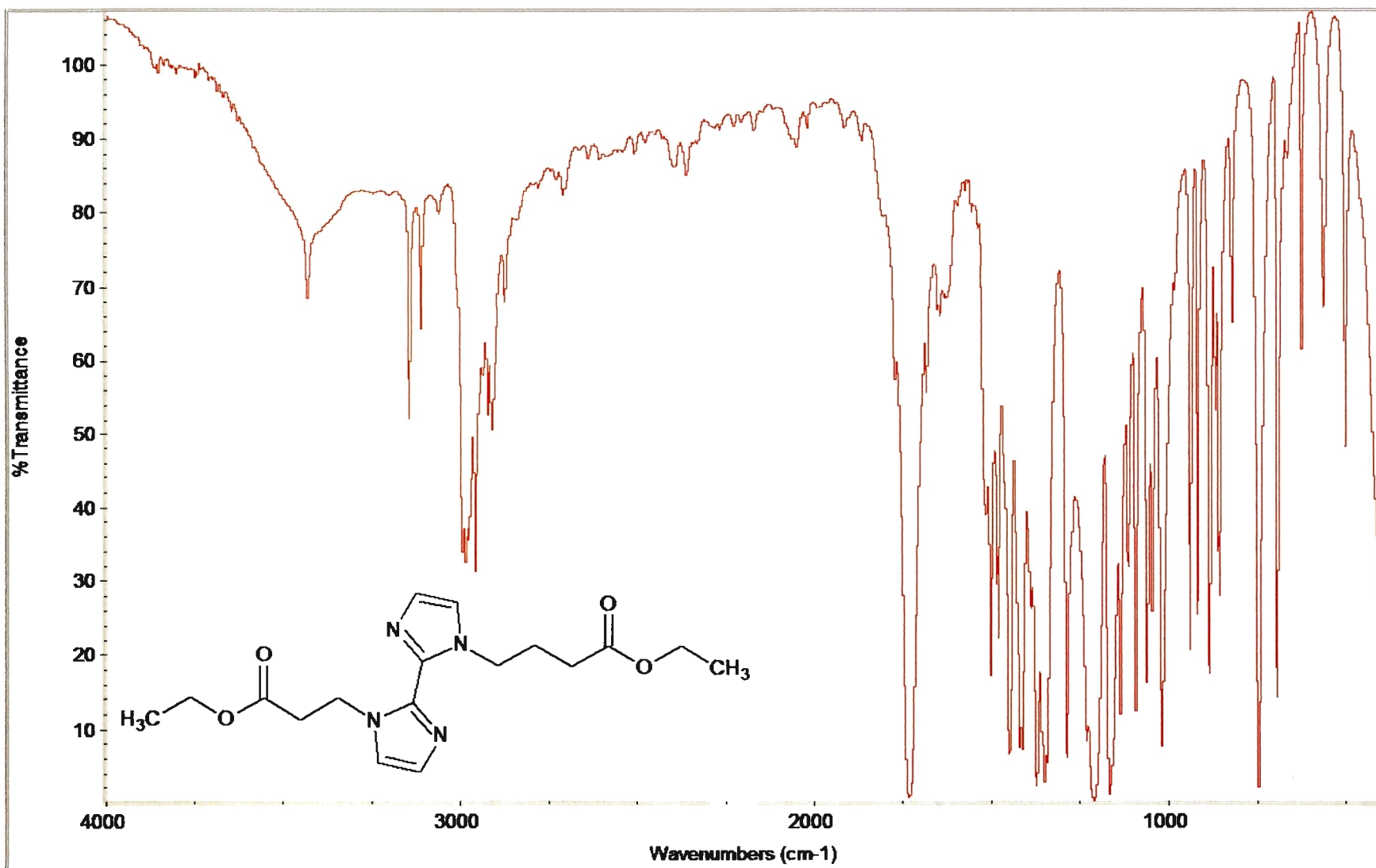


Figure A.3. Infrared spectrum of 1,1'-di(ethylpropionato)-2,2'-biimidazole.

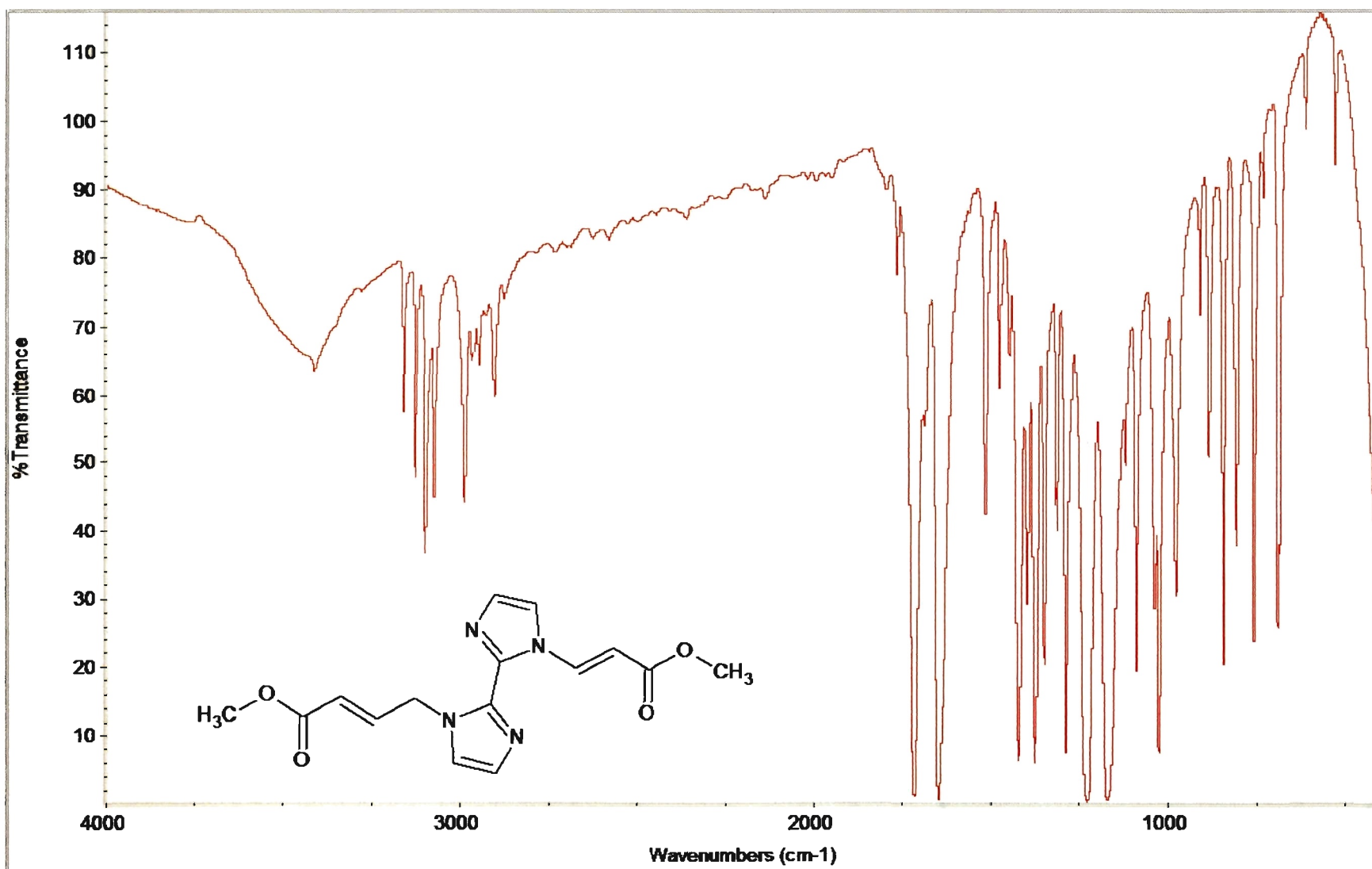


Figure A.4. Infrared spectrum of 1,1'-di(ethylacrylate)-2,2'-biimidazole.

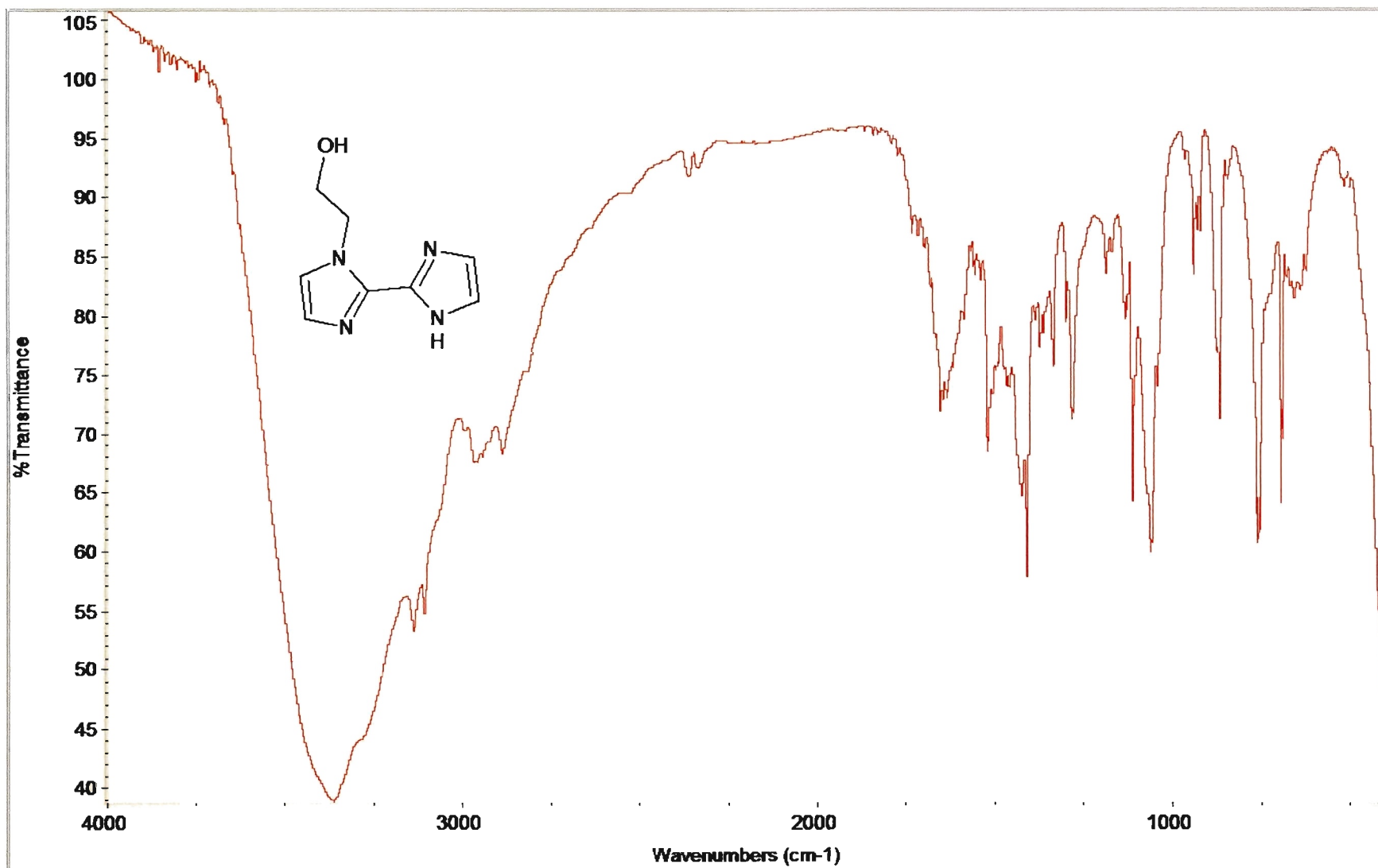


Figure A.5. Infrared spectrum of 1-hydroxyethyl-2,2'-biimidazole.

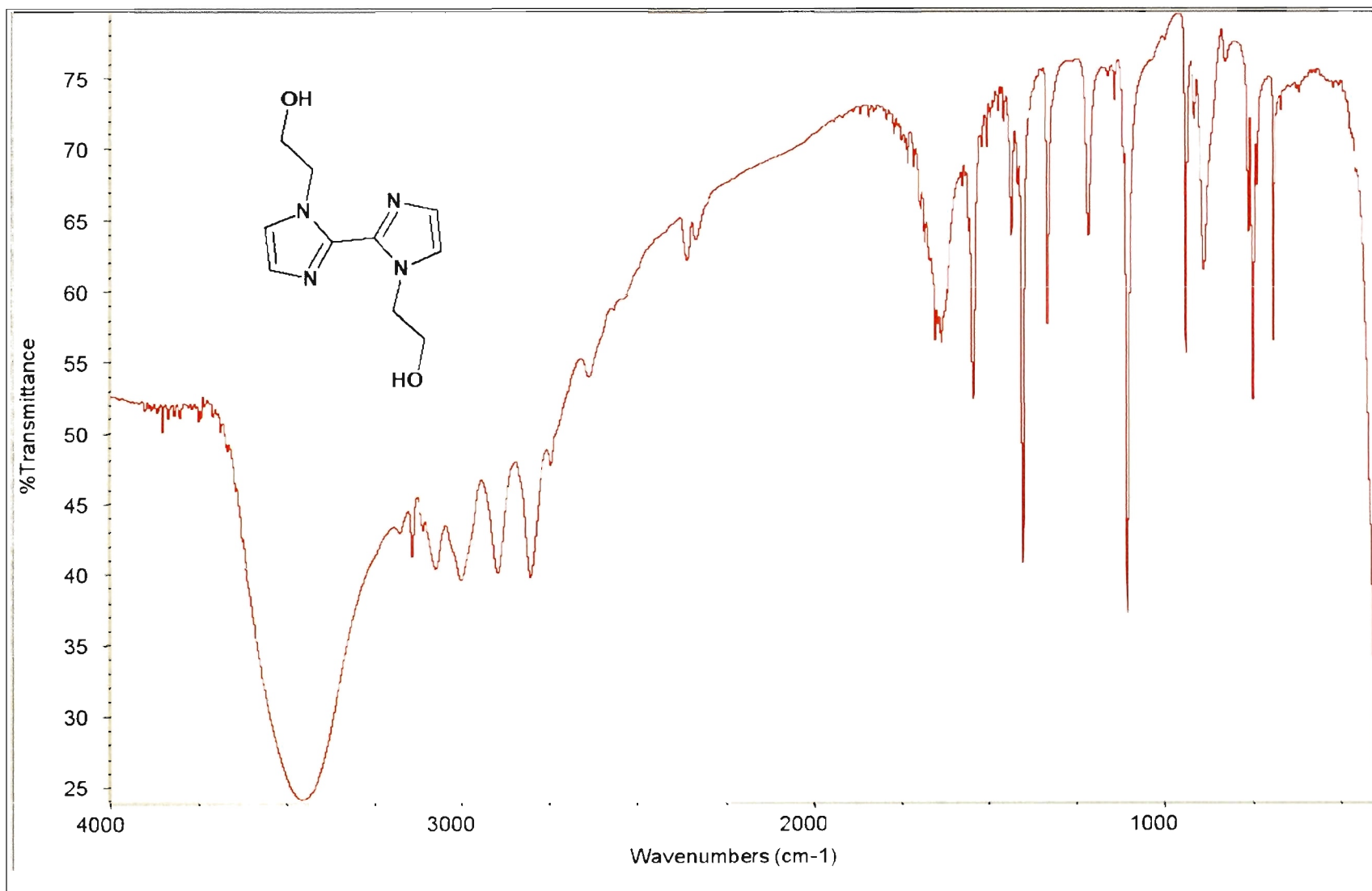


Figure A.6. Infrared spectrum of 1,1'-di(hydroxyethyl)-2,2'-biimidazole.

### Rxn I - HEB:DMPB

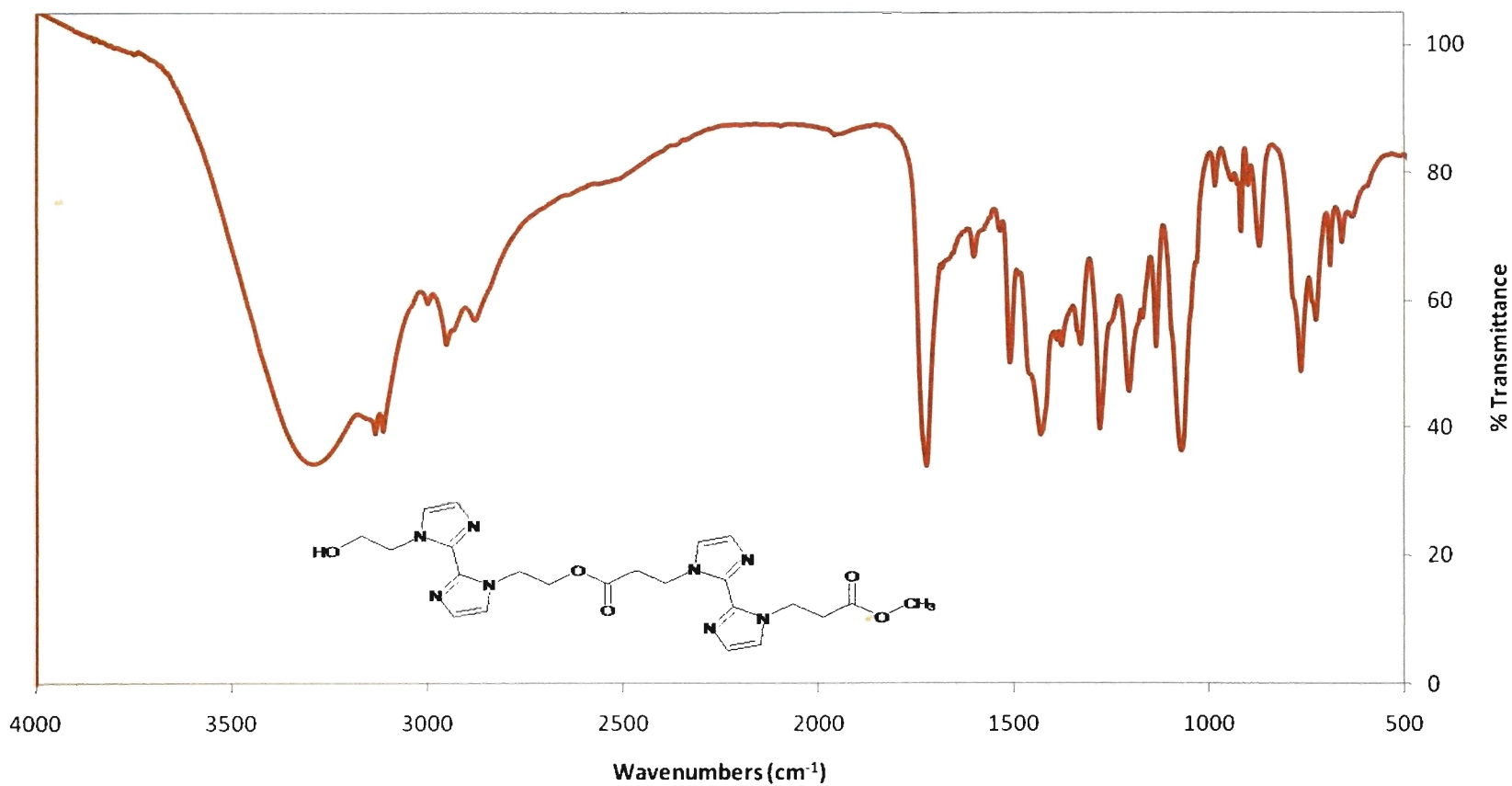


Figure A.7. Infrared spectrum of HEB:DMPB

### Rxn II - HEB:DEPB

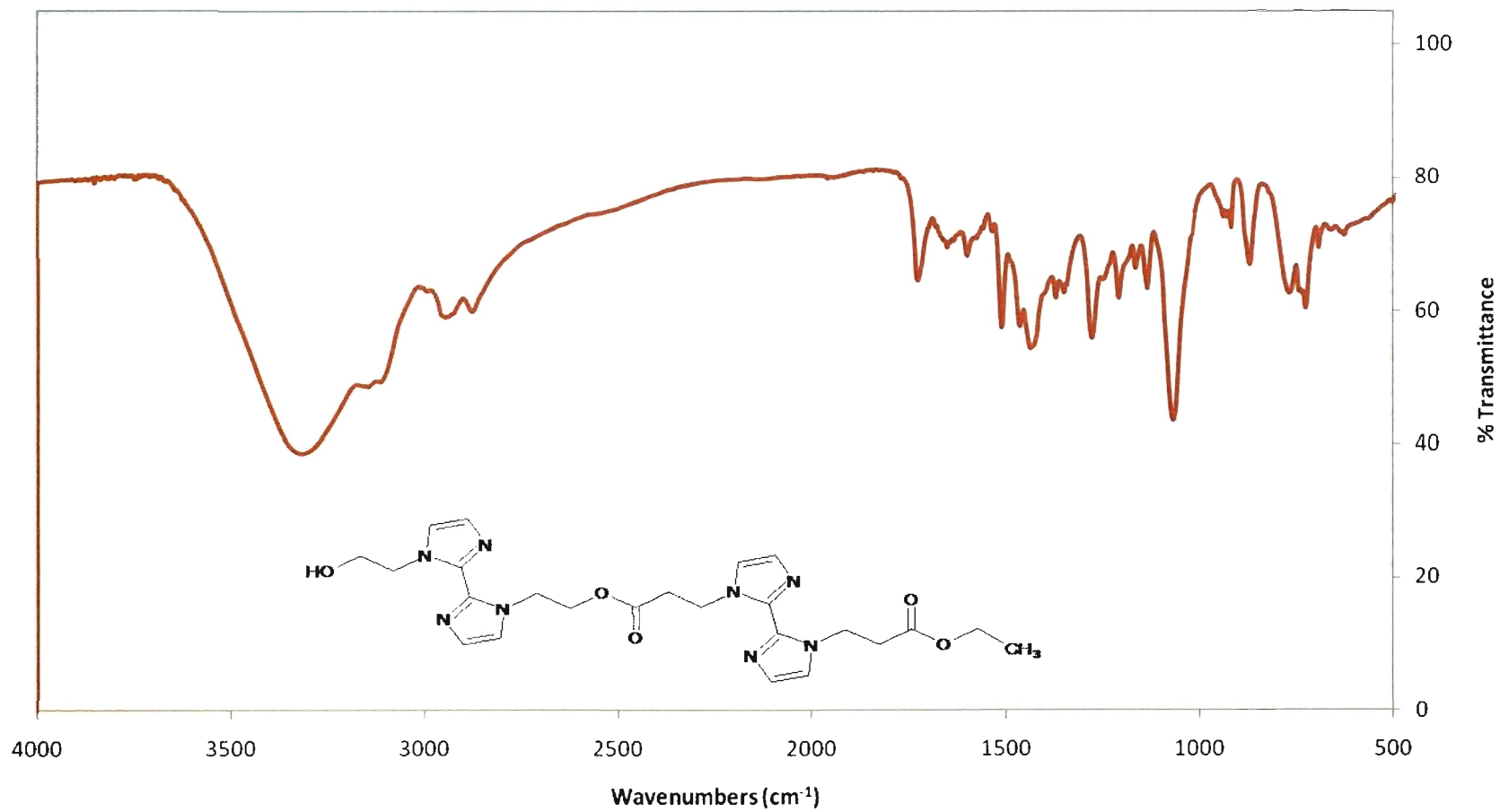


Figure A.8. Infrared spectrum of HEB:DEPB product .

### Rxn III - DEPB:mock-HEB w EtOH

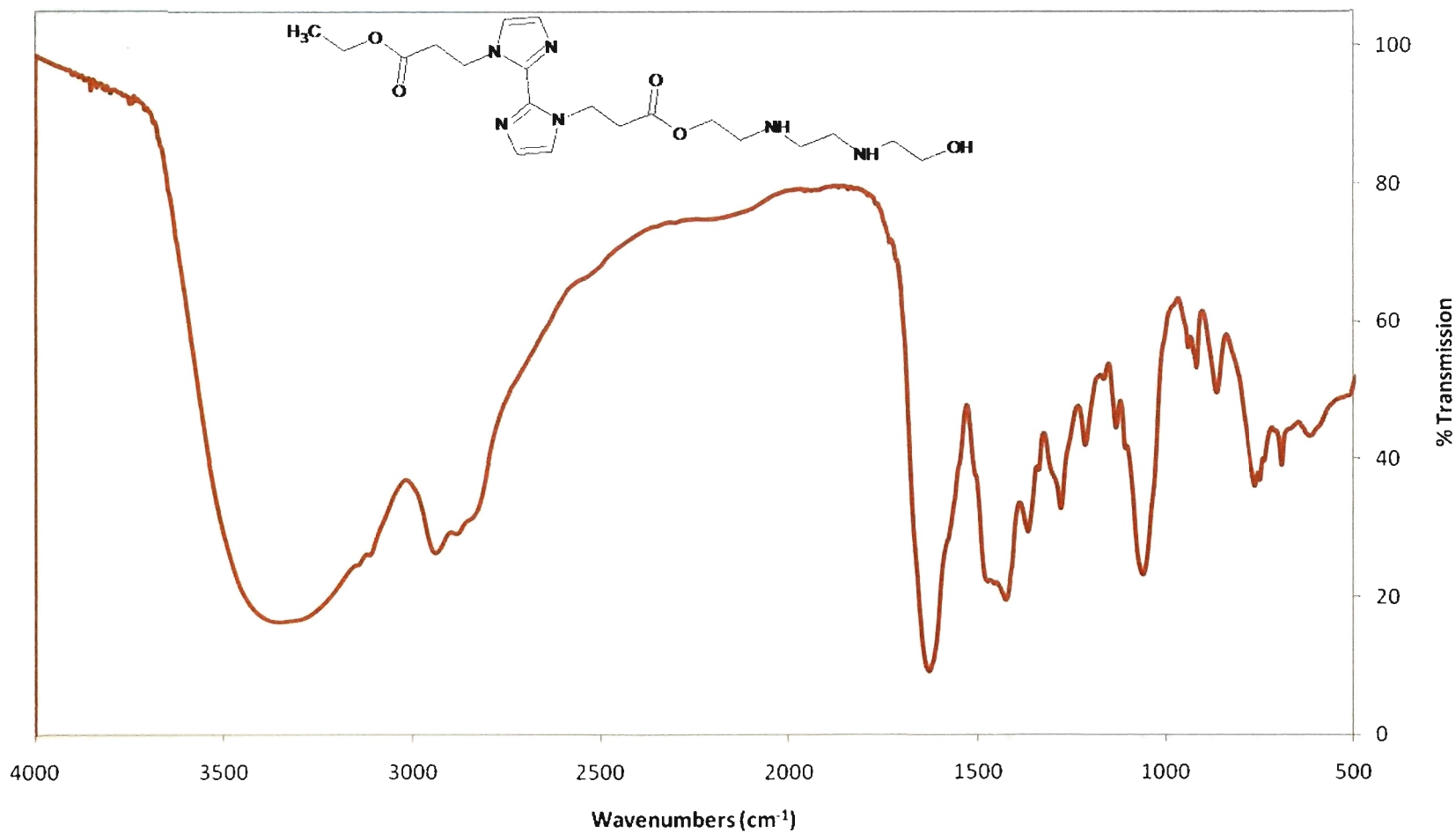


Figure A.9. Infrared spectrum of DEPB:mock-HEB product with ethanol.

### Rxn IV - DEPB:mock-HEB w H2O

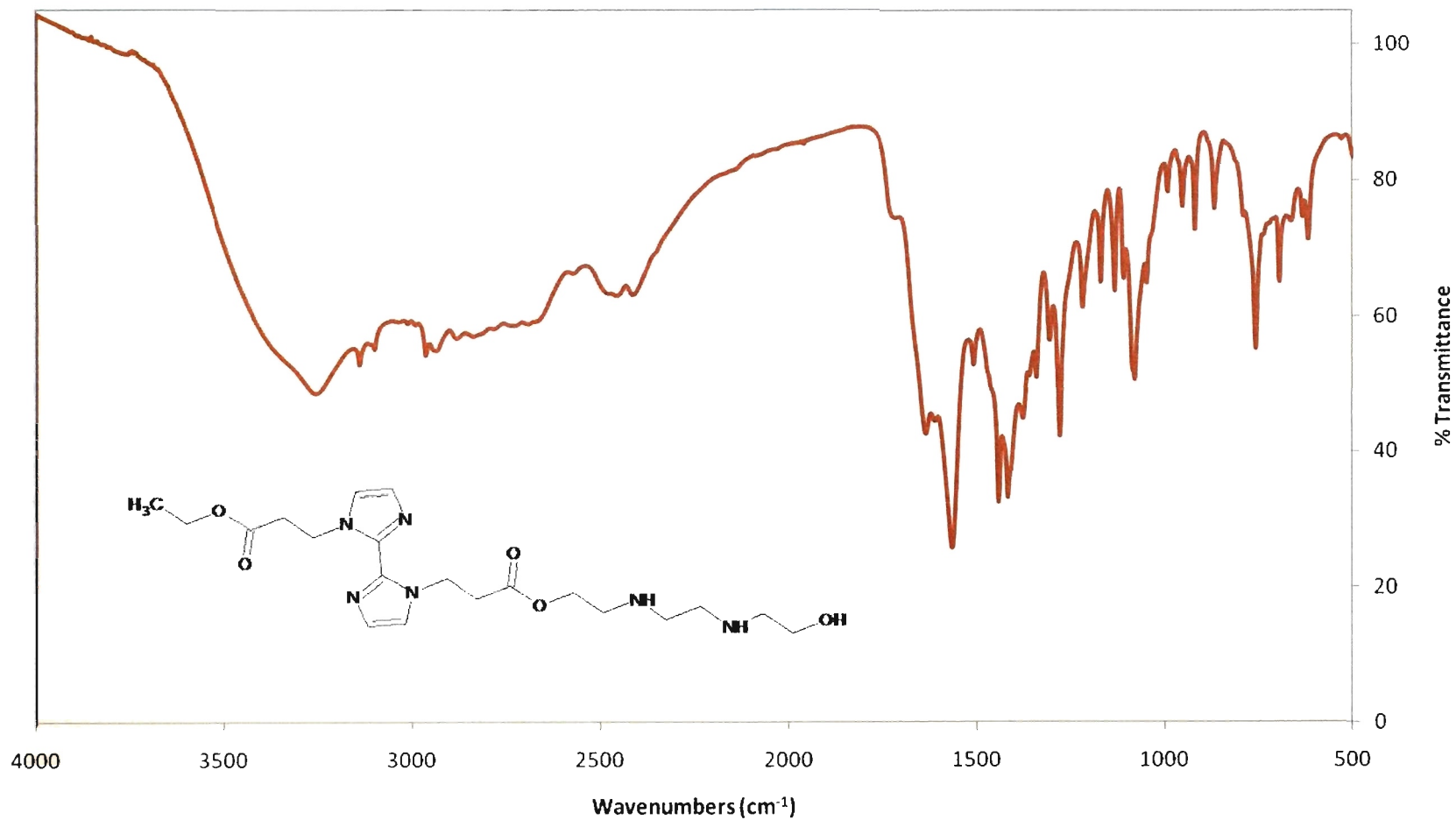


Figure A.10. Infrared spectrum of DEPB:mock-HEB product with water.



APPENDIX B

CRYSTALLOGRAPHIC TABLES

Table B.1. Crystal Data and Structure Refinement for [biimH<sub>2</sub>][NO<sub>3</sub>]<sub>3</sub>

Identification code	fincham	
Empirical formula	C <sub>8</sub> H <sub>10.67</sub> N <sub>8</sub> O <sub>8</sub>	
Formula weight	346.91	
Temperature	298 K	
Wavelength	0.71073 Å	
Crystal system	Orthorhombic	
Space group	P2(1)2(1)2	
Unit cell dimensions	a = 12.9534(10) Å	α = 90°.
	b = 7.2114(6) Å	β = 90°.
	c = 11.3479(9) Å	γ = 90°.
Volume	1060.03(15) Å <sup>3</sup>	
Z	3	
Density (calculated)	1.630 Mg/m <sup>3</sup>	
Absorption coefficient	0.146 mm <sup>-1</sup>	
F(000)	536	
Crystal size	? x ? x ? mm <sup>3</sup>	
Theta range for data collection	1.79 to 28.42°.	
Index ranges	-17 ≤ h ≤ 17, -9 ≤ k ≤ 9, -14 ≤ l ≤ 15	
Reflections collected	11298	
Independent reflections	2653 [R(int) = 0.1402]	
Completeness to theta = 28.42°	100.0 %	
Absorption correction	None	
Refinement method	Full-matrix least-squares on F <sup>2</sup>	
Data / restraints / parameters	2653 / 0 / 165	
Goodness-of-fit on F <sup>2</sup>	1.108	
Final R indices [I > 2σ(I)]	R1 = 0.0634, wR2 = 0.1488	
R indices (all data)	R1 = 0.0699, wR2 = 0.1546	
Absolute structure parameter	0.7(18)	
Largest diff. peak and hole	0.325 and -0.503 e.Å <sup>-3</sup>	

Table B.2. Atomic Coordinates ( $\times 10^4$ ) and Equivalent Isotropic Displacement Parameters ( $\text{\AA}^2 \times 10^3$ ) for  $[\text{biimH}_2][\text{NO}_3]_3$ .  $U(\text{eq})$  is Defined as One Third of the Trace of the Orthogonalized  $U^{ij}$  Tensor

	x	y	z	$U(\text{eq})$
O(31)	0	10000	6042(3)	72(1)
N(2)	985(1)	2205(2)	1143(2)	36(1)
N(11)	1373(2)	7352(2)	2500(1)	35(1)
C(1)	1788(1)	2031(3)	1857(2)	31(1)
N(10)	1030(1)	2655(2)	3806(2)	38(1)
N(7)	2659(2)	3202(3)	3638(2)	43(1)
N(5)	2554(1)	1253(3)	1268(2)	41(1)
O(11)	2310(2)	7225(3)	2556(1)	66(1)
C(6)	1825(2)	2611(3)	3074(2)	33(1)
O(13)	894(1)	8503(2)	3112(2)	51(1)
O(12)	884(1)	6323(3)	1815(2)	59(1)
C(4)	2226(2)	928(3)	143(2)	50(1)
C(8)	2382(2)	3624(3)	4765(2)	53(1)
C(3)	1257(2)	1514(3)	63(2)	47(1)
C(9)	1381(2)	3279(3)	4875(2)	50(1)
O(22)	4182(1)	10098(3)	2603(2)	73(1)
O(21)	5000	10000	960(2)	68(1)
N(21)	5000	10000	2048(3)	43(1)
N(31)	0	10000	7132(2)	41(1)
O(32)	675(2)	9180(3)	7704(2)	66(1)

Table B.3. Bond Lengths [ $\text{\AA}$ ] and Angles [ $^\circ$ ] for  $[\text{biimH}_2][\text{NO}_3]_3$ 

O(31)-N(31)	1.237(4)
N(2)-C(1)	1.325(2)
N(2)-C(3)	1.368(3)
N(11)-O(11)	1.219(3)
N(11)-O(12)	1.247(2)
N(11)-O(13)	1.248(2)
C(1)-N(5)	1.322(2)
C(1)-C(6)	1.443(3)
N(10)-C(6)	1.323(3)
N(10)-C(9)	1.372(3)
N(7)-C(6)	1.327(3)
N(7)-C(8)	1.363(3)
N(5)-C(4)	1.366(3)
C(4)-C(3)	1.328(4)
C(8)-C(9)	1.327(4)
O(22)-N(21)	1.234(2)
O(21)-N(21)	1.235(4)
N(21)-O(22)#1	1.234(2)
N(31)-O(32)#2	1.239(2)
N(31)-O(32)	1.239(2)
C(1)-N(2)-C(3)	108.12(18)
O(11)-N(11)-O(12)	119.58(18)
O(11)-N(11)-O(13)	121.07(18)
O(12)-N(11)-O(13)	119.3(2)
N(5)-C(1)-N(2)	108.67(18)
N(5)-C(1)-C(6)	125.59(17)
N(2)-C(1)-C(6)	125.74(16)
C(6)-N(10)-C(9)	107.80(19)
C(6)-N(7)-C(8)	108.1(2)
C(1)-N(5)-C(4)	108.21(19)
N(10)-C(6)-N(7)	108.84(17)
N(10)-C(6)-C(1)	125.57(16)

Table B.3. (Continued) Bond Lengths [Å] and Angles [°] for [biimH<sub>2</sub>][NO<sub>3</sub>]<sub>3</sub>

N(7)-C(6)-C(1)	125.58(17)
C(3)-C(4)-N(5)	107.6(2)
C(9)-C(8)-N(7)	107.7(2)
C(4)-C(3)-N(2)	107.4(2)
C(8)-C(9)-N(10)	107.6(2)
O(22)#1-N(21)-O(22)	118.7(3)
O(22)#1-N(21)-O(21)	120.67(16)
O(22)-N(21)-O(21)	120.67(16)
O(31)-N(31)-O(32)#2	121.57(15)
O(31)-N(31)-O(32)	121.57(15)
O(32)#2-N(31)-O(32)	116.9(3)

---

Symmetry transformations used to generate equivalent atoms:

#1 -x+1,-y+2,z #2 -x,-y+2,z

Table B.4. Anisotropic Displacement Parameters ( $\text{\AA}^2 \times 10^3$ ) for  $[\text{biimH}_2][\text{NO}_3]_3$ . The Anisotropic Displacement Factor Exponent Takes the Form:  $-2\pi^2 [h^2 a^{*2} U_{11} + \dots + 2 h k a^* b^* U_{12}]$

	U11	U22	U33	U23	U13	U12
O(31)	75(2)	98(2)	41(1)	0	0	-9(2)
N(2)	35(1)	41(1)	31(1)	-2(1)	-2(1)	4(1)
N(11)	30(1)	38(1)	38(1)	6(1)	-2(1)	0(1)
C(1)	29(1)	35(1)	30(1)	4(1)	1(1)	1(1)
N(10)	40(1)	44(1)	29(1)	-2(1)	3(1)	-2(1)
N(7)	38(1)	55(1)	35(1)	4(1)	-9(1)	-12(1)
N(5)	38(1)	51(1)	35(1)	5(1)	6(1)	10(1)
O(11)	31(1)	115(2)	52(1)	-8(1)	-1(1)	4(1)
C(6)	35(1)	38(1)	27(1)	4(1)	-3(1)	-4(1)
O(13)	39(1)	50(1)	62(1)	-14(1)	-2(1)	1(1)
O(12)	39(1)	58(1)	80(1)	-24(1)	-8(1)	3(1)
C(4)	68(2)	51(1)	31(1)	-2(1)	13(1)	11(1)
C(8)	74(2)	53(1)	32(1)	0(1)	-15(1)	-20(1)
C(3)	67(2)	47(1)	26(1)	-2(1)	-6(1)	4(1)
C(9)	75(2)	50(1)	25(1)	-3(1)	2(1)	-3(1)
O(22)	39(1)	104(2)	74(1)	37(1)	17(1)	16(1)
O(21)	81(2)	80(2)	42(1)	0	0	-21(2)
N(21)	33(1)	48(1)	48(2)	0	0	-4(1)
N(31)	34(1)	46(1)	43(1)	0	0	0(1)
O(32)	55(1)	84(1)	59(1)	-7(1)	-7(1)	30(1)

Table B.5. Hydrogen Coordinates ( $\times 10^4$ ) and Isotropic Displacement Parameters ( $\text{\AA}^2 \times 10^3$ ) for  $[\text{biimH}_2][\text{NO}_3]_3$

	x	y	z	U(eq)
H(2)	395	2671	1325	43
H(10)	405	2348	3641	45
H(7)	3269	3302	3344	51
H(5)	3155	995	1546	50
H(4)	2612	392	-458	60
H(8)	2817	4073	5352	64
H(3)	840	1464	-603	56
H(9)	988	3432	5554	60

Table B.6. Crystal Data and Structure Refinement for Ag(biimH)<sub>2</sub>(NO<sub>3</sub>)<sub>3</sub>

Identification code	sad	
Empirical formula	C <sub>12</sub> H <sub>14</sub> AgN <sub>11</sub> O <sub>9</sub>	
Formula weight	564.21	
Temperature	298(2) K	
Wavelength	0.71073 Å	
Crystal system	Monoclinic	
Space group	Cc	
Unit cell dimensions	a = 24.095(6) Å	α=90°
	b = 12.037(3) Å	β=91.319(6) °
	c = 6.8262(18) Å	γ=90°
Volume	1979.3(9) Å <sup>3</sup>	
Z	4	
Density (calculated)	1.893 Mg/m <sup>3</sup>	
Absorption coefficient	1.094 mm <sup>-1</sup>	
F(000)	1128	
Crystal size	0.05 x 0.1 x 0.5 mm <sup>3</sup>	
Theta range for data collection	1.69 to 28.36°.	
Index ranges	-32 ≤ h ≤ 32, -16 ≤ k ≤ 16, -9 ≤ l ≤ 9	
Reflections collected	9952	
Independent reflections	2467 [R(int) = 0.0669]	
Completeness to theta = 28.36°	99.6 %	
Absorption correction	SADABS	
Refinement method	Full-matrix least-squares on F <sup>2</sup>	
Data / restraints / parameters	2467 / 0 / 163	
Goodness-of-fit on F <sup>2</sup>	0.998	
Final R indices [I>2σ(I)]	R <sub>1</sub> = 0.0472, wR <sub>2</sub> = 0.0983	
R indices (all data)	R <sub>1</sub> = 0.0718, wR <sub>2</sub> = 0.1098	
Largest diff. peak and hole	0.511 and -0.430 e.Å <sup>-3</sup>	



Table B.7. Atomic Coordinates ( $\times 10^4$ ) and Equivalent Isotropic Displacement Parameters ( $\text{\AA}^2 \times 10^3$ ) for  $\text{Ag}(\text{biimH})_2(\text{NO}_3)_3$ .  $U(\text{eq})$  is Defined as One Third of the Trace of the Orthogonalized  $U_{ij}$  Tensor

	x	y	z	$U(\text{eq})$
N(5)	10000	2473(5)	7500	51(1)
Ag(1)	10000	5401(1)	7500	47(1)
O(1)	9967(2)	3011(3)	5933(5)	72(1)
O(2)	10000	1460(4)	7500	88(2)
O(3)	8549(1)	8071(3)	1638(5)	74(1)
O(4)	7785(1)	8052(3)	3229(4)	58(1)
O(5)	7819(2)	8774(4)	349(5)	97(1)
N(1)	9121(1)	5447(3)	7454(4)	40(1)
N(2)	8236(1)	5862(3)	7127(5)	47(1)
N(3)	9294(1)	7974(3)	8094(5)	44(1)
N(4)	8583(2)	8185(3)	6179(5)	49(1)
N(6)	8055(2)	8294(3)	1686(6)	54(1)
C(1)	8813(2)	4480(3)	7442(6)	46(1)
C(2)	8267(2)	4741(4)	7231(6)	51(1)
C(3)	8759(1)	6265(3)	7270(5)	38(1)
C(4)	8882(1)	7443(3)	7182(5)	38(1)
C(5)	8816(2)	9210(4)	6473(7)	59(1)
C(6)	9258(2)	9085(3)	7681(6)	53(1)

Table B.8. Bond Lengths [Å] and Angles [°] for Ag(biimH)<sub>2</sub>(NO<sub>3</sub>)<sub>3</sub>

N(5)-O(2)	1.220(7)
N(5)-O(1)#1	1.251(4)
N(5)-O(1)	1.251(4)
N(5)-Ag(1)	3.525(6)
Ag(1)-N(1)	2.118(3)
Ag(1)-N(1)#1	2.118(3)
O(3)-N(6)	1.221(4)
O(4)-N(6)	1.285(4)
O(5)-N(6)	1.211(5)
N(1)-C(3)	1.319(5)
N(1)-C(1)	1.380(5)
N(2)-C(3)	1.352(5)
N(2)-C(2)	1.353(6)
N(3)-C(4)	1.326(5)
N(3)-C(6)	1.369(5)
N(4)-C(4)	1.327(5)
N(4)-C(5)	1.368(6)
C(1)-C(2)	1.358(6)
C(3)-C(4)	1.449(5)
C(5)-C(6)	1.341(7)
O(2)-N(5)-O(1)#1	121.1(3)
O(2)-N(5)-O(1)	121.1(3)
O(1)#1-N(5)-O(1)	117.7(5)
O(2)-N(5)-Ag(1)	180.000(1)
O(1)#1-N(5)-Ag(1)	58.9(3)
O(1)-N(5)-Ag(1)	58.9(3)
N(1)-Ag(1)-N(1)#1	177.00(17)
N(1)-Ag(1)-N(5)	91.50(9)

Table B.8. (Continued) Bond Lengths [ $\text{\AA}$ ] and Angles [ $^\circ$ ] for  $\text{Ag}(\text{biimH})_2(\text{NO}_3)_3$ 

N(1)#1-Ag(1)-N(5)	91.50(9)
C(3)-N(1)-C(1)	105.9(3)
C(3)-N(1)-Ag(1)	132.8(3)
C(1)-N(1)-Ag(1)	121.0(3)
C(3)-N(2)-C(2)	107.7(3)
C(4)-N(3)-C(6)	109.3(4)
C(4)-N(4)-C(5)	108.4(4)
O(5)-N(6)-O(3)	121.7(4)
O(5)-N(6)-O(4)	119.3(4)
O(3)-N(6)-O(4)	119.0(4)
C(2)-C(1)-N(1)	109.0(4)
N(2)-C(2)-C(1)	106.7(4)
N(1)-C(3)-N(2)	110.6(3)
N(1)-C(3)-C(4)	126.8(3)
N(2)-C(3)-C(4)	122.6(3)
N(3)-C(4)-N(4)	108.0(4)
N(3)-C(4)-C(3)	127.1(3)
N(4)-C(4)-C(3)	124.8(3)
C(6)-C(5)-N(4)	107.8(4)
C(5)-C(6)-N(3)	106.4(4)

---

Symmetry transformations used to generate equivalent atoms:

#1  $-x+2, y, -z+3/2$

Table B.9. Anisotropic Displacement Parameters ( $\text{\AA}^2 \times 10^3$ ) for  $\text{Ag}(\text{biimH})_2(\text{NO}_3)_3$ . The Anisotropic Displacement Factor Exponent Takes the Form:  $-2\pi^2 [ h^2 a^{*2} U_{11} + \dots + 2 h k a^* b^* U_{12} ]$

	$U_{11}$	$U_{22}$	$U_{33}$	$U_{23}$	$U_{13}$	$U_{12}$
N(5)	46(3)	52(3)	54(3)	0	-5(2)	0
Ag(1)	34(1)	47(1)	60(1)	0	-2(1)	0
O(1)	90(3)	72(2)	53(2)	12(2)	-20(2)	-16(2)
O(2)	94(4)	46(3)	122(5)	0	-8(3)	0
O(3)	54(2)	77(2)	91(3)	9(2)	22(2)	17(2)
O(4)	44(2)	76(2)	53(2)	11(2)	6(1)	3(1)
O(5)	73(2)	149(4)	67(2)	39(3)	-11(2)	7(3)
N(1)	39(2)	41(2)	41(2)	2(2)	-1(1)	-2(1)
N(2)	33(2)	56(2)	51(2)	3(2)	-2(1)	0(2)
N(3)	44(2)	47(2)	41(2)	1(2)	-1(2)	-2(2)
N(4)	51(2)	48(2)	46(2)	6(2)	-3(2)	7(2)
N(6)	49(2)	53(2)	59(2)	2(2)	3(2)	2(2)
C(1)	47(2)	42(2)	48(2)	-1(2)	1(2)	-3(2)
C(2)	47(2)	54(3)	52(3)	2(2)	-1(2)	-14(2)
C(3)	32(2)	44(2)	37(2)	-2(2)	-3(1)	1(2)
C(4)	36(2)	41(2)	36(2)	1(2)	2(2)	3(2)
C(5)	71(3)	41(2)	65(3)	7(2)	11(2)	8(2)
C(6)	61(3)	42(2)	56(3)	-6(2)	16(2)	-5(2)

Table B.10. Hydrogen Coordinates ( $\times 10^4$ ) and Isotropic Displacement Parameters ( $\text{\AA}^2 \times 10^3$ ) for  $\text{Ag}(\text{biimH})_2(\text{NO}_3)_3$

	x	y	z	U(eq)
H(1)	8956	3766	7559	55
H(2)	7971	4246	7171	61
H(5)	8689	9875	5932	71
H(6)	9494	9642	8145	63
H(2N)	7925(18)	6230(30)	7230(60)	50(12)
H(3)	9508(16)	7630(30)	8930(60)	44(12)
H(4)	8296(19)	8090(40)	5310(70)	69(15)

Table B.11. Torsion Angles [°] for Ag(biimH)<sub>2</sub>(NO<sub>3</sub>)<sub>3</sub>


---

O(2)-N(5)-Ag(1)-N(1)	0(100)
O(1)#1-N(5)-Ag(1)-N(1)	-93.8(2)
O(1)-N(5)-Ag(1)-N(1)	86.2(2)
O(2)-N(5)-Ag(1)-N(1)#1	0(100)
O(1)#1-N(5)-Ag(1)-N(1)#1	86.2(2)
O(1)-N(5)-Ag(1)-N(1)#1	-93.8(2)
N(1)#1-Ag(1)-N(1)-C(3)	6.7(3)
N(5)-Ag(1)-N(1)-C(3)	-173.3(3)
N(1)#1-Ag(1)-N(1)-C(1)	-179.9(3)
N(5)-Ag(1)-N(1)-C(1)	0.1(3)
C(3)-N(1)-C(1)-C(2)	0.5(4)
Ag(1)-N(1)-C(1)-C(2)	-174.5(3)
C(3)-N(2)-C(2)-C(1)	0.1(5)
N(1)-C(1)-C(2)-N(2)	-0.4(5)
C(1)-N(1)-C(3)-N(2)	-0.5(4)
Ag(1)-N(1)-C(3)-N(2)	173.7(3)
C(1)-N(1)-C(3)-C(4)	-179.2(4)
Ag(1)-N(1)-C(3)-C(4)	-5.0(6)
C(2)-N(2)-C(3)-N(1)	0.2(5)
C(2)-N(2)-C(3)-C(4)	179.0(3)
C(6)-N(3)-C(4)-N(4)	0.5(4)
C(6)-N(3)-C(4)-C(3)	-178.2(4)
C(5)-N(4)-C(4)-N(3)	-0.1(5)
C(5)-N(4)-C(4)-C(3)	178.7(4)
N(1)-C(3)-C(4)-N(3)	-33.4(6)
N(2)-C(3)-C(4)-N(3)	148.0(4)
N(1)-C(3)-C(4)-N(4)	148.1(4)
N(2)-C(3)-C(4)-N(4)	-30.5(6)
C(4)-N(4)-C(5)-C(6)	-0.4(5)

Table B.11. (Continued) Torsion Angles [°] for Ag(biimH)<sub>2</sub>(NO<sub>3</sub>)<sub>3</sub>

N(4)-C(5)-C(6)-N(3)	0.7(5)
C(4)-N(3)-C(6)-C(5)	-0.7(5)

---

Symmetry transformations used to generate equivalent atoms:

#1  $-x+2, y, -z+3/2$

## APPENDIX C

### NUCLEAR MAGNETIC RESONANCE SPECTRA



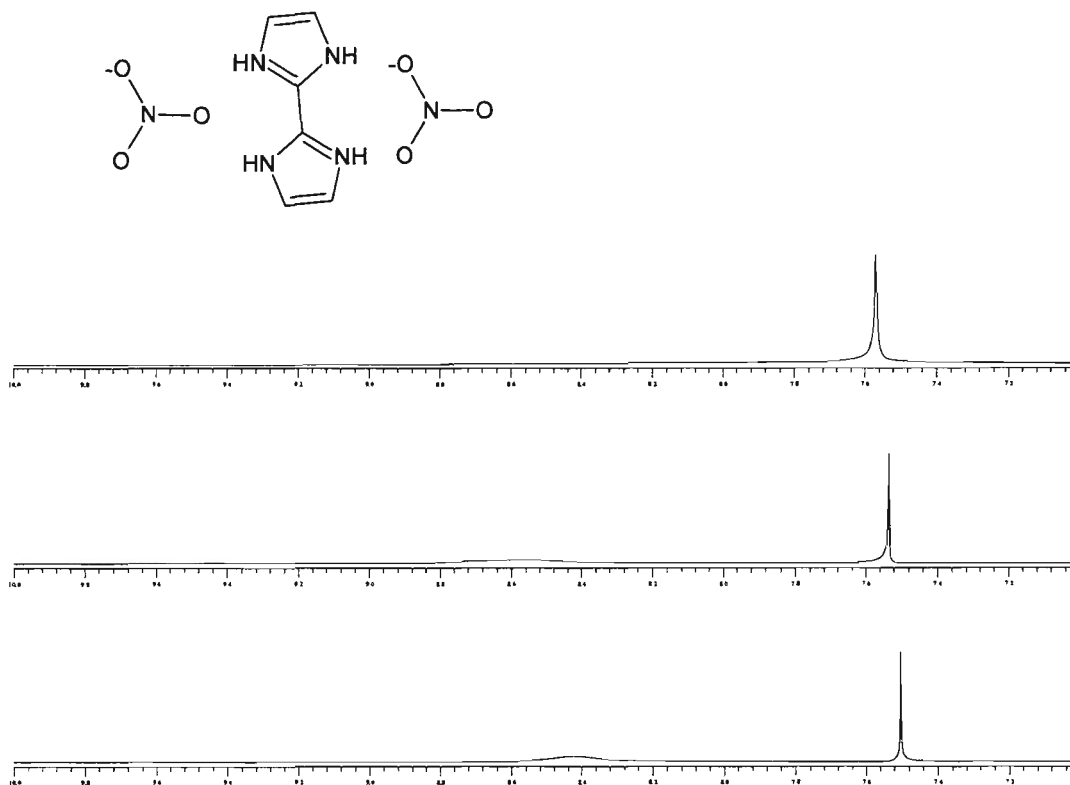


Figure C.1. Proton NMR spectra at 20°, 50°, and 75° C (from bottom to top) of 2,2'-bis(1H-imidazolium) dinitrate.

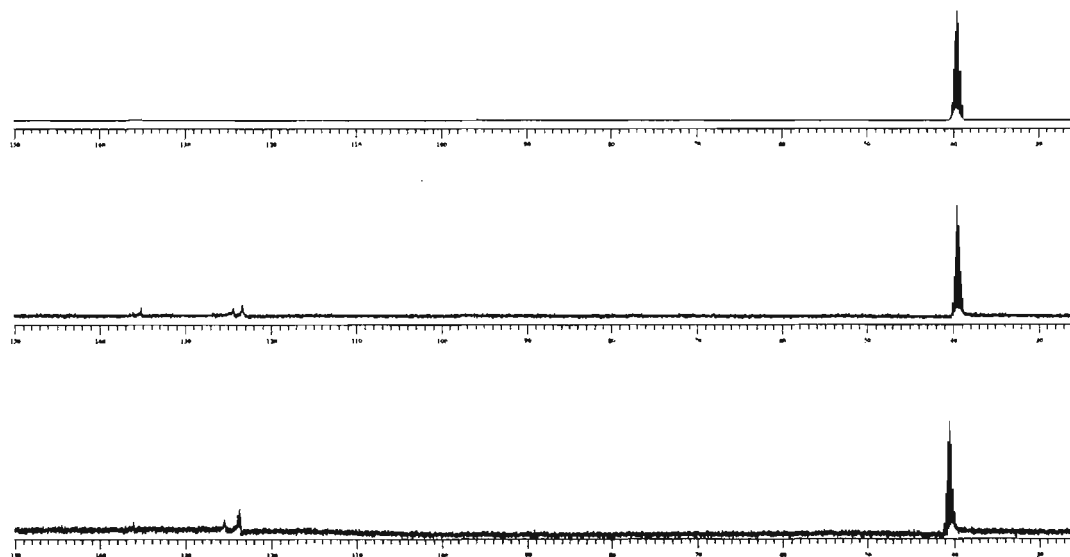


Figure C.2. Carbon NMR spectra at 20°, 50°, and 75°C (from bottom to top) of 2,2'-bis(1H-imidazolium) dinitrate.

APPENDIX D

THERMOGRAVIMETRIC ANALYSIS SPECTRA

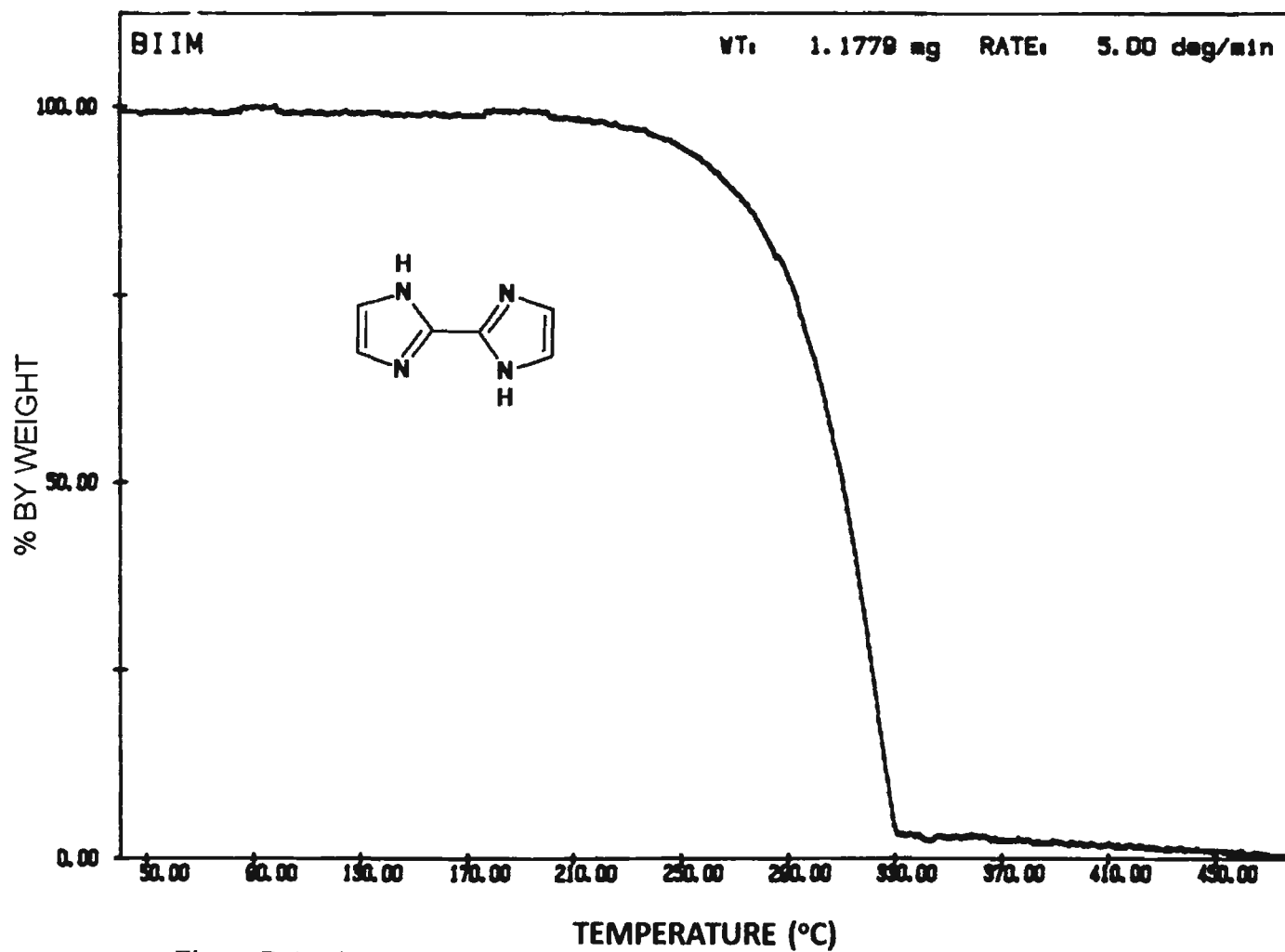


Figure D.1. Thermal gravimetric spectrum of 2,2'-biimidazole.

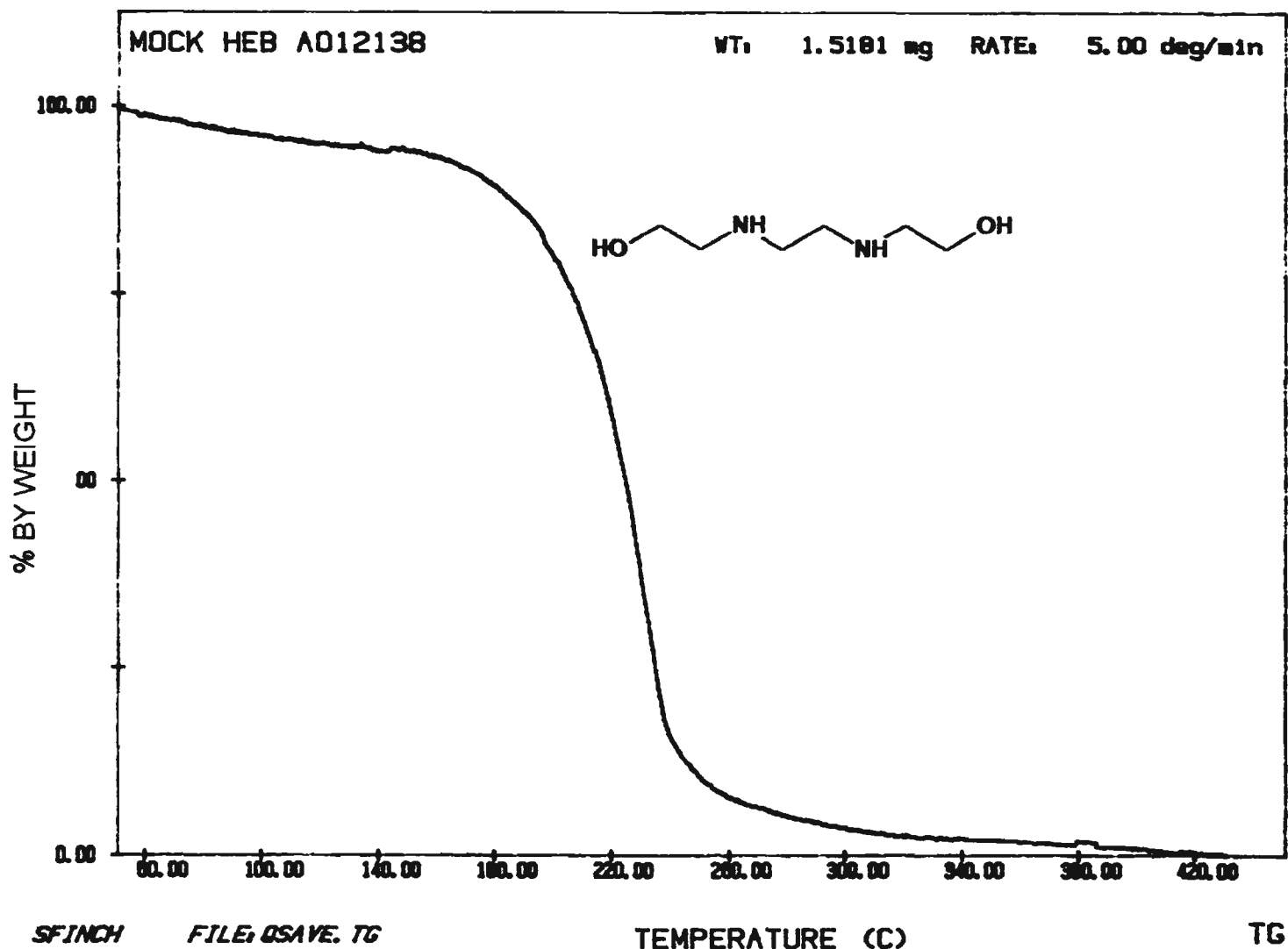


Figure D.2. Thermal gravimetric spectrum of mock-HEB.

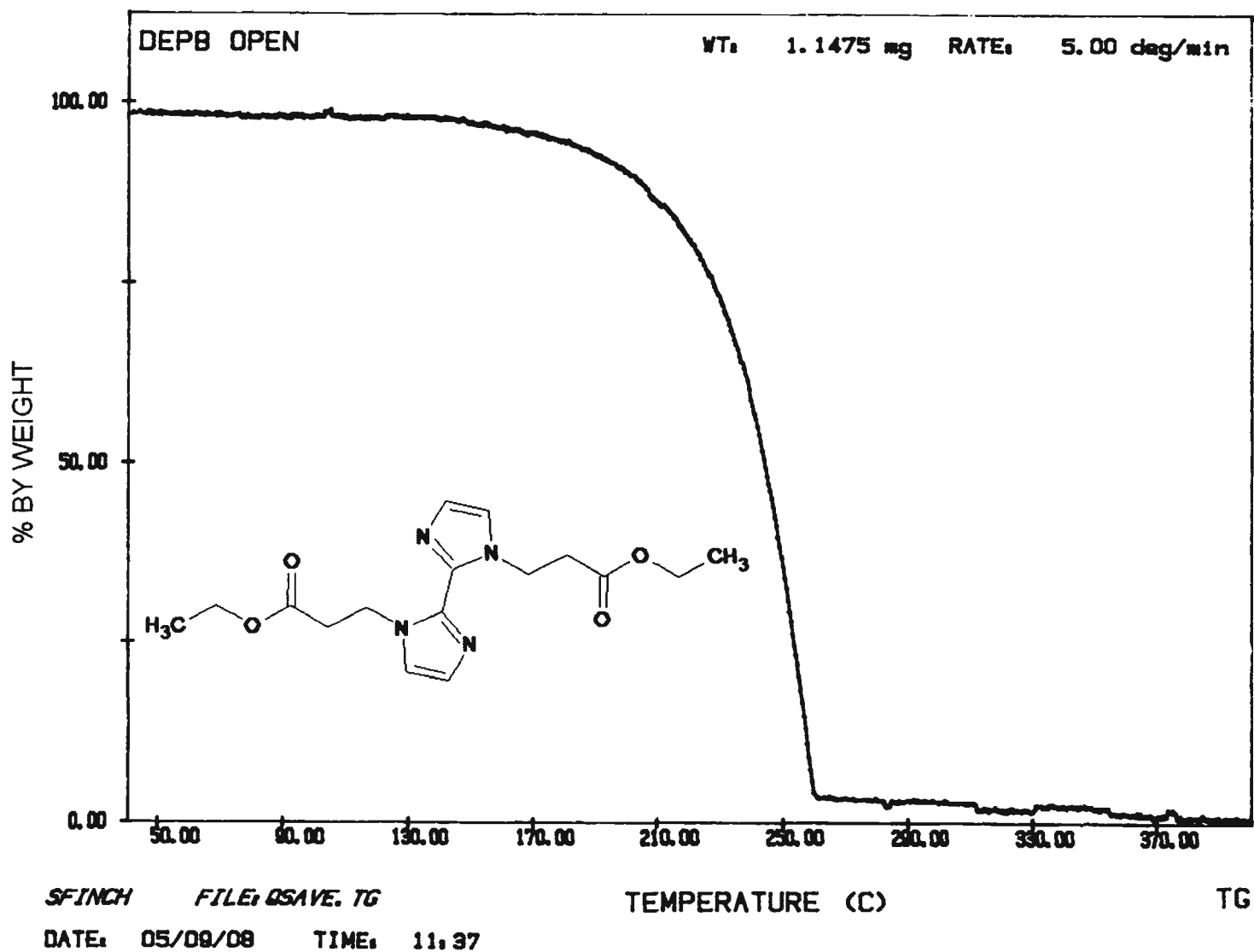


Figure D.3. Thermal gravimetric spectrum of DEP8.

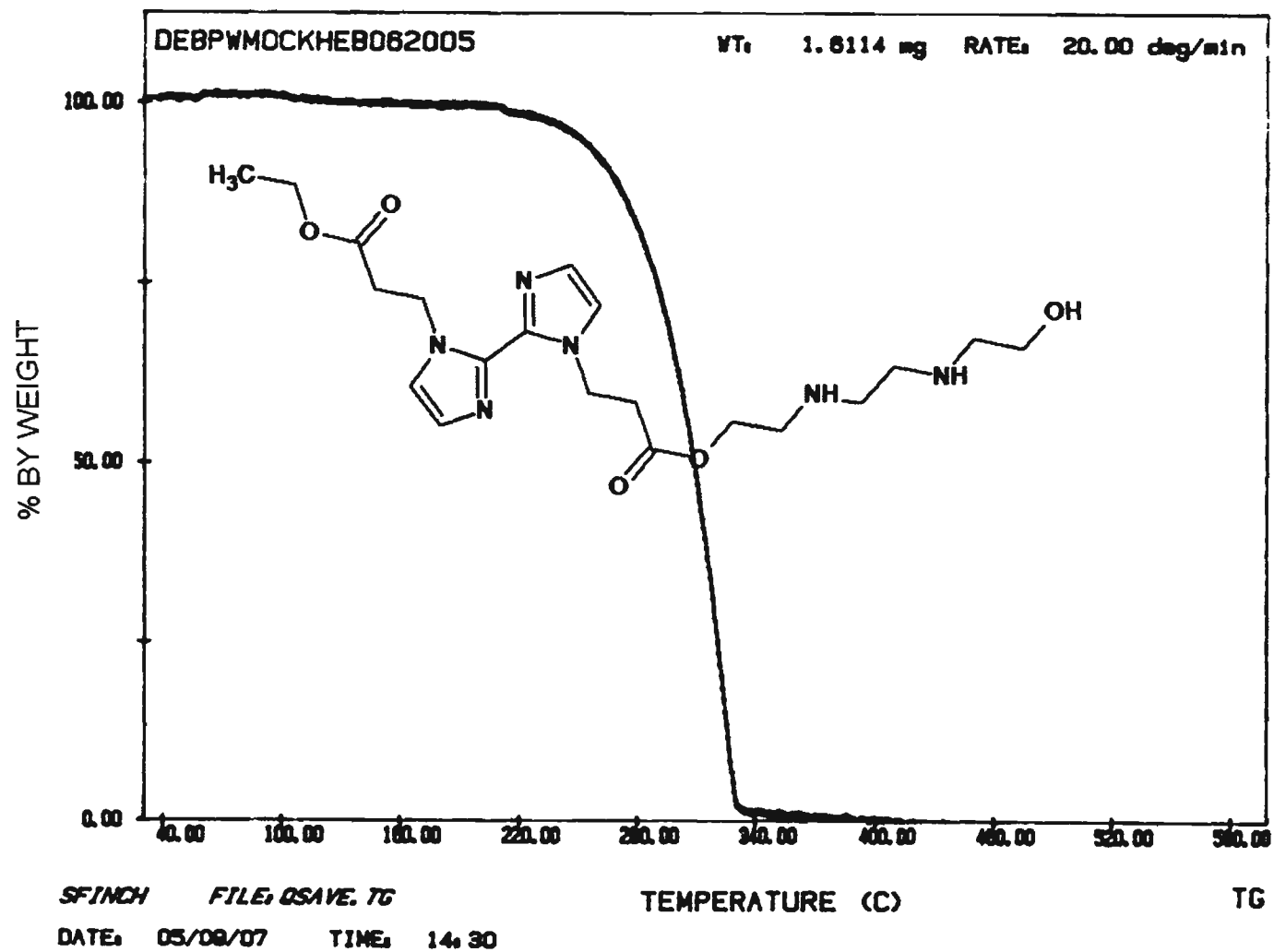


Figure D.4. Thermal gravimetric spectrum of DEPB:mock-HEB.

## REFERENCES

1. Debus, H. *Justus Liebigs Annalen Der Chemie* **1858**,107, 199-208.
2. Melloni, P., Metelli, R., Bassini D. F., Confalonieri, C., Logemann, W., De Carneri, I. *Arzneimittel-Forschung* **1975**,25(1), 9-14.
3. Matthews, D.P., McCarthy, J.R., Whitten, J. P., Kastner, P. R., Barney, C. L., Marshall, F. N., Ertel, M. A., Burkhard, T., Shea, P. J., and Kariya, T. *Journal of Medicinal Chemistry*, **1990**, 33(1), 317-327.
4. Matthews, D. P., McCarthy, J. R., and Whitten, J. P. *United States Patent* 88-111954 301456, 25 July **1988**. (Merrell Dow Pharmaceuticals, Inc., USA). **1989**. 10 pp.
5. Mestroni, G., Alessio, E., Sava, G., and Bergamo, A. *Italian Patent* 2002076998, 22 March **2002**. (Sigea S. R. L., Italy). **2002**. 17 pp.
6. Mestroni, G., Alessio, E., Sava, G., Iengo, E., Zorzet, S., and Bergamo, A. *Italian Patent* 2000063218, 19 April **1999**. (Sigea S. R. L., Italy). **2000**. 42 pp.
7. Cromer, D. T., Ryan, R. R., and Storm C.B. *Acta Crystallographica* **1987**, C43(7), 1435-1437.
8. Akutagawa, T., Saito, G., Yamochi, H., Kusunoki, M., and Sakaguchi, K. *Synthetic Metals* **1995**, 69(1-3), 591-592.
9. Akutagawa, T., and Saito, G. *Bulletin of the Chemical Society of Japan*, **1995**, 68(7), 1753-1773.
10. Tadokoro M, Kanno H, Kitajima, T., Shimada-Umemoto, H, Nakanishi, N., Isobe, K., and Nakasuji, K.. *Proceedings of the National Academy of Sciences of the United States of America*, **2002**, 99(8), 4950-4955.
11. Tadokoro, M., Sato, K., Shiomi, D., Takui, T., and Itoh, K. *Molecular Crystals and Liquid Crystals Science and Technology Section A*,**1997**, 306, 49-56.
12. Tadokoro, M., and Takui, T. *Molecular Crystals and Liquid Crystals Science and Technology Section A*, **1996**, 278, 225-228.
13. Tadokoro, M., Isobe, K., and Nakasuji, K. *Molecular Crystals and Liquid Crystals Science and Technology Section A*, **1996**, 278, 217-220.
14. Tadokoro, M., Isobe, K., Miyazaki, A., Enoki, T., and Nakasuji, K. *Molecular Crystals and Liquid Crystals Science and Technology Section A*, **1996**, 278, 199-207.

15. Tadokoro, M., Isobe, K., and Nakasuji, K. *Molecular Crystals and Liquid Crystals Science and Technology, Section A*, **1996**, 278, 213-216.
16. Tadokoro, M., Isobe, K., and Nakasuji, K. *Molecular Crystals and Liquid Crystals Science and Technology Section A*, **1996**, 285, 269-274.
17. Tadokoro, M., and Nakasuji, K. *Coordination Chemistry Reviews* **2000**, 198, 205-218.
18. Tadokoro, M., Toyoda, J., Isobe, K., Itoh, T., Miyazaki, A., Enoki, T., and Nakasuji, K. *Chemistry Letters* **1995**, (8), 613-614.
19. Tadokoro, M., Shiomi, T., Shiromizu, T., Isobe, K., Matsumoto, K., and Nakasuji, K. *Molecular Crystals and Liquid Crystals Science and Technology Section A*, **1997**, 306, 235-239.
20. Tadokoro, M., Sato, K., Shiomi, D., Bae, J., Takui, T., and Itoh, K. *Molecular Crystals and Liquid Crystals Science and Technology Section A*, **1996**, 278, 241-246.
21. Schuchardt, U., Sercheli, R., and Vargas, R. M. *Journal of the Brazilian Chemical Society*, **1998**, 9(3), 199-210.
22. Xiang, J., Toyoshima, S., Orita, A., and Otera, J. *Angewandte Chemie, International Edition*, **2001**, 40(19), 3670-3672.
23. Kuhn, R., and Blau, W. *Justus Liebigs Annalen Der Chemie* **1957**, 605, 32-35.
24. Ginzburg, B. M., Nurgatin, V. V., Beskrovnaya, T. G., and Kovalenko, V. I. *Russian Patent* 83-3591321 1122655, 4 March **1983** (USSR). **1984**.
25. Matthews, D. P., Whitten, J. P., and McCarthy, J. R. *Synthesis*, **1986**, (4), 336-337.
26. Nurgatin, V. V., Ginzburg, B. M., Sharnin, G. P., and Polyanskii, V.F. *Khimiya Geterotsiklicheskikh Soedinenii*, **1987**, (8), 1069-1070.
27. Duranti, E., and Balsamini, C. *Synthesis*, **1974**, (11), 815-816.
28. Oida, M., and Hirohata, H. *Japanese Patent* 71-65305 51049577, 25 August **1971** (Matsushita Electric Industrial Co., Ltd., Japan). **1976**. 2 pp.
29. Heinisch, E., and Hussong, M. *German Patent* 1105377. (Zschimmer & Schwarz). **1961**.



30. Mal'tsev, N. D., Bodina, N. N., Sidorova, R. P., Agapova, O. I., Petrysheva, Z. N., Ratnovskaya, E. D., and Izrael'son, B. I. *Russian Patent* 137884. **1961**.
31. Melloni, P., Dradi, E., Logemann, W., De Carneri, I., and Trane, F. *Journal of Medicinal Chemistry*, **1972**, 15(9), 926-930.
32. Melloni, P., Logemann, W., De Carneri, I., and Trane, F. *Advan. Antimicrob. Antineoplastic Chemother., Proc. Int. Congr. Chemother., 7th*, **1972**, 1(1), 405-407.
33. Melloni, P., Logemann, W., and De Carneri, I. *German Patent* 71-2149825 2149825, 6 October **1971**. (Erba, Carlo, S.P.A.). **1972**. 38 pp.
34. Jpn. Kokai Tokkyo Koho. *Japanese Patent* 62135461 (Merrell Dow Pharmaceuticals, Inc., USA). **1987**. 5 pp.
35. Mestroni, G., Alessio, E., Gianni, S., Iengo, E., Zorzet, S., and Bergamo, A. *Italian Patent* 2002-EP3256 2002076998, 22 March **2002** (Sigea S.R.L., Italy). **2000**. 17 pp.
36. Sanchez Gonzalez, A., Casas, J. S., Sordo, J., Russo, U., Lareo, M. I., and Regueiro, B. J. *Journal of Inorganic Biochemistry*, **1990**, 39(3), 227-235.
37. Borchers, A., Engler, H., Szelenyi, I., and Schunack, W. *Arzneimittel-Forschung*, **1982**, 32(12), 1509-1512.
38. von Euler, H., Hasselquist, H., and Heidenberger, O. *Arkiv för Kemi*, **1959**, 14, 419-428.
39. Roehling, H. *Zeitschrift für Naturforschung, Teil B: Anorganische Chemie, Organische Chemie, Biochemie, Biophysik, Biologie*, **1970**, 25(9), 631-634.
40. Haga, M.A. *Inorganica Chimica Acta*, **1983**, 75(1), 29-35.
41. Kokai Tokkyo Koho. *Japanese Patent* 80-125164 57049962, 9 September **1980** (Ricoh Co., Ltd., Japan). **1982**. 6 pp.
42. Rasmussen, P. G., Bailey, O. H., Anderson, J. E., Kolowich, J. B., and Bayon, J. *C. Molecular Crystals and Liquid Crystals*, **1985**, 126(1), 87-94.
43. *Netherlands Patent* 6505529 (E. I. du Pont de Nemours & Co.). **1965**. 39 pp.
44. Goff, D. L. *United States Patent* 82-427415 4416973, 29 September **1982** (E. I. du Pont de Nemours & Co.) **1983**. 7pp.

45. Goff, D. L., Yuan, E. L., and Proskow, S. *United States Patent* 81-334164 4414312, 24 December 1981 (E. I. du Pont de Nemours & Co.). 1983. 4 pp.
46. Goff, D. L., Yuan, E. L., and Proskow, S. *United States Patent* 81-334166 4410612, 24 December 1981 (E. I. du Pont de Nemours & Co. USA). 1983. 5 pp.
47. Goff, D. L., Yuan, E. L., and Proskow S. *United States Patent* 81-334163 4369247, 24 December 1981 (E. I. du Pont de Nemours & Co. USA). 1983. 5 pp.
48. Strilko PS. Deactivating dual-response photosensitive composition with visible and ultraviolet light. (du Pont de Nemours, E. I., and Co.). 1972.
49. Dessauer, R., and Looney, C. *Photographic Science and Engineering*, 1979, 23(5), 287-289.
50. Schuster, C., Gehm, R., Abrahamczik, E., and Schwarte, G. *German Patent* 1028338 (Badische Anilin- & Soda-Fabrik Akt.-Ges.). 1958.
51. Surovtsev, L. G., Blokhin, V. E., Rozin, Y. A., Lukina, G. A., and Bulatov, M. A. *Tezisy Dokladov-Simpozium po Khimii i Tekhnologii Geterotsiklicheskih Soedinenii Goryuchikh Iskopaemykh, 2nd*, 1973, 203-204.
52. Skvortsova, G. G., Domnina, E. S., Baikalova, L. V., Val'kova, A. K., Lyubomilova, M. V., and Nikolenko, L. N. *Russian Patent* 78-2669161 740771, 2 October 1978. (USSR) 1980.
53. Nikolenko, L. N., Tolmacheva, N. S., Semenova, M. N., Babievskaya, I.Z., Kotkova, G. V., and Teterin, Y. A. *Koordinatsionnaya Khimiya*, 1975, 1(8), 1054-1058.
54. Beck, W., Goetzfried, F., and Riederer, M. *Zeitschrift fuer Anorganische und Allgemeine Chemie*, 1976, 423(2), 97-102.
55. Kaiser, S. W., Saillant, R. B., Butler, W. M., and Rasmussen, P. G. *Inorganic Chemistry*, 1976, 15(11), 2688-2694.
56. Kaiser, S. W., Saillant, R. B., Butler, W.M., and Rasmussen, P. G. *Inorganic Chemistry*, 1976, 15(11), 2681-2688.
57. Dose, E. V., and Wilson, L. J.. *Inorganic Chemistry*, 1978, 17(9), 2660-2666.
58. Abushamleh, A. S., and Goodwin, H. A. *Australian Journal of Chemistry*, 1979, 32(3), 513-518.
59. Sakaguchi, U., and Addison, A. W. *Journal of the Chemical Society, Dalton Transactions: Inorganic Chemistry* 1979, (4), 600-608.

60. Calhorda, M. J., and Dias, A. R. *Journal of Organometallic Chemistry*, **1980**, 197(3), 291-302.
61. Dance, I. G., Abushamleh, A. S., and Goodwin, H. A. *Inorganica Chimica Acta*, **1980**, 43(2), 217-221.
62. Holmes, F., Jones, K. M., and Torrible, E. G. *Journal of the Chemical Society*, **1961**, 4790-4794.
63. Bernhard, P., Lehmann, H., and Ludi, A. *Journal of the Chemical Society, Chemical Communications*, **1981**, (23), 1216-1217.
64. Keiko, V. V., Baikalova, L. V., Domnina, E. S., Skvortsova, G. G., Taryashinova, D. D., Chipanina, N. N., Voronov, V. K., and Nikolenko, L. N. *Zhurnal Obshchei Khimii*, **1981**, 51(4), 892-897.
65. Uson, R., and Gimeno, J. *Journal of Organometallic Chemistry*, **1981**, 220(2), 173-179.
66. Uson, R., Gimeno, J., Fornies, J., and Martinez, F. *Inorganica Chimica Acta*, **1981**, 50(2), 173-177.
67. Uson, R., Gimeno, J., Oro, L. A., Valderrama, M., Sariego, R., and Martinez, E. *Transition Metal Chemistry* **1981**, 6(2), 103-107.
68. Rasmussen, P. G., and Anderson, J. E. *Polyhedron*, **1983**, 2(6), 547-550.
69. Uson, R., Gimeno, J., Oro, L. A., Aznar, M.A., and Cabeza, J. A. *Polyhedron*, **1983**, 2(3), 163-166.
70. Uson, R., Oro, L. A., Ciriano, M. A., Naval, M. M., Apreada, M. C., Foces-Foces, C., Cano, F. H., and Garcia-Blanco, S. *Journal of Organometallic Chemistry*, **1983**, 256(2), 331-347.
71. Hester, C. A., Baughman, R. G., and Collier, H. L. *Polyhedron*, **1997**, 16(16), 2893-2895.
72. Hester, C. A., Collier, H. L., and Baughman, R. G. *Polyhedron*, **1996**, 15(23), 4255-4258.
73. Hu, M. L., Cai, X. Q., and Chen, J. X. *Acta Crystallographica*, **2005**, C61(9), m403-m405.
74. Tadokoro, M. *Nippon Kessho Gakkaishi*, **2003**, 45(4), 240-248.

75. Tadokoro, M. *Yuki Gosei Kagaku Kyokaishi*, **2004**, 62(6), 629-640.
76. Tadokoro, M., Daigo, M., Isobe, K., Matsumoto, K., and Nakasuji, K. *Molecular Crystals and Liquid Crystals Science and Technology, Section A*, **1997**, 306, 391-396.
77. Tadokoro, M., Daigo, M., Isobe, K., Matsumoto, K., and Nakasuji, K. *Molecular Crystals and Liquid Crystals Science and Technology, Section A*, **1997**, 306, 41-47.
78. Tadokoro, M., Isobe, K., Uekusa, H., Ohashi, Y., and Nakasuji, K. *Molecular Crystals and Liquid Crystals Science and Technology, Section A*, **1996**, 278, 221-224.
79. Tadokoro, M., Isobe, K., Uekusa, H., Ohashi, Y., Toyoda, J., Tashiro, K., and Nakasuji, K. *Angewandte Chemie, International Edition*, **1999**, 38(1/2), 95-98.
80. Tadokoro, M., Shiomi, T., Isobe, K., and Nakasuji, K. *Inorganic Chemistry*, **2001**, 40(22), 5476-5478.
81. Lehn, J. M., and Regnouf de Vains, J. B. *Helvetica Chimica Acta*, **1992**, 75(4), 1221-1236.
82. Dhal, P. K., and Arnold, F. H. *Journal of the American Chemical Society*, **1991**, 113(19), 7417-7418.
83. Xu, J., Huang, J., and Deng, A. *Chinese Patent* 2002-138392 1486986, 3 October **2002** (Huatai Chemistry Co., Ltd., Changzhou, Peop. Rep. China). **2004**. 10 pp.
84. Fu, Y.-M., Zhao, Y.-H., Lan, Y.-Q., Shao, K.-Z., Qiu, Y.-Q., Hao, X.-R. and Su, Z.-M. *Inorganic Chemistry Communications*, **2007**, 10(6), 720-723.
85. Akutagawa, T., Saito, G., Kusunoki, M., and Sakaguchi K-I. *Bulletin of the Chemical Society of Japan*, **1996**, 69(9), 2487-2511.
86. Herbstein, F. H., Hu, S., and Kapon, M. *Acta Crystallographica*, **2002**, B58(5), 884-892.
87. Yuan, J. X. *Acta Crystallographica*, **2005**, E61(10), 3294-3296.
88. Ramirez, K., Reyes, J. A., Briceno, A., and Atencio, R. *CrystEngComm*, **2002**, 4, 208-212.
89. Li, Y. P., and Yang, P. *Acta Crystallographica*, **2006**, E62(8), 3223-3224.

90. Hu, M. L., and Chen, F. *Zeitschrift fuer Kristallographie - New Crystal Structures*, 2006, 221(1), 47-48.
91. Belanger, S., and Beauchamp, A. L. *Acta Crystallographica*, **1996**, C52(10), 2588-2590 (1996).
92. Finch S, Collier H. 2,2-bis(1H-imidazolium) dinitrate. *Acta Crystallographica*, 2011 (In preparation).
93. Baughman, R.G. Truman State University, Chemistry Department, Kirksville MO, personal communication. June **2003**.
94. Lemke, M., Knoch, F., Kisch, H., and Salbeck, J. *Chemische Berichte*, **1995**, 128(2), 131-136.
95. Majumdar, P., Kamar, K. K., Goswami, S., and Castineiras, A. *Chemical Communications*, **2001**, (14), 1292-1293.
96. Majumdar, P., Peng, S.-M., and Goswami, S. *Journal of the Chemical Society, Dalton Transactions*, **1998**, (10), 1569-1574.
97. Atencio, R., Chacon, M., Gonzalez, T., Briceno, A., Agrifoglio, G., and Sierraalta, A. *Journal of the Chemical Society, Dalton Transactions*, **2004**, (4), 505-513.
98. Olah, G. A. *Journal of Organic Chemistry*, **2001**, 66(18), 5943-5957.
99. Lammertsma, K., Schleyer, P. v. R., and Schwarz, H. *Angewandte Chemie*, **1989**, 101(10), 1313-1335.
100. Kamar, K. K., Falvello, L. R., Fanwick, P. E., Kim, J., and Goswami, S. *Journal of the Chemical Society, Dalton Transactions.*, **2004**, (12), 1827-1831.
101. Sheldrick, G. M. *Acta Crystallographica Section A: Foundations of Crystallography* **2008**, 64, no, 1, 112-122.
102. Deady, L. W. *Australian Journal of Chemistry*, **1981**, 34(12), 2569-2576.
103. Rasmussen, P. G., Hough, R. L., Anderson, J. E., Bailey, O. H., and Bayon, J. C. *Journal of the American Chemical Society*, **1982**, 104(22), 6155-6156.
104. Barnett, M., Secondo, P., and Collier, H. *Journal of Heterocyclic Chemistry*, **1996**, 33(4), 1363-1365.
105. Barnett, W. M., Baughman, R. G., Collier, H. L., and Vizueté, W. G. *Journal of Chemical Crystallography*, **1999**, 29(7), 765-768.

106. He, F. Aspects of convenient synthesis of 2,2'-biimidazole derivatives and aliphatic poly(amino-ester)s. (2002).
107. Barnett, W. M., Lin, G., Collier, H. L., and Baughman, R. G. *Journal of Chemical Crystallography*, **1997**, 27(7), 423-427.
108. He, F., Shooshtari, K., and Collier, H. Abstracts of Papers, 222nd ACS National Meeting, Chicago, IL, United States, **2001**, August 26-30, 2001, POLY-159.
109. Maiboroda, A., Rheinwald, G., and Lang, H. *Inorganic Chemistry Communications*, **2001**, 4(8), 381-383.
110. Lin, G. *Investigations of several new 2,2'-biimidazole derivatives and styrenic and methacrylic polymers*. **1998**.
111. Lin, G., Collier, H., and Baughman, R. G. *Acta Crystallographica*, **1999**, C55(3), 476-478.
112. Lister, R. L. *Synthesis and characterization of metal ion binding polyesters containing 2,2'-bimidazole*. **1997**.
113. Breslow, R., Anslyn, E., and Huang, D. L. *Tetrahedron*, **1991**, 47(14-15), 2365-2376.
114. Breslow R. Enzyme mimics. Ciba Foundation Symposium, 158(Host-Guest Mol. Interact.: Chem. Biol.), 115-127 (1991).
115. Constable, E. C. *Australian Journal of Chemistry*, **2006**, (59), 1-2.
116. Mighell, A. D., Reimann, C. W., and Mauer, F. A. *Acta Crystallographica, Section B: Structural Crystallography and Crystal Chemistry*, **1969**, 25(Pt. 1), 60-66.
117. Marsh, R. E., Kapon, M., Hu, S., and Herbstein, F.H. *Acta Crystallographica*, **2002**, B58(1), 62-77.
118. Marsh, R. E. *Acta Crystallographica*, **2002**, B58(5), 893-899.
119. Sang, R.-L., and Xu, L. *European Journal of Inorganic Chemistry*, **2006**, (6), 1260-1267.
120. Finch, S. R., Harper, J. P., Choudhury, A., Sinn, E., and Collier, H. L. *Acta Crystallographica*, **2011**, E67(7), m909.

121. Ding, B.-B., Weng, Y.-Q., Cui, Y., Chen, X.-M., and Ye, B.-H. *Supramolecular Chemistry*, **2005**, 17(6), 475-483.
122. Sang, R.-L., and Xu, L. *Inorganica Chimica Acta*, **2006**, 359(8), 2337-2342.
123. Jana, A. D., Ghosh, A. K., Ghoshal, D., Mostafa, G., and Chaudhuri, N. R. *CrystEngComm*, **2007**, 9(4), 304-312.
124. Ghosh, A. K., Jana, A. D., Ghoshal, D., Mostafa, G., and Chaudhuri, N. R. *Crystal Growth & Design*, **2006**, 6(3), 701-707.
125. Gruia, L. M., Rochon, F. D., and Beauchamp, A. L. *Inorganica Chimica Acta*, **2007**, 360(6), 1825-1840.
126. Ye, B.-H., Ding, B.-B., Weng, Y.-Q., and Chen, X.-M. *Crystal Growth & Design*, **2005**, 5(2), 801-806.
127. Sang, R.-L., and Xu, L. *Polyhedron*, **2006**, 25(10), 2167-2174.
128. Hester, C., Baughman, R. G., and Collier, H. *Journal of Chemical Crystallography*, **1996**, 26(10), 695-699.
129. Tadokoro, M., Fukui, S., Kitajima, T., Nagao, Y., Ishimaru, S., Kitagawa, H., Isobe, K. and Nakasuji, K. *Chemical Communications*, **2006**, (12), 1274-1276.
130. Larsson, K., and Oehrstroem, L. *CrystEngComm*, **2004**, 6, 354-359.
131. Aviles, T., Dinis, A., Calhorda, M. J., Pinto, P., Felix, V., and Drew, M. G. B. *Journal of Organometallic Chemistry*, **2001**, 625(2), 186-194.
132. Ohrstrom, L., Larsson, K., Borg, S., and Norberg, S. T. *Chemistry--A European Journal*, **2001**, 7(22), 4805-4810.
133. Ye, B.-H., Ding, B.-B., Weng, Y.-Q., and Chen, X.-M. *Inorganic Chemistry*, **2004**, 43(22), 6866-6868.
134. Marshall, S. R., Incarvito, C. D., Shum, W. W., Rheingold, A. L., and Miller, J. S. *Chemical Communications*, **2002**, (24), 3006-3007.
135. Ding, B.-B., Weng, Y.-Q., Mao, Z.-W., Lam, C.-K., Chen, X.-M., and Ye, B.-H. *Inorganic Chemistry*, **2005**, 44(24), 8836-8845.
136. Gruia, L. M., Rochon, F. D., and Beauchamp, A. L. *Canadian Journal of Chemistry*, **2006**, 84(7), 949-959.
137. Larsson, K., and Oehrstroem, L. *CrystEngComm*, **2003**, 5, 222-225.

138. Sang, R., and Xu, L. *Acta Crystallographica*, **2005**, E61(4), m793-m795.
139. Atencio, R., Ramirez, K., Reyes, J. A., Gonzalez, T., and Silva, P. *Inorganica Chimica Acta*, **2005**, 358(3), 520-526.
140. Gao, X. L., Wei, Y. B., Li, Y. P., and Yang, P. *Acta Crystallographica*, **2005**, C61(1), m10-m12.
141. Hu, M. L., Cai, X. Q., and Chen, J. X. *Acta Crystallographica*, **2005**, C61(9), m403-m405.
142. Haj, M. A., Quiros, M., Salas, J. M., Dobado, J. A., Molina, J. M., Basollote, M. G. and Manez, M. A. *European Journal of Inorganic Chemistry*, **2002**, (4), 811-818.
143. Carranza, J., Brennan, C., Sletten, J., Vangdal, B., Rillema, P., Lloret, F., and Julve, M. *New Journal of Chemistry*, **2003**, 27(12), 1775-1783.
144. Haj, M. A., Quiros, M., and Salas, J. M. *Journal of Chemical Crystallography*, **2004**, 34(8), 549-552.
145. Matouzenko, G. S., Letard, J.-F., Lecoq, S., Bousseksou, A., Capes, L., Salmon, L., Perrin, M., Kahn, O. and Collet, A. *European Journal of Inorganic Chemistry*, **2001**, (11), 2935-2945.
146. Ziessel, R., Youinou, M.-T., Balegroune, F., and Grandjean, D. *Journal of Organometallic Chemistry*, **1992**, 441(1), 143-154.
147. Ghoshal, D., Ghosh, A. K., Ribas, J., Zangrando, E., Mostafa, G., Maji, T. K. and Chaudhuri, N. R. *Crystal Growth & Design*, **2005**, 5(3), 941-947.
148. Pereira, C. C. L., Braga, S. S., Paz, F. A. A., Pillinger, M., Klinowski, J., and Goncalves, I. S. *European Journal of Inorganic Chemistry*, **2006**, (21), 4278-4288.
149. Drew, M. G. B., Felix, V., Goncalves, I. S., Kuhn, F. E., Lopes, A. D., and Romao, C. C. *Polyhedron*, **1998**, 17(7), 1091-1102.
150. Yang, L. N., Li, J., and Zhang, F. X. *Acta Crystallographica*, **2005**, E61(10), m2169-m2171.
151. Ni, Z. H., Cai, Z. N., Zhong, W. F., and Wei, S. Z. *Acta Crystallographica*, **2007**, E63(6), m1570.



152. Comba, P., Mayboroda, A., and Pritzkow, H. *European Journal of Inorganic Chemistry*, **2003**, (16), 3042-3046.
153. Maiboroda, A., Rheinwald, G., and Lang, H. *European Journal of Inorganic Chemistry*, **2001** (9), 2263-2269.
154. Mayboroda, A., Comba, P., Pritzkow, H., Rheinwald, G., Lang, H., and van Koten, G. *European Journal of Inorganic Chemistry*, **2003**, (9), 1703-1710.
155. Fortin, S., and Beauchamp, A. L. *Inorganic Chemistry*, **2000**, 39(21), 4886-4893.
156. Fortin, S., and Beauchamp, A. L. *Inorganic Chemistry*, **2001**, 40(1), 105-112.
157. Fortin, S., Fabre, P.-L., Dartiguenave, M., Beauchamp, A. L. *Journal of the Chemical Society, Dalton Transactions*, **2001**, (23), 3520-3527.
158. Derossi, S., Adams, H., Ward, M. D. *Journal of the Chemical Society, Dalton Transactions*, **2007**, (1), 33-36.
159. Ion, L., Morales, D., Perez, J., Riera, L., Riera, V., Kowenicki, R. A., and McPartlin, M. *Chemical Communications*, **2006**, (1), 91-93.
160. Cancela, J., Gonzalez Garmendia, M. J., and Quiros, M. *Inorganica Chimica Acta*, **2001**, 313(1-2), 156-159.
161. Sang, R., Zhu, M., and Yang, P. *Acta Crystallographica*, **2002**, E58(5), m172-m175.
162. Ye, B.-H., Xue, F., Xue, G.-Q., Ji, L.-N., Mak, T. C. W. *Polyhedron*, **1999**, 18(12), 1785-1790.
163. Kirchner, C., and Krebs, B. *Inorganic Chemistry*, **1987**, 26(21), 3569-3576.
164. Drew, M. G. B., Felix, V., Goncalves, I. S., Kuehn, F. E., Lopes, A. D., and Romao, C. C. *Polyhedron*, **1998**, 17(7), 1091-1102.
165. Nakasuji, K., Tadokoro, M., Toyoda, J., Mitsumi, M., Itoh, T., and Iijima, K. *Molecular Crystals and Liquid Crystals Science and Technology, Section A: Molecular Crystals and Liquid Crystals*, 285(Nagoya Conference Proceedings on Perspectives in Organic-Inorganic Hybrid Solids: Molecular Design and Functionality, 1996), 241-248 (1996).
166. Allen, F. H., Battle, G. M., and Robertson, S. *Comprehensive Medical Chemistry II*, **2006**, 3, 389-410.

167. Bernarducci, E. E., Bharadwaj, P. K., Lalancette, R. A., Krogh-Jespersen, K., Potenza, J. A., and Schugar, H. J. *Inorganic Chemistry*, **1983**, 22(26), 3911-3920.
168. Uson, R., Gimeno, J., Oro, L. A. *Journal of the Chemical Society, Dalton Transactions: Inorganic Chemistry*, **1983**, (1972-1999), (8), 1729-1737.
169. Rasmussen, P. G., Anderson, J. E., and Bayon, J. C. *Inorganica Chimica Acta*, **1984**, 87(2), 159-164.
170. Rasmussen, P. G., Bailey, O. H., and Bayon, J. C. *Inorganica Chimica Acta*, **1984**, 86(2), 107-111.
171. Rasmussen, P. G., Bailey, O. H., and Bayon, J. C. *Inorganic Chemistry*, **1984**, 23(3), 338-343.
172. Rasmussen, P. G., Bailey, O. H., Bayon, J. C., and Butler, W. M. *Inorganic Chemistry*, **1984**, 23(3), 343-349.
173. Rasmussen, P. G., and Bayon, J. C. *Inorganica Chimica Acta*, **1984**, 81(1), L15-L17.
174. Somerville AN. *SciFinder Scholar*, edited by Edward J. Walsh. **1998**.
175. Yamamoto, T., Uemura, T., Tanimoto, A., and Sasaki, S. *Macromolecules*, **2003**, 36(4), 1047-1053.
176. Forster, R. J., Walsh, D. A., Mano, N., Mao, F., and Heller, A. *Langmuir*, **2004**, 20(3), 862-868.
177. Ternay A. *Contemporary Organic Chemistry*, W. B. Saunders Co., **1979**.
178. Painter PC, Coleman MM. *Fundamentals of Polymer Science An Introductory Text*, Technomic Publishing Company, Inc., **1997**.
179. Lister, R. L., and Collier, H. L. *Polymer Preprints*, **1993**, 34(1), 360-361.

## VITA

Shelonda Rena Taylor Finch was born May 12, 1968 at Fort Campbell, Kentucky. She completed her elementary and secondary education with the Christian County School District in Kentucky, graduating from Hopkinsville High School in May 1986. She attended various colleges and universities receiving an Associate of Science degree with High Distinction from Hopkinsville Community College in July 1993, a Bachelor of Science degree in Chemistry and minor in Mathematics from Austin Peay State University in December 1996, and a Master of Science degree in Chemistry from the University of Missouri-Rolla in May 2001. While at Austin Peay State University, she was inducted into Kappa Mu Epsilon and received the Analytical Chemistry award in 1996.

She has been enrolled in the Chemistry graduate program at the University of Missouri-Rolla since August 1998 and has been the recipient of the Missouri Alliance for Graduate Education for the Professorate fellowship.